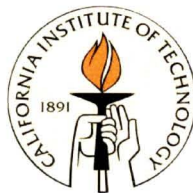# Microfabricated Devices for Rapid DNA Diagnostics

Thesis by

Hou-Pu Chou

In Partial Fulfillment of the Requirements

for the Degree of

Doctor of Philosophy

California Institute of Technology

Pasadena, California

2000

(Submitted May 30th, 2000)

Acknowledgements

It has always been a great pleasure to come to Caltech, enjoying American culture, studying in a new discipline, electrical engineering, and doing research with my great advisors and colleagues in the Nanofabrication Lab and the Biophysics Lab. I'd like to thank all of you, who have ever helped me, advised me, worked with me, or even played with me. Without you, the world, or at least this thesis, would have no value at all.

First, I would like to thank my wonderful advisors, Dr. Axel Scherer and Dr. Stephen Quake. Axel lets me have a chance to lay down my foundation in experiments, especially, fabrication skills, gives me mental support, and tolerates all my ignorance to the new world. He is such a great advisor who always says, "I *share* all the equipment with my students." Don't just tell him your progress. He would like to hear your problems more and then give you valuable suggestions. As for Steve, he is a great scientist. He has profound knowledge, excellent skills, perspective insights, and good management. Through working with him, I could be trained as a real scientist, enjoy my research, and get good experimental results. It is such an unforgettable pleasure and honor to work with both of them.

Second, I would like to thank all my colleagues, especially, Chuan-Cheng Cheng, Charles Spence, and Marc A. Unger. I am so grateful to Chuan-Cheng for his sincere training, instructions, and help during my first three years. Through working with him and Atul A. Salvekarand, the polarization beam splitter project using 2-D photonic band-gap structure became my first good achievement in Caltech[76]. There are thousands of thankful words that I'd like to say but they just won't fit into such a small space. Charles is a wonderful guy, who knows almost all the good stores and companies. He is my tutor in machining and hands-on electronics. It was such a pleasure to work with him in the DNA sizing system[14], which gave us a great memory of making a state-of-the-art avalanche photodiode detector and obtaining good results for this big project. Marc is a great and innovative postdoc in Steve's lab. It was an amazing time when we worked on the silicone miniature valves and pumps day and night[77]. It was truly a big accomplishment to both of us. I am also grateful to Anne Y. Fu for her spiritual discussions and excellent work in the cell-sorting project[25], to Shuli Eyal for her continuing work on the DNA sizing project and important results about

the strong variation dependence on the laser polarization, and to Joyce Y. Wong for her organization, notification, discussions, help, and encouragement. Many thanks also go to Dr. Yu-Chong Tai for his sincere teaching in microfabrication and microelectromechanical systems (MEMS), and to Reynolds Johnson, Atul A. Salvekar, Cherri Chao-Ping Hsu, and Sangdun Choi for their precious help and/or nice work done together. Of course, I'd like to thank my advisor and colleague, Dr. Yang-Fang Chen and Dr. Y.-T. Dai, respectively, in National Taiwan University. The computer and optics experience I learned from the PDS projects there[12, 13] were always helpful throughout my whole graduate study here.

At last, I give sincere thanks to my Mom and Dad. Their care, help and support are always there no matter when, where, or what. I am also grateful to Grace Chia-Hsuan Kuan. Even though she was not in America, or more accurately, never came to California, she is always with me in my mind, which gives me much strength, joy, and fulfillment.

To you and to all of the above, my gratitude.

Hou-Pu Chou

Pasadena, California

March, 2000

Abstract

Science makes new technology and technology pushes science forward. For biological studies and hospital diagnoses, knowledge and techniques accumulated from other fields, such as semiconductors, optics, electronics, and chemistry, are generating huge impacts in almost every aspect and for almost everyone involved. Among these, tools for DNA diagnostics play a very important role. They are also essential to many genetic studies, drug discovery, and even forensic identifications.

Working with Professor Stephen Quake, Professor Axel Scherer, and my colleagues in Caltech, I have developed several building blocks for rapid DNA sizing, cell sorting, molecular fingerprinting, and hybridization assays, based on those newly available technologies. First, a microfabricated flow-cell device was developed using 'soft lithography'. It offers a small, cheap, robust, and contamination-free alternative to the complicated glass-capillary structure used in a conventional flow cytometer. Based on this device, a highly sensitive single-molecule DNA sizing system was demonstrated. It is 100 times faster and requires a million times less sample than pulsed-field gel electrophoresis. For DNA molecules of 1–200 kbp, it has comparable resolution, which improves with increasing DNA length. To serve as a real substitute for a conventional flow cytometry, DNA and cell sorting has also been demonstrated under this system. Simple enclosed actuation schemes are implemented and system downtime due to capillary cleaning is totally eliminated because the device costs only pennies to make and thus becomes disposable. Therefore, there is no cross-contamination issue for both DNA sizing and cell sorting applications. Using this system, prototype work for rapid DNA molecular fingerprinting was devised as an alternative to the widely used Southern blot fingerprinting protocol. Molecular evolution, VNTR fingerprinting of human forensic samples, disease diagnosis based on restriction fragment length polymorphism (RFLP), and simple DNA genomic mapping can all be accomplished with this system. Because of the great flexibility of microfabrication, more complicated functions can also be designed and incorporated into these flow-cell devices. Therefore, this single-molecule sizing system can become a key component in the family of lab-on-a-chip devices.

In addition, a multilayer soft lithography technique was invented, allowing monolithic microvalves and micropumps to be built into these flow-channel devices. Active microfluidic systems containing on-off valves, switching valves and pumps were made, entirely out of elastomer. The softness of these materials allows the device area to be reduced by more than two orders of magnitude compared with silicon-based devices. An actuation volume as small as about one picoliter is demonstrated. The other advantages of soft lithography, such as rapid prototyping, ease of fabrication, and biocompatibility, are retained. Based on these active components, an integrated diagnostic chip was built. More than two orders of magnitude improvement in terms of binding speed and efficiency over passive devices was shown. Selective surface patterning of DNA molecules, biotin, and avidin within the chips by elastomeric flow channels was also shown. With active pumping, we are able to make a rotary motion in these microfluidic devices and show fast inline mixing which overcomes the limitation of laminar flow in this low-Reynolds number regime. Moreover, the problem of buffer depletion due to electrolysis in electroosmotic or electrophoretic flow control does not exist in these devices.

All of these serve as fast, cheap, and robust alternatives to many conventional techniques used widely in biological studies and hospital pathogenic diagnosis. They are all very simple to fabricate and easy to use. If desired, more complicated flow patterns and functions can also be incorporated with much less effort than their silicon counterparts. We anticipate that more applications and devices based on these systems and techniques will be developed rapidly in the near future.

Contents

List of Figures

List of Tables

Chapter 1 Overview

1.1 Introduction

Biology is always an amazing subject to study: to see how beautifully all the small molecules and living things react with each other, and to find out those elegant processes and regulations behind it. Within it, genomics, a study of genetic information stored in the form of nucleic acids in almost every living organism[1], has been a great success in 20th-century science and well marched into the 21st century as the basis of modern molecular biology. A series of Nobel Prizes were awarded to recognize the significance of this work:

- To Watson, Crick and Wilkins in 1962 for their discovery of the structure of DNA.

- To Nirenberg, Khorana and Holley in 1968 for their elucidation of the genetic code.

- To Arber, Smith and Nathans in 1978 for their discovery of Restriction Enzymes.

- To Sanger and Gilbert in 1980 for their development of methods for determining the nucleotide sequence of DNA molecules.

- To Berg in 1980 for developing the first methods for cloning genes, recombinant DNA.

- To Bishop and Varmus in 1989 for the use of recombinant DNA techniques to identify cellular origin of several genes involved in cancer, retroviral oncogenes.

- To Sharp and Roberts in 1993 for their discovery of RNA splicing and split genes.

- To Mullis and Smith in 1993 for the polymerase chain reaction (PCR), which allows one to selectively amplify chosen DNA molecules, for methods that allow the production of biologically useful mutant DNA molecules.

- To Lewis, Nüsslein-Volhard and Wieschaus in 1995 for their research into the genetic blueprint that runs a single cell into a fruit fly, a contribution toward the understanding of genetic control of early embryonic development.

---

[1]Except Prion diseases, which are believed to be composed of only proteins with their genetic codes stored in the genome of their hosts.

As always, great discoveries came from elegant minds and also the advancement of technologies, the giant for us to sit on. With the method of x-ray diffraction, the double-helix structure of DNA was identified. With the continuous development of DNA sequencing techniques, bigger and bigger genomes of various species were unveiled, such as bacterium *Escherichia coli*, worm *Caenorhabditis elegans*, fruit fly *Drosophila* and very soon human beings. With the discoveries of restriction enzymes, DNA recombination factors, and PCR, many interesting biological manipulations and experiments become possible. Looking around beyond biology, tremendous improvements has also been made in the fields of semiconductors, electronics, optics and also chemistry. Based upon all of these, a blooming research and industrial field was formed: *biotechnology*. DNA chips made by Affymetrix, the Human Genome Project under vigorous competition between Celera Genomics and US National Human Genome Research Institute, proteomics in terms of functional studies of proteins and computer-assisted designs, and the idea of lab-on-a-chip devices are all good examples. While institutional research is focused on basic studies and development of technique prototypes, industrial efforts are taking place on instrumentation, protocol perfection, disease diagnostics, and drug development.

Working with Professor Axel Scherer, Professor Stephen Quake and my colleagues, I have developed several essential building blocks of biotechniques based on semiconductor fabrication, micromachining (MEMS), advanced optics and electronics, and also several biological techniques, such as DNA hybridization and high quantum-efficiency DNA intercalating dyes. The results could speed up our future biological studies, reduce significant amount of reagents and samples required, eliminate some intrinsic problems and complexity of previous instrumentation designs, serve as components for future lab-on-a-chip devices, and do many automatic in-situ sizing, sorting and diagnostics. A short summary is listed chronically as follows.

1.1.1 Single-Molecule DNA Sizing

Many assays in biology require measurement of the length distribution of DNA molecules in a heterogeneous solution. This measurement is commonly done with gel electrophoresis — the molecules are separated by mobility, from which the lengths are inferred. However, gel electrophoresis is time-consuming and tens to hundreds of nanograms of samples are generally required. Moreover, its performance degrades significantly for longer DNA molecules.

Even though pulsed-field gel electrophoresis has been invented to partially alleviate this problem[8, 66], the running time can take days.

Instead of relying on mobility, we have developed a single-molecule DNA sizing apparatus[14], in which the length of a DNA fragment is directly inferred from its fluorescence when stained with intercalating dyes. This system is 100 times faster than conventional pulsed-field gel electrophoresis and has a resolution that improves with increasing DNA length. Moreover, it requires a million times less sample than pulsed-field gel electrophoresis and has comparable resolution for large molecules. The device is made of silicone and is extremely easy and cheap to fabricate. An extension of this work, fluorescence-activated cell sorting, has also been demonstrated[15, 25, 60]. Currently, both systems are under commercialization by Mycometrix Corporation.

1.1.2 Monolithic Microvalves and Micropumps

Soft lithography is an alternative to silicon-based micromachining that uses replica molding of nontraditional elastomeric materials to fabricate stamps and microfluidic channels. An extension to the soft lithography paradigm, multilayer soft lithography, was developed, with which devices consisting of multiple layers may be fabricated from soft materials[77]. We used this technique to build active microfluidic systems containing on-off valves, switching valves, and peristaltic pumps entirely out of elastomer. The softness of these materials allows the device area to be reduced by more than two orders of magnitude compared with silicon-based devices. The other advantages of soft lithography, such as rapid prototyping, ease of fabrication, low cost and biocompatibility are all retained.

This new technique greatly enhanced our progress toward *active* lab-on-a-chip devices. Instead of using electroosmosis, electrophoresis and dielectrophoresis, which are problematic due to their intrinsic electrolysis complexity, we can now build complicated multilayer fluidic networks with components of only a few microns to tens of microns in size. There is no worry about the composition of aqueous buffers and samples used. Interesting flow patterns and actuation schemes can also be incorporated to explore greater research subjects and application possibilities.

1.1.3 Multiple Disease Diagnosis on a Single Chip

DNA chips introduced by Affymetrix and many other research groups[61] have demonstrated multiple DNA diagnoses on the same chip. However, due to slow diffusion processes, only DNA molecules close to the right detection spots have a chance to hybridize with their corresponding probes. Therefore, most of the target DNA in the sample is actually lost. PCR is thus typically required to amplify the original sample first, which gives some possible errors and makes it very hard to do multiple disease diagnostics of various distinct infectious diseases.

Based upon the monolithic microvalves and micropumps, an *active* lab-on-a-chip was designed and successfully fabricated. DNA, biotin or avidin could be patterned selectively on the glass substrate. They then intersect with a central reaction fluidic channel loop and form the diagnostic pads. A model system where avidin-coated beads were used as the target objects was constructed. After 4 minutes of rotary pumping, most beads moving in this loop were quickly grabbed onto all the biotinylated diagnostic pads, several orders of magnitude improvement over a passive diffusion scheme. Precise flow control, reagent metering, and fast inline mixing were also demonstrated.

1.2 Organization

In order for readers to easily digest the information and implement these techniques, the contents of this dissertation are categorized according to the subjects of different technologies.

Chapter 2. Microfabricated flow-cell devices.

> Fabrication techniques of soft lithography using a silicone rubber material developed in our lab are discussed. Studies of surface treatments and actuation schemes associated with such a silicone device are described. They are the basis for all the following chapters.

Chapter 3. Microvalves and micropumps.

> The technique of multilayer soft lithography is described. With it, monolithic elastomeric microvalves and micropumps were fabricated and characterized. Different designs of structures and consideration of fabrication processes are given. Its speed

limitation is also fully discussed. This is a fundamental building block to the multiple disease diagnostics devices in Chapter 5.

Chapter 4. Single-molecule DNA sizing.

A successful rapid single-molecule DNA sizing system based on a microfabricated device is shown here. Details of system design and implementation are discussed, such as the selection of the optical components, the detection methods, the fluorescent dyes, and the staining protocols. Performance and resolution of a well-tuned system are given. Two important applications based on this system, DNA mapping by bacteria artificial chromosomes and DNA molecular fingerprinting, are described and results of prototype work, such as protocols, are shown. This chapter also includes some interesting phenomena observed in this system: strong laser polarization dependence and a DNA clamping effect by intercalating dye molecules.

Chapter 5. Multiple disease diagnostics.

A design of an active DNA hybridization lab-on-a-chip device is described. Key components, surface patterning, inline mixing and rotary pumping, are demonstrated. A biotin/avidin model system has also been constructed and significant enhancement of the reaction speed and efficiency is shown.

Part I

Device Microfabrication

Chapter 2   Microfabricated Flow-Cell Devices

Flow Cytometry :

A technique for identifying and sorting cells and their components (as DNA) by staining with a fluorescent dye and detecting the fluorescence usually by laser beam illumination.

— *Merriam-Webster Dictionary*

2.1   Introduction

Flow cytometry was invented many decades ago[67]. It started from counting microscopic cells in a flowing fluidic chamber under a microscope[52] and went on to become a delicate system capable of sorting mammalian and bacterial cells according to their light absorption, scattering, fluorescence, or other characteristics. Recently, single-molecular DNA sizing has also been demonstrated, due to the improvements in optical detection and DNA intercalating dyes[10, 28]. However, such a system is generally costly (US$250,000), mechanically complex and requires trained personnel for operation and maintenance. Inexpensive devices that could rapidly count small particles, determine the sizes of DNA molecules and even sort genetically modified cells would be welcomed by many educational, medical, environmental and industrial institutions. They could greatly enhance genomic studies by fast DNA fingerprinting and mapping, and by facilitating screening of combinatorial chemistry libraries or cell populations during in-vitro molecular evolution. In addition, such devices would have wide applications in clinical medicine, forensic identification, and basic biological and materials research.

In order to achieve small flow diameters for higher illumination uniformity, all modern flow cytometers are designed to have a flow chamber with a nozzle and are based on the principle of hydrodynamic focusing[17]. When the sample-carrying medium exits the nozzle, a central flow stream of tens of microns in diameter is obtained by means of the sheath pulling from the surrounding buffer flowing at a higher speed. If sorting is desired, an

ink-jet head is built in and charged droplets are formed and shoot out when biased under a high voltage. Electrostatic deflection is then used to achieve high sorting rates[26, 74]. However, this mechanism is delicate and many failures of the instrument can result from problems in the flow chamber. For example, clogging of the orifice and particle adsorption and contamination in the tubing can cause turbulent flow in the central jet stream, inducing variation in illumination and detection. Sample carryover can occur during consecutive runs when remnants of previous samples backflush into the new sample stream, and sterilizing the system between runs is time-consuming and results in machine downtime. Furthermore, cells or particles passing the orifice of the ink-jet head may perturb droplet formation: Larger objects can change the droplet size, nonspherical cells tend to align with the long axis parallel to the flow axis, and deformable cells may elongate in the direction of the flow[67]. Such perturbation in droplet formation can introduce variation in the time from the analysis to the actual sorting event. Finally, a number of technical problems make it difficult to generate identically charged droplets, in turn increasing the deflection error.

Replacing the conventional flow chamber with microfabricated devices potentially can allow more sensitive optical detection, easier mechanical setup, and innovative sizing and sorting schemes. Higher sensitivity can be obtained by using a high-NA oil immersion objective lens because there is no need of a surrounding sheath buffer for hydrodynamic focusing or an air gap between the glass capillary and the collection lens. In addition, channels of a few microns in width can be easily fabricated. It allows us to achieve higher illumination uniformity, to use lower excitation laser power, and it also reduces the device complexity. Moreover, instead of high-voltage electrostatic deflection, sorting can be accomplished simply by electrophoresis, electroosmotic flow, differential pressure drive or direct mechanical actuation with embedded microvalves[4, 23, 44, 77]. Compared to conventional flow cytometry systems, all of these are easier, more robust and less sensitive to the size, shape and orientation of the flowing objects. Most important of all, many additional functions can be designed and incorporated into the same device, such as DNA digestion, hybridization, cell lysing, transinfection, and so on. This is mainly due to the convergence of matured micromachining technology (MEMS) and the idea of lab-on-a-chip. Simple microfabricated flow devices can be mass produced and therefore become disposable. It eliminates the possibility of cross-contamination and the necessity of tedious cleaning procedures and system downtime.

Here, I would like to describe the efforts I have made in the attempt to make microfabricated flow-cell devices. Several different material and fabrication methods were developed and successful devices of each type were demonstrated. Important issues, such as surface treatment and actuation mechanisms, are also discussed as follows.

2.2 Design and Fabrication

A microfabricated flow cell consists of at least one input channel and one output channel. If sorting is desired, two or more output channels are necessary. Figure 2.1 shows an example of a microfabricated flow cell with three channels arranged in the shape of the letter T. The central channel is where the sample comes in and the two branches are the output channels for sorting. Detection and analysis of DNA or cells is done at the narrowed part of the input channel near the T-junction. To obtain a good illumination uniformity, the width of the central detection channel is usually 2 μm to 10 μm. Moreover, in order to achieve higher sensitivity by using an high-NA oil-immersion objective lens, the depths of the channels are limited to 4 μm maximum because of the short depth-of-focus of this kind of lens[1]. All of this can be done with various fabrication techniques currently available. Thus, the success of this project relies on a smart choice of the fabrication process, the related surface chemistry treatment, and the actuation mechanism.

2.2.1 Fabrication

In order to substitute the conventional glass capillary in flow cytometry with microfabricated devices, many fabrication methods have been explored and working devices of different types have been demonstrated.

Silicon

Silicon is the most straightforward material to use because extensive studies have been done over the years in the semiconductor field. Silicon wafers patterned with thick photoresist (Shipley SJR 5740) can be etched by a reactive ion etch system (RIE) using a mixture of reactive gases, NF_3 (10 sccm) and CCl_2F_2 (13 sccm). With an RF power of 150 W and

---

[1]Channels of 20 μm to 50 μm in width and depth were also fabricated to facilitate mammalian cells. However, a lower NA objective lens has to be used in this case.
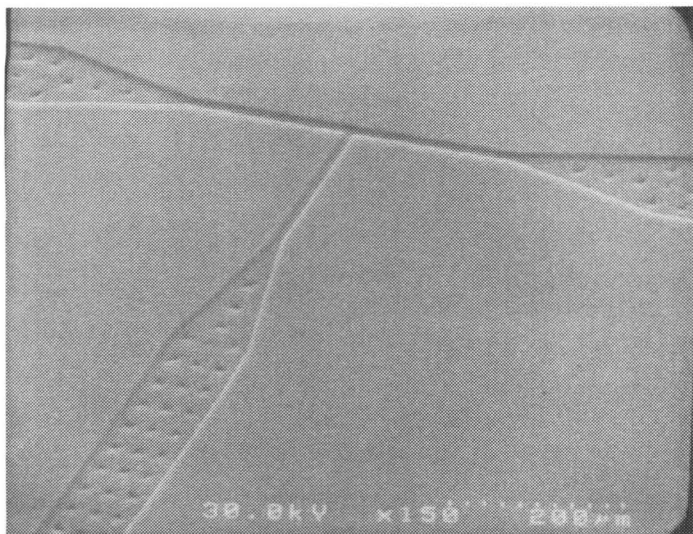
Figure 2.1: An SEM image of a microfabrication flow channel made by RTV soft lithography. Channels at the T-junction are 10 μm wide and 4 μm deep. Input and output channels are 100 μm wide. Square corrugated supports in the wider channels can also be seen.

a chamber pressure of 20 mtorr, an etch rate of 100 nm/min was obtained. Etched for 30 minutes, a T-shaped silicon channel of 3 μm in depth was fabricated. To make channels of further depth and small lateral dimension, stronger masking material, chromium, was used. It was thermally evaporated on and patterned by a photoresist lift-off process[2].

After a flow channel was made by RIE dry etch, the channel was sealed against a sodium-rich glass cover slip, such as Corning #7740 (Pyrex), by anodic bonding[48]. First, masking material photoresist or chromium was removed from the Si substrate. Both the silicon wafer and the glass cover slip were thoroughly washed by RCA cleaning procedure (see B.1). Then, they were pressed together on a hot plate of ~350°C. A 800-volt bias voltage was applied and the bonding process began. It usually takes about 10 minutes to finish sealing of the whole device . Buffer containing DNA or cells could easily flow through the sealed channel simply by capillary action because the silicon and glass surfaces had been rendered highly hydrophilic by the RCA treatment.

Even though the fabrication process of silicon devices are relatively easy, silicon itself is not a transparent material in the visible light region. Since most flow cytometry is done by optical detection at a visible wavelength, search of a transparent substitute is important. Glass, polyimide and RTV silicone have all been studied.

---

[2]Dipping the photoresist-coated wafer in chlorobenzene for a short time during the baking process helps the lift-off process significantly, especially when there are isolated small features, such as those square supports in the channels (Fig. 2.1).
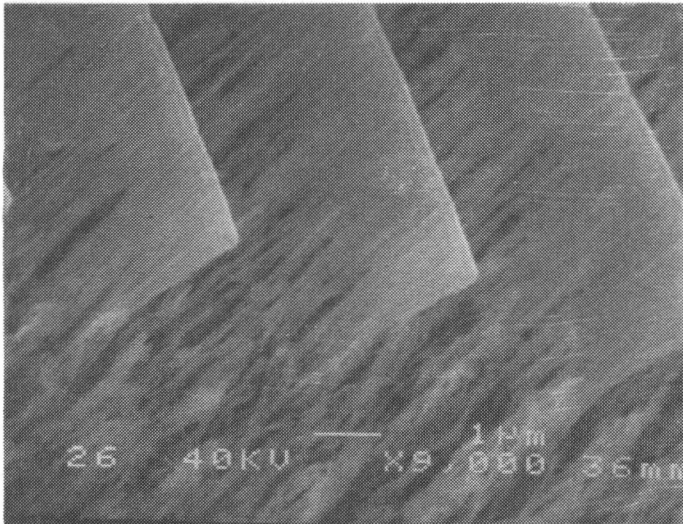
Figure 2.2: Micrograss formed on a glass substrate after C_2F_6 RIE for two hours.

Glass

Glass substrates such as microscope slides or cover slips can be etched either by RIE dry etch or HF chemical wet etch. HF etch is fast but isotropic. It causes severe undercutting and generates rounded corners at the T-junction, where cells or large particles could get stuck easily. Therefore, the wet etch was quickly abandoned after several tries. However, because of the chemical stability of silicon dioxide (glass), the etch rate is generally slow under an RIE system, $\sim$ 20 nm/min: 50 W RF power, 30 mtorr chamber pressure and a mixture of reactive gases, C_2F_6 (20 sccm) and CHF_3 (8 sccm). Moreover, the etch stopped when the depth approached 2 μm because grass-shaped obstacles formed at the bottom as shown on Figure 2.2. It is due to the high-aspect-ratio etching condition and the masking effect of contamination.

A combined dry-wet etch process was created[3]. After 30 minutes of RIE dry etch, the glass sample was dipped into a 10% HF solution for 10 seconds. Such a short time of wet-etch process cleaned out the accumulated micrograss at the bottom, increased the depth of the channel from 0.7 μm to 0.95 μm, and left the side walls almost untouched. With a little bit higher dry-etch power and six rounds of dry-wet etch process described above, a T-channel of 7.6 μm deep was made on a regular cover slip. A SEM image of this T-junction is shown on Figure 2.3. The bottom surface of the glass channel was much smoother. Little

---

[3]First done 4/12/1997 to 4/18/1997.
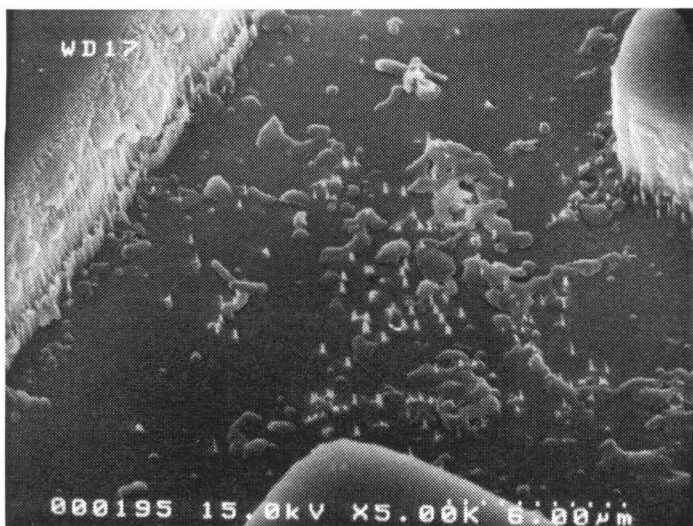
Figure 2.3: T-channel made on a regular glass cover slip by the dry-wet etch process. Channel width: 10 μm. Channel depth: 7.6 μm. Wet-etch process: 10 seconds in 10% HF. Dry-etch process: 35 minutes of RIE, C_2F_6 20 sccm, CHF_3 8 sccm, 100W RF power, and 30 mtorr chamber pressure.

undercut was observed and the corners were still sharp. No cell sticking problem was seen in these kinds of device.

After dry-wet etching, the glass channel was sealed hermetically by a block of RTV silicone (GE RTV615). Because of the softness of RTV, metal pins attached with input- and output-fluid tubing can pierce it and form a complete flow cytometry device. Manual pressure sorting of fluorescent beads was first demonstrated with one of these devices in our lab.

Polyimide

Instead of going through lengthy etching process to make channels in glass, polyimide was chosen and had been used to make flow cells successfully.

Adhesion promoter (2% 3-aminopropylethoxysilane in methanol) was first spun onto a RCA-cleaned glass cover slip, which was first attached onto a supporting microscope slide, using 2% PMMA as the glue (baked for 30 min at 150°C). Polyimide (DuPont PI-2566) was then spun on at 1,000 RPM and the sample was baked at 300°C on a hot plate for 40 minutes. Cured polyimide film of 5.5 μm in thickness was obtained. After patterning with thick photoresist (Shipley SJR 5740), a T-channel of 3.5 μm deep could be formed by oxygen RIE for 20 minutes (flow rate: 20 sccm, chamber pressure: 20 mtorr, RF power: 150 W). The power was chosen to be at the high end so as to increase the temperature, at which the etching selectivity between polyimide and photoresist was increased to 5:4. After
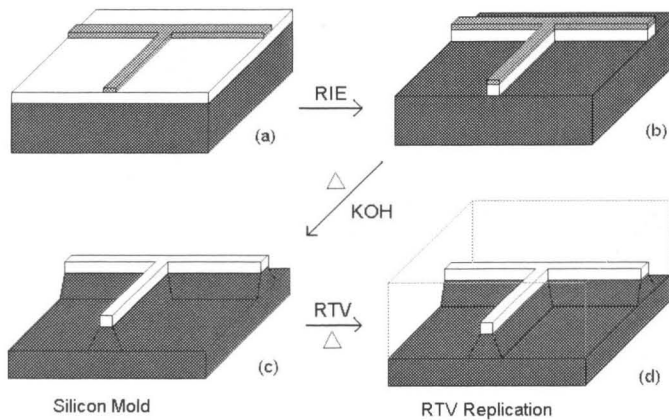
Figure 2.4: Silicone fabrication process. (a)–(c) Fabrication of a silicon master mold using photolithography, RIE oxide etching and silicon anisotropic KOH wet etching. (d) RTV replication process, molding and heat curing.

etching, the cover slip was released from the supporting slide by soaking in acetone, which also cleans out photoresist left on the surface. Then, the channel can be sealed against a RTV block as described in previous glass section.

A polyimide device is much easier to fabricate than a glass one. However, the sealing between polyimide and RTV is slightly weaker. Its yellowish color may also interfere with optical detection by absorbing part of the light and by generating background fluorescence. Further investigation is necessary for any specific applications.

Silicone

Silicone rubber (GE RTV 615) is the final choice in our lab to make microfabricated flow-cell devices. It has many benefits. The fabrication process is simple, as shown in Figure 2.4. Once a master negative mold was made, hundreds of RTV devices could be made simply by a molding and curing process. The material, RTV silicone, has good optical properties, being transparent and yielding very low fluorescent background. It is also extremely cheap, especially compared with single crystal silicon: $\sim\$.05/cm^3$ vs. $\sim\$2.50/cm^3$. After the molding process, it could seal hermetically on a glass cover slip, on a Plexiglass gadget or simply on another RTV block. This binding is reversible. Therefore, the RTV device could be peeled off from the glass substrate, washed clean, put back onto another clean glass cover slip, and then be reused. However, because of the easy fabrication process and the low material cost, the devices can simply be discarded after each use. Hence, the cross-contamination and system downtime problems in the conventional flow cytometers

are eliminated. The softness and elastic property of RTV silicone also makes the devices robust and makes the binding much more insensitive to the dust. RTV simply wraps around any micron-sized particles which would generate big voids in the case of silicon-glass anodic bonding. With careful handling, devices could be made with very high yield without a clean-room facility.

Various materials can be used to fabricate the master channel molds. Two methods were developed and used commonly in our lab: silicon molds made by KOH anisotropic etch[14] and photoresist molds treated by trimethylchlorosilane (TMCS)[77]. The first one is illustrated in Figure 2.4, (a) to (c). A <100> lightly-doped silicon wafer with thermally grown oxide of 200 nm to 300 nm in thickness was first patterned by photolithography. After C_2F_6 RIE as described in the glass section above, the pattern was transferred into the oxide layer[4], which was then used as the mask for the following KOH anisotropic etching: 50 g of solid KOH in 100 ml of deionized water, heated to 50°C, with an etch rate of 0.2 μm/min. Then, a T-shaped intrusive channel with 54.7°-tilted sidewalls (<111> planes) was formed. This mold can be used for the RTV replication process indefinitely as long as it doesn't get broken. Channels of 2 μm to 10 μm in width and 2 μm to 40 μm in depth at the T-junction have been fabricated. An SEM image of one RTV device made with this process is shown in Figure 2.1.

Another easier way to make master molds is to use photoresist itself. Shipley SJR 5740 was patterned on a suitable substrate, usually a silicon wafer. A one-minute HMDS vapor treatment can be applied to enhance the photoresist adhesion for patterns with small channel dimensions. Before each RTV replication process, a one-minute TMCS vapor treatment was applied to protect the photoresist surface from adhesion to the curing RTV silicone. With this protective coating, a photoresist mold can be used many times without showing any significant deterioration. Channels of 4 μm to 15 μm in depth can be fabricated easily with this method. For other depths, different photoresist or multi-layer spin-coated SJR 5740 should be used.

After a master mold was made and proper surface treatment was applied, the RTV replication process began. Ten parts of RTV 615A and one part of RTV 615B were weighed

---

[4]The only trick I found here is a three-minute oxygen RIE (50 W) followed immediately after the C_2F_6 etch. This is intended to remove any carbonfluoride residue C_xF_y left on the surface after C_2F_6 etches through the oxide region and enters the oxygen-poor silicon region. A very thin layer of Teflon-like carbonfluoride deposit is strong enough to block the following KOH anisotropic etch entirely.

Temperature	Time
150°C	15 min
100°C	1 hr
65°C	4 hr
25°C	24 hr

Table 2.1: Curing time of GE RTV 615 at different temperatures. Generally, RTV can stand temperature up to about 400°C. Source: GE technical support.
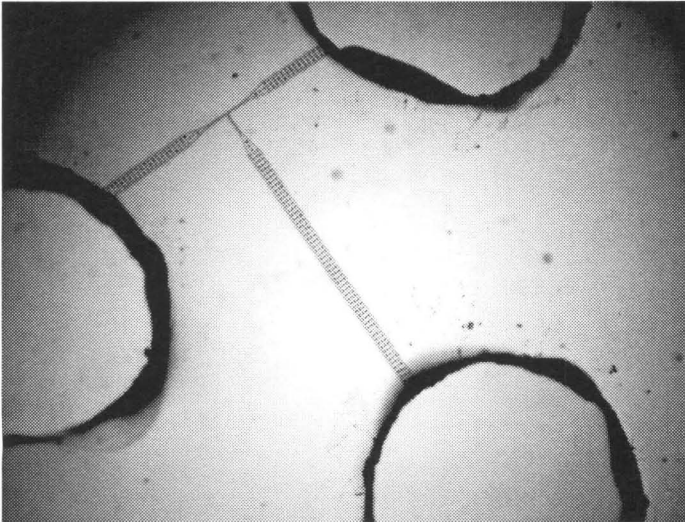
Figure 2.5: An assembled silicone flow-channel device on a glass cover slip with punched sample wells[25].

and mixed thoroughly. Air bubbles introduced during mixing were removed by degassing in an evacuation chamber for 30 minutes. The liquid elastomer was then poured on the mold and cured in an oven of 90°C for two hours. Table 2.1 gives a list of proper curing times at different temperatures. After curing, the RTV device could be peeled off from the mold. Fluid wells or holes were punched with a sharp metal tool or a metal pin. Then it bonded hermetically to a glass cover slip. A complete flow-cell device was made. One example is shown in Figure 2.5.

Since RTV silicone is a soft material, in the early prototypes we found that the RTV at the top of a 100 μm-wide channel actually sagged down and pinched off the fluid pass. Therefore, when designing a fabrication mask, adding supports whenever channels have a width-to-height ratio more than 20 to 1 is strongly recommended (see Figure 2.1 and 2.5).

This novel replication process is part of a new set of fabrication techniques called soft lithography[86], pioneered by Whitesides's group at Harvard University. A recent review in

fabrication of microfluidic systems using this soft silicone material, poly(dimethylsiloxane) (PDMS), can be found in [50]. GE RTV is essentially PDMS. However, some of the methyl groups in RTV 615A are substituted by vinyl groups, $-C=C$, whereas some of the methyl groups in RTV 615B are replaced by hydrogen atoms. After mixing and heating, with the help of a catalyst inside, these two react with each other and then form a cross-linked polymer matrix.

$$-O(CH_3)Si-CH=CH_2 + H-Si(CH_3)O- \xrightarrow{\triangle} -O(CH_3)Si-(CH_2)_2-Si(CH_3)O- \qquad (2.1)$$
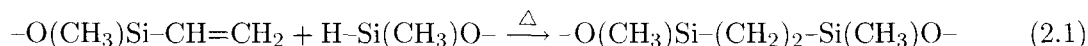
We started by using this material to seal microfabricated glass channels because of its superior natural adhesion property. However, we later discovered that we could use this material to make devices simply by replication against a negative master silicon mold in early 1997. Many interesting applications and technical advances have been made as we will discuss further in the following chapters.

2.2.2 Surface Treatment

When a fluidic channel is just a few microns wide, the *surface* suddenly plays an important role in almost every aspect. In the case of microfabricated flow cells, there are at least two things we have to think about first: hydrophilicity and sample adsorption. The former applies to almost every running condition because aqueous solutions are commonly used. The latter refers to the probability that particles in the sample stick onto the channel walls, which may then change the flow rate, disturb the flow pattern, offset the optical measurement, and even clog up the tiny channel opening. In general, we can unify these problems into a single word: affinity; that is, the affinities between the channel, the flow medium and the sample. We would like to have high affinity between the channel and the medium while maintaining low affinity between the channel and the sample. This is kind of an art, or sometimes called 'black magic,' because it is always hard for us to tell what is exactly happening at the surface when there are just a few important molecular layers. Nevertheless, I would like to give a survey of some successful methods we have developed in our lab to overcome this challenge.

Generally speaking, there are two ways to modify the surface property. One is to apply a special treatment to modify the surface of the flow channel before using it, especially to

achieve enhanced hydrophilicity. The other is to flow certain surfactants together with the sample in the fluidic medium.

Soap is a well-known surfactant used to reduce the surface tension of water, especially between water and nonpolar organic materials. 0.5% neutral Tween-20 is commonly added to our running buffer for DNA sizing[14] and 10^{-5}M of anionic SDS is used in cell sorting project[25]. No significant side effects, such as background fluorescence, were observed. With lowered surface tension, the fluid can flow more smoothly and the sample adhesion problem is significantly reduced, especially in the case of fluorescent beads. For cells, single nucleotides, proteins, and so on, which tend to stick on the walls frequently, BSA (1 mg/ml or less) could also be added to the solution and/or flowed through the channel before running. BSA is known to coat the surface and thus leaves fewer binding sites for the following biological objects to stick on.

When a microfabricated channel is made of silicon or silicon oxide, it usually has high hydrophilicity for an aqueous solution to flow through easily, especially when it is treated with RCA cleaning protocol in advance (see B.1). Yet, the opposite happens when silicone RTV is used because it is designed to be hydrophobic in order to achieve high adhesion affinity to many nonpolar materials. If channel dimensions are bigger than 10 μm, we could push the solution through a silicone channel by applying back pressure at the input or applying vacuum at the output. However, when the channel becomes smaller and smaller, it becomes harder and harder proportionally. With a simple calculation, one can verify that the pressure difference at an interface between liquid and air is

$$\Delta P = \eta \left(\frac{1}{r_1} + \frac{1}{r_2} \right), \tag{2.2}$$

where η is the surface tension of the liquid and r_1 and r_2 are the two principal radii of curvature of the liquid-air interface. At 20°C, η is 0.0728 N/m for water and 0.0223 N/m for ethanol. As discussed before, soap can generally reduce the surface tension of water. However, the improvement is at most a factor of two since η will not be less than that of ethanol according to our experience. As to the radius of curvature, it depends on the width of the channel, w, and the contact angle of the liquid to the wall, θ.

$$r \cos(180° - \theta) \approx \frac{w}{2}. \tag{2.3}$$

When the liquid does not like the channel material, it shows up with a contact angle larger than 90°. In the extreme case when θ is nearly 180°, the radius of curvature would get very close to half of the channel width, $w/2$. For a channel of 5 μm in width and 2 μm in height, the ΔP would get as high as 10^5 Pa, exactly one extra normal atmosphere pressure. The adhesion between silicone and glass usually could not stand such a high back pressure unless a post-heating treatment was applied (85°C for an hour). However, it takes more work to load the sample and it is not a good solution either because the low affinity between water and silicone would aggravate the problem of sample adsorption, i.e, the natural tendency to reduce energy and increase entropy. Therefore, a way to increase the silicone-water affinity so as to lower the contact angle θ close to 90° or even below it became a very important task. There are many methods we have tried. Each has its own benefits and drawbacks as we shall discuss below.

Hydrophilic Polyurethane Coating

Hydrophilic polyurethane (Hydrogel RL#153-87; Tyndale), 0.15%–0.5% w/v solution dissolved in 95:5 ethanol:water, can be used to paint or spin-coat onto a silicone device. It dries at room temperature for about 15 minutes or we can bake the device in an oven of 90° for an hour to enhance the binding of polyurethane to silicone. After this process, the channel is rendered so hydrophilic that aqueous solution can quickly flow through it as loaded. This method gives a very high hydrophilicity and yields the lowest fluorescent background. One drawback is that this treatment is not suitable for long-term running (more than an hour) because the flowing buffer would eventually wash the coating away. The other difficulty is that the surface tension of polyurethane tends to pull itself together and leaves a nonuniform coating, which may block channels of shallow depth (2–3 μm). Spin-coating at high speed and baking dry immediately can somehow alleviate this problem. However, it also reduces the adhesion between RTV silicone to glass because it unavoidably coats the whole surface. This actually happens to all hydrophilic treatments. Usually the higher the hydrophilicity, the worse the binding between RTV to glass substrate. So, a compromise protocol should always be advised.

Oxygen Plasma

Oxygen plasma surface treatment is the most common method used in the field of soft lithography[20]. After a 5-minute reactive treatment (2.8 W) in an oxygen plasma chamber, the surface of a silicone device was oxidized and a thin layer of silicon oxide was formed, which rendered the surface hydrophilic. After this process, the surface becomes reactive; therefore, careful handling and storage is required. However, because of the fragility of the oxide layer, a fine cracking network was generated at the moment when the silicone surface was in contact with a sealing glass cover slip. Along the crack lines, the hydrophobic silicone underneath was exposed. It could then prevent fluid flow in channels of dimension of 5 μm or less. A spin coat of hydrophilic polyurethane at 3,000 RPM immediately after the oxygen plasma treatment could neutralize the reactive surface and keep the fluid flow even when cracks were formed. This method was used for a while until the following HCl treatment was invented.

Hydrochloric Acid Treatment

A hydrochloric acid treatment to directly modify the silicone surface was created while working with Anne Y. Fu[5]. Soaking in dilute HCl (pH 2.7, 0.0074% in water) for 40 minutes at 43°C, the silicone device was chemically modified to be hydrophilic[14]. Buffer containing 0.5% Tween-20 can pass through channels as small as 3 μm by 1.75 μm simply by capillary action without any extra help. Since this is not a coating, treated devices can be used for a long running time. They can even be peeled off from the cover slip, washed by isopropanol (IPA) and acetone, and then reused many times without any signs of losing hydrophilicity. They are also suitable for long-term storage. No degradation has ever been observed.

We suspect that the mechanism behind this is a well-known chemical reaction that can be found in every textbook of organic chemistry. A hydrogen halide molecule can attach to a carbon double-bond as shown:

$$\overset{\backslash}{\underset{/}{C}} = \overset{/}{\underset{\backslash}{C}} + HX \xrightarrow{\triangle} -\overset{|}{\underset{|}{C}}-\overset{|}{\underset{|}{C}}-, \qquad (2.4)$$

$$\underset{H \quad X}{}$$
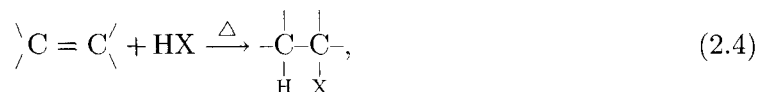
where X represents a halogen atom such as Cl, in this case. As discussed in Section 2.2.1, RTV has a lot of vinyl groups, –C=C. Any of them left after polymerization become sub-

---

[5]On 12/22/1997.

strates for this reaction to happen. Because of high electron affinity, the attached chlorine atoms can form weak hydrogen bonds with water molecules and thus render the surface hydrophilic[6]. The chlorine atoms can be further substituted into hydroxyl groups, –OH, by dipping the device in a heated base solution for 10 to 30 minutes. The hydrophilicity gets even better by observing the contact angle of water droplets on the surface. However, the silicone device now starts to lose its natural adhesion to the glass substrate. Because HCl treatment itself is good enough for even the smallest channel we would like to use, there is no need for any further treatment at this point.

Add-In Surfactants

Another way to make the silicone device hydrophilic is to add surfactants directly into it. One example is MAKON 6 (Stepan Canada, Longford Mills, Canada), an oil-based surfactant. By mixing 0.2% MAKON 6 with the 10:1 RTV, the cured device instantly becomes hydrophilic[7]. The ability to bind to a glass substrate is still retained. This is a faster and easier way to get a hydrophilic silicone device. The only drawback is its optical property. The device is slightly whitish and has much higher fluorescent background than HCl and polyurethane devices. It makes it unsuitable for sensitive DNA sizing experiment. However, for brighter objects, it surely would become a good candidate.

2.2.3 Actuation

In conventional flow cytometry systems, sorting is mostly accomplished by electrostatic deflection of charged droplets formed at the end of the glass capillary. Such a scheme can also be incorporated into microfabricated flow-cell devices. However, with the flexibility of fabrication design, many other simpler schemes can be used. Problems associated with the jet head and high voltage could then be avoided. Three different ways of sorting actuation based upon the T-shaped microfabricated flow cells have been successfully demonstrated in our lab as discussed in the following sections. Unlike electrostatic deflection, the fluid is kept

---

[6]It can also be argued that hydroxyl groups were put on instead of chlorine atoms. It is surely possible and also preferable. It depends on whether hydrogen atoms are a catalyst that attaches water molecules to excited carbon double-bonds or are simply a reactant (remember that $[Cl^-] \gg [OH^-]$). In either case, the hydrophilicity of the RTV is achieved. They are both the intentions for the development of this treatment. The other possibility is due to hydrolysis of some of the Si–O–Si bonds[50]. This could be determined experimentally with PDMS of which polymerization is not based on carbon double-bonds (vinyl groups).

[7]One trick to obtain a good mixing is to mix the MAKON 6 with the one-part RTV 615B first and then mix with the ten-part RTV 615A.

inside the input and output channels and never comes in contact with the air. Therefore, there is no concern about water evaporation and a very small actuation volume can be used.

Pressure-Driven Scheme

With a sealed fluidic system, the direction of objects in the channel can be controlled by adjusting the pressure differences of the input, P_I, and the two output sides, P_{O1} and P_{O2}. When $P_{O1} < P_{O2} < P_I$ and the actual P_{O2} is set to be equal to the pressure at the T-junction, the fluid flow goes to output channel 1; whereas reversing P_{O1} and P_{O2}, the fluid flow goes to output channel 2. Any object inside the channel, such as DNA, beads and cells, would be carried over according to the flow direction. By switching between these two conditions, sorting can be accomplished easily. There are no concerns about which aqueous buffer is being used and what kind of objects are present. Flow speed can also be easily determined by choosing the right pressure combinations.

There are numerous ways to make an enclosed (sealed) flow cytometry system using microfabricated devices. Systems made of glass, Plexiglass and RTV silicone have all been demonstrated in our lab. The easiest method currently is to use the RTV channel itself as the supporting body. Before sealing against a glass cover slip, the RTV T-channel device was punched by a Luer gauge-20 needle to obtain three through-holes — one input and two outputs. Fluid can then be introduced into this device by inserting a pin-tubing assembly: gauge-23 pin attached with a plastic tubing (I.D. 0.020") filled with the desired solution. The pressure difference was determined by adjusting the relative height of the fluid level in each tubing:

$$\Delta P = \rho g \Delta h, \qquad (2.5)$$

where ρ is the density of the fluid. By raising and lowering the tubing attached to the two output sides, respectively, manual sorting of fluorescent beads and DNA molecules was accomplished.

Instead of raising and lowering the tubing mechanically, there is a better way to make fast pressure switching[4]. We can set up three constant air pressures using pressure regulators. Then they would be applied to the end of each tubing with tubing fitting and fixture (such as those from Upchurch Scientific). By maintaining constant fluid levels in the tubing, the

pressure differences would be determined by the difference of the air pressures applied to each tubing. Fast switching between different air pressures can be done with a fast 3-way pneumatic valve, such as Lee LHDA1211111H, which can go up to 300 Hz according to the specification. Rapid switching of fluid flow carrying fluorescent beads with this simple setup has been demonstrated in our lab. A small leakage flow to or from the stopped channel was seen, $\sim 1\%$ of the main flow. This can be alleviated when better pressure regulators were in place.

Speed limitation is the main concern for such a pressure-driven system; that is, how fast can we switch the fluid pressure at the T-junction? It is mainly determined by the latency of the pneumatic valve, the RC time constant of the switching air chamber, and the speed of sound. For a fast 3-way pneumatic valve, such as LHDA1211111H, the on-off time is about 1.6 ms. After that, the valve position is changed and different air pressure is connected to the tiny air chamber at the end of the tubing, which can be considered as a small capacitor in a circuit. The constant air pressure swapped in can be considered as a large capacitor, while the connection between these two through the channel in the pneumatic valve acts like a resistor. Therefore, a RC time constant can be calculated accordingly. Tubing with small diameter should be used for the fluid to maintain the output capacitor small whereas tubing with larger diameter should be used for the input air pressure sources connected to the pneumatic valve. This was verified in our results with the microvalve and micropump project discussed in Chapter 3. Suppose a fluid tubing of inner diameter 0.020" (5.08×10^{-5} m) is used and the length of air portion at the end of the tubing is 6.8 cm. Then the capacitance C is 1.36×10^{-15} m^3/Pa at 27°C when the operating pressure is close to 1 atm. The resistance R from the pneumatic valve, say LHDA1211111H, is 1100 Lohms[43], that is 3.00×10^{10} Pa·s/m^3. Therefore, the time constant τ, $2\pi RC$, is 0.256 ms. Let 3τ be an effective switching time. The time for pressure switching would be about 0.8 ms. Once the air pressure in the fluid tubing is switched, this event would be conducted to the junction by the speed of sound, which is 340 m/s in air and 1,230 m/s in water at room temperature. Supposed the length of air portion of the tubing is 6.8 cm, as used above, and the length of the whole aqueous solution to the T-junction is 12.3 cm. The time needed is 0.3 ms total. A rough estimation of the pressure-switching response time would be 2.7 ms, which is very reasonable according to our experience. A maximum cycling frequency of ~ 180 Hz would be achievable under this actuation configuration.

Electrophoresis and Electroosmotic Flow

Manipulating particles in solution using electric fields is the most commonly used method. According to the underlying mechanisms, it can be divided into three categories: electrophoresis[14, 21, 31, 81], dielectrophoresis[23, 53, 59] and electroosmosis[25, 44, 64, 81]. The first one is to move charged particles in a solution directly by an electric field, such as negatively charged DNA molecules, which would flow toward the positive electrode. This serves as the basis of DNA gel electrophoresis. Dielectrophoresis refers to moving neutral particles by polarizing them with an AC electric field and manipulating them with the field gradient because

$$U = -\boldsymbol{p} \cdot \boldsymbol{E}, \qquad (2.6)$$

where U is the energy, $\boldsymbol{p}$ is the polarization, and $\boldsymbol{E}$ is the electric field. Laser tweezers can be considered as a special application of this mechanism. Electroosmosis refers to carrying particles (slightly charged or neutral) with the ionic flow inside the buffer solution. It is hard to differentiate electrophoretic and electroosmotic flows because they both happen at the same time. Usually strongly charged particles are dominated by electrophoresis and lightly charged or neutral particles are dominated by electroosmosis. Of course, it also depends on the ionic strength, i.e, the ion concentration, of the buffer used.

Sorting of DNA molecules using electrophoresis[14] and fluorescent beads and *E. coli* cells using electroosmotic flow[15, 25] have been demonstrated in our lab with microfabricated flow-cell devices by inserting electrodes in the three sample wells as shown in Figure 2.5. Detailed discussion of the whole system will be given in Chapter 4.

These methods are easy and very powerful. Many biotechnology companies, such as Caliper Technology, Aclara Biosciences, and Nanogen, are working on building lab-on-a-chip devices using components based upon these mechanisms. The main drawback of these methods is 'electrolysis.' In order to obtain higher sorting rate, we have to increase the electric field and thus the voltages, which then starts to electrolyze the buffer, form air bubbles, and electroplate reduced metal ions onto the electrodes. Eventually it causes severe deterioration of the ionic conditions in the solution. Therefore, it becomes an unavoidable task for every specific sample object to play with the composition and ionic strength of the buffer, to find out the right voltage range, to keep refreshing buffer or design big buffer wells,

and to ensure there is no interference with the properties we are interested in for sorting and also the viability of biological samples. Precise control of flow requires calibration for each new buffer or solute and can be difficult when the exact composition of a sample is not known in advance. Electroporation occurring at a high electric field (a few kilovolts per centimeter) can lead to the death of cells. It sets the upper limit of the applied voltage, which in turn limits the flow rate of many biological samples. The condition becomes even more stringent for bigger neutral objects, such as mammalian cells.

Direct Mechanical Actuation

The most straightforward method for sorting actuation is to build micromechanical on-off actuators, i.e, microvalves, near the junction. Opening a selected valve will direct the flow and the objects into the desired output channel. This is obviously independent of the buffer used as long as it is compatible with the building material and thus suitable for a long-term run of cell sorting.

In the field of microelectromechanical systems (MEMS), many microfabricated valves have been demonstrated[69]. However, one that is fast and also compatible with such a small actuation volume (subnanoliter) has not been demonstrated until recently [77] (see Chapter 3). A complete on-off cycling speed of 75 Hz has been demonstrated with this new system powered by external pneumatic valves. An actuation volume as small as ~ 1 pl (20 μm by 20 μm by $\sim$3 μm) has also been made and shown working on-off switching behavior[24]. Moreover, these microvalves are robust. After more than four million on-off cycles, no signs of fatigue or rupture have ever been observed. A working flow-cell device based upon this newly developed technique is currently under development in our lab (Fig. 2.6).

2.3   Conclusion

We have demonstrated successful microfabricated flow-cell devices to replace conventional glass capillaries. Silicone rubber (GE RTV 615) is the final choice of the building material because of its easy fabrication process, low cost, excellent optical properties, and natural adhesion to numerous materials, especially glass cover slips. High-NA oil-immersion objective lenses can then be used to obtain higher sensitivity. The problem of hydrophobicity
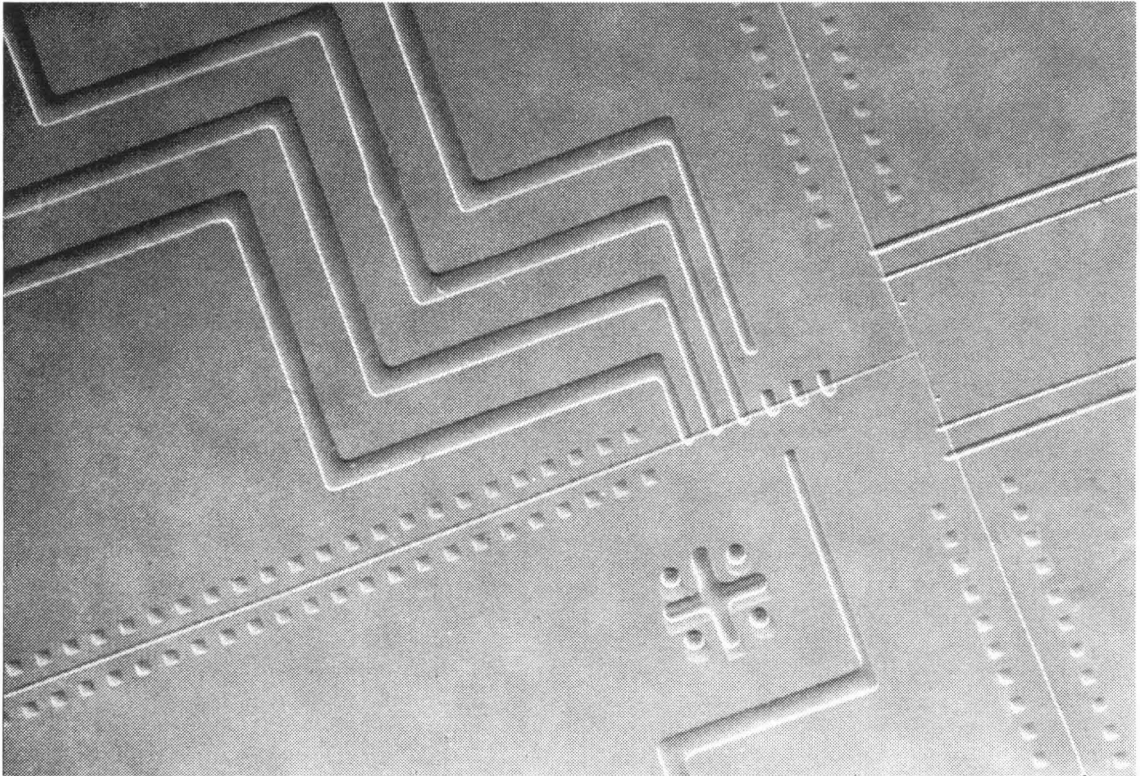
Figure 2.6: A preliminary version of sorting devices based on microvalves. A peristaltic micropump can be seen on the input channel and sets of switching microvalves are present at the two output branches. [24].

property of RTV silicone can be alleviated using hydrophilic polyurethane coating, oxygen plasma or HCl treatment. With the flexibility of microfabrication, extra functions can be designed and incorporated into the same device, such as inline digestion, cell lysis, and in-vitro trans-infection. Because of the softness of the silicone material, miniature microvalves can be built into it to directly control the flow direction. Wells or through-holes can also be punched easily to facilitate electrophoretic or electroosmotic sorting or to use a pressure-driven scheme, respectively. Since the devices are so cheap, they are therefore disposable. There is no worry about sample cross-contamination and system downtime for flow-cell cleaning can be eliminated. The basic device design and sorting scheme are also simple. Many complexities associated with hydrodynamic focusing and electrostatic deflection are no longer of concern. In principle, there is no need to have a well-trained technician to operate a system based upon this microfabricated flow-cell device.

Chapter 3   Monolithic Elastomeric Microvalves and Micropumps

3.1   Introduction

The application of micromachining technology is growing rapidly, driven by the dramatic success of a few key applications such as microfabricated accelerometers[62, 88], pressure sensors[75], and ink-jet print heads[41]. New applications are appearing in other fields, in particular fiber-optic communications[45, 54], displays[33], and microfluidics[31, 36, 69]. The two most widespread methods for the production of microelectromechanical systems (MEMS) are bulk micromachining and surface micromachining. Bulk micromachining is a subtractive fabrication method, whereby single-crystal silicon is lithographically patterned and then etched to form three-dimensional structures. Surface micromachining, in contrast, is an additive method where layers of semiconductor-type materials (polysilicon, metals, silicon oxide, silicon nitride and so forth) are sequentially added and patterned to make 3-D structures.

Bulk and surface micromachining methods are limited by the materials used. The semiconductor-type materials typically used in bulk and surface micromachining are stiff materials with Young's modulus ~100 GPa (see Table 3.1). Because the forces generated by micromachined actuators are limited, the stiffness of the materials limits the minimum size of many devices. Furthermore, because multiple layers must be built up to make active devices, adhesion between layers is a problem of great practical concern. For bulk

Material	Young's Modulus	
PDMS [47]	~ 750	kPa
Silicon	107	GPa
SiO_2	71.7	GPa
Si_3N_4 [5]	100–200	GPa

Table 3.1: Comparison of Young's moduli of PDMS (RTV) and other common MEMS materials.

micromachining, wafer-bonding techniques must be used to create multilayer structures. For surface micromachining, thermal stress between layers limits the total device thickness to about 20 μm. Clean-room fabrication and careful control of process conditions are required to realize acceptable device yields.

An alternative microfabrication technique based on replication molding is gaining popularity. Typically, an elastomer is patterned by curing on a micromachined mold. Loosely termed soft lithography, this technique has been used to make blazed grating optics[85], stamps for chemical patternining[86], and microfluidic devices[19, 21, 34, 50] (also the flow-cell devices[14] described in Chapter 2). Soft lithography's advantages include the capacity for rapid prototyping, easy fabrication without expensive capital equipment, and forgiving process parameters. For applications with moderate-sized features (≥ 20 μm) such as microfluidics, molds can be patterned by using a high-resolution transparency film as a contact mask for a thick photoresist layer. A single researcher can design, print, pattern the mold, and create a new set of cast-elastomer devices within one day, and subsequent elastomer casts can be made in just a few hours. The tolerant process parameters for elastomer casting allow devices to be produced in ambient laboratory conditions instead of a clean room. However, soft lithography also has limitations: It is fundamentally a subtractive method (in the sense that the mold defines where elastomer is removed), and with only one elastomer layer it is difficult to create active device or moving parts. A method for bonding elastomer components by plasma oxidation has been described previously[20] and has been used to seal microfluidic channels against flat elastomer substrates[50].

Postdoc Marc A. Unger in our lab and I developed a technique called 'multilayer soft lithography,' which combines soft lithography with the capability to bond multiple patterned layers of elastomer together by varying the relative composition of a two-component silicone rubber between them[77]. The ease of producing multilayers makes it possible to have multiple layers of fluidics, a difficult task with conventional micromachining. We created test structures of up to seven patterned layers in this fashion, each of ~ 40 μm in thickness (Fig. 3.4F). Because the devices are monolithic (i.e, all of the layers are composed of the same material), interlayer adhesion failures and thermal stress problems are completely avoided. Particulates disturb interlayer bonding very little, if at all. Perhaps most importantly for the actuation of microstructures, the elastomer is a soft material with Young's modulus ~ 750 kPa (see Table 3.1), allowing large deflections with small actuation

forces. Therefore, it makes this technique a good candidate for fabrication of passive-sensing and active microelectromechanical systems in general.

With the power of multilayer soft lithography and also to serve as an intuitive actuation mechanism for the flow-cell devices described in Chapter 2, we fabricated active microvalves and micropumps entirely out of this elastomeric material[77]. Like other mechanical microfluidic devices, these monolithic elastomeric devices avoid several practical problems affecting flow systems based on electroosmotic flow, electrophoresis or dielectrophoresis, as we discussed previously on page 23. Electrolytic bubble formation, although not a problem for laboratory devices, seriously restricts the use of electroosmotic flow in integrated microfluidic devices. Besides, neither electroosmotic, electrophoretic, nor dielectrophoretic flow can easily be used to stop flow or balance pressure difference. Rotary flow patterns obtained with such a mechanically pumped device[16] cannot be achieved by these electrically pumped methods either, because of the existence of two electric polarities.

Moreover, the softness of the silicone material allows the device areas to be reduced by more than two orders of magnitude compared with silicon-based devices[69]. Microvalves with dead volumes as small as one picoliter were demonstrated[24]. It is even smaller than the unit volume of tens of picoliters achieved by a state-of-the-art bubble-jet print head. Maximum on-off cycling frequency of 75 Hz to 100 Hz has also been demonstrated[77]. Linear response of these microvalves to the applied air pressure also makes them suitable for metering fluid flow precisely, which is important for many biological and chemical lab-on-a-chip devices. The other advantages of soft lithography, such as rapid prototyping, ease of fabrication and biocompatibility, are all retained.

In the following sections, I would like to describe the principle and protocols behind multilayer soft lithography, give characterization data about monolithic elastomeric valves and pumps with various dimensions and control setting, and discuss the huge set of possible applications in the future.

3.2 Multilayer Soft Lithography

The idea behind multilayer soft lithography is actually very simple (Figure 3.1). Two bonding layers are separately cast against microfabricated molds (see Silicone Fabrication on page 13). The elastomer used is a two-component addition-cure silicone rubber (GE RTV
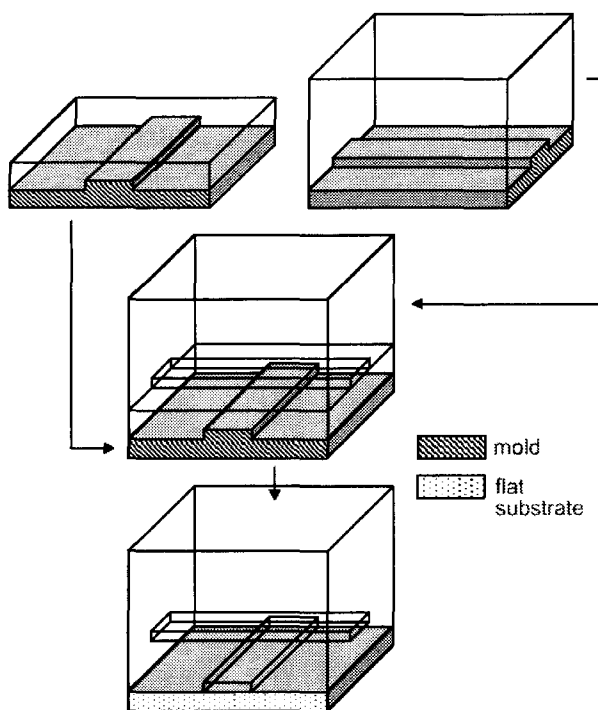
Figure 3.1: Process flow of multi-layer soft lithography[77].

615). The bottom layer has an excess of one of the components, (A), whereas the upper layer has an excess of the other, (B). After separate curing of the layers, the upper layer is removed from its mold and placed on top of the lower layer, where it forms a hermetic seal. Because each layer has an excess of one of the two components, reactive molecules remain at the interface between the layers. Further curing causes the two layers to irreversibly bond. The strength of the interface equals the strength of the bulk elastomer. This process creates a monolithic three-dimensional structure composed entirely of elastomer. Additional layers are added by simply repeating the process: Each time the device is sealed on a layer of opposite 'polarity' (A versus B) and cured, another layer is added.

Typically, to make a cured silicone device, a 10-to-1 mixing ratio between RTV 615A and 615B is recommended by the manufacturer, General Electric. RTV 615A contains a polydimethylsiloxane bearing vinyl groups and a platinum catalyst, whereas RTV 615B contains a cross-linker with silicon hydride (Si–H) groups, which form covalent bonds with vinyl groups while heat curing (Eq. 2.1). However, in the case of multilayer soft lithography, unbalanced mixing ratios between two bonding layers are used, for example, 30 A : 1 B versus 3 A : 1 B. The bottom layer is spin-coated onto the mold in order to precisely control

the thickness, while the top layer is simply poured onto the mold for easier handling in the later process (shown on the top of Figure 3.1). Spin-coating of 30 A: 1 B RTV at 2,000 RPM yields a layer of ~ 40 μm in thickness. After spin-coating or pouring, each layer was baked in an oven of 80°C for 20 minutes to 1.5 hours. Afterwards, the RTV from the top mold is peeled off and fluid or air accessing through-holes are punched along the channels. It is then aligned and placed on top of the bottom RTV layer. A second baking of 80°C for 1.5 hours would chemically bond these two layers irreversibly. The whole assembly is thus ready to be peeled off from the bottom mold. Through-holes to access the bottom channels are punched and it is then sealed against a glass cover slip, a Plexiglass gadget or another thin layer of RTV. After attaching tubing with metal pins at the end for air control lines or fluid flow, a complete active elastomeric device is formed. A multilayer device could also be made easily by keeping all intermediate baking time short (20–30 min). Each mold is spin-coated with alternative RTV polarity. The assembly starts from the top and goes downward layer by layer. A long 1.5-hour curing is applied at the end to get a final 3-D microfluidic device.

Generally speaking, a 10:1 mixing ratio yields the stiffest RTV. The relation of stiffness between three different common ratios is as follows:

$$10:1 > 3:1 > 30:1. \tag{3.1}$$

30:1 RTV is so soft that it is hard to handle when it is used for the RTV block on the topmost mold. There is a good way to solve this kind of problem: Spin-coat the RTV of desired polarity on the topmost mold, bake for 20 minutes, pour 10:1 RTV on top, and bake for another 20 to 30 minutes. Devices made in this fashion are much easier for the bonding process and have the best mechanical stability to hold the tubing-attached metal pins straight. This modification is used commonly in most active lab-on-a-chip devices in our lab, which I will talk about briefly later.

One can also control the physical properties of the building material[77]. We created magnetic layers of elastomer by adding fine iron powders (~ 1 μm in diameter), up to 20% by weight. Electrically conducting layers were also demonstrated by doping with carbon black (Vulcan XC72; Cabot, Billerica, MA) above the percolation threshold, i.e, 10% or higher by weight. Conductivity increased with carbon black concentration from

Figure 3.2: Schematic of valve closing for square and rounded channels[77]. The dotted lines indicate the contour of the top of the channel for rectangular (left) and rounded (right) channels as pressure is increased.

5.6×10^{-16} to $\sim 5 \times 10^{-3}$ $(\Omega \cdot cm)^{-1}$. For both conductive and magnetic silicones, multilayer bonding functioned normally. Therefore, there is the possibility of creating all-elastomer electromagnetic devices.

3.3   Monolithic Elastomeric Microvalves

Monolithic elastomeric microvalves are fabricated using a crossed-channel architecture as shown in Figure 3.1. Typical channels are 100 μm wide and 10 μm high, making the active area of the valve 100 μm by 100 μm. The membrane of polymer between the channels is engineered to be relatively thin (typically 30 μm). When pressure is applied to the upper channel ("control channel"), the membrane deflects downward. Sufficient pressure closes the lower channel ("flow channel"). For optical convenience, we typically seal our structures with glass as the bottom layer; this bond with glass is reversible, so devices may be peeled up, washed, and reused. We also fabricated devices where the bottom layer is another layer of elastomer, which is useful when higher fluid back-pressures are used. The response time of devices actuated in this fashion is on the order of 1 ms, and the applied pressures are on the order of 100 kPa, so a 100 μm by 100 μm area gives actuation forces on the order of 1 mN. Pneumatic actuation allows active devices to be densely packed; we built microfluidics with densities of 30 active components per square millimeter, and greater densities are also achievable. The actuation speed, pressure, and device density are more than adequate for the vast majority of microfluidic applications.

The shape of the flow channel is important for proper actuation of the valve (Figure 3.2). Rectangular and even trapezoidal-shaped channels will not close completely under pressure from above. Flow channels with a round cross-section close completely; the round shape transfers force from above to the channel edges and causes the channel to close from the

edges to the center. This can be observed under an optical microscope, in which the sealed edges appear as distinct lines. Incomplete sealing as with a rectangular channel shows as an "island" of contact at the center of the flow channel; complete sealing (as observed with rounded channels) gives continuous contact from the left and the right edges toward the center in the flow channel. We found that 100 μm by 100 μm by 10 μm valves over trapezoidal channels made from KOH-etched silicon molds would not close completely even at 200 kPa of applied pressure, whereas rounded channels sealed completely at only 40 kPa.

Therefore, making rounded fluid channel molds becomes a critical issue. This is the opposite direction of most fabrication techniques where high-aspect-ratio structures are favored. However, this rounded shape could be obtained by hard baking a photoresist channel mold above its glass transition temperature, at which the photoresist reflows and becomes perfectly rounded due to the pulling of its surface tension. Usually, photoresist, Shipley SJR 5740, was used, which has a glass transition temperature of $\sim$ 120°C. After channels are formed by photolithography, the mold was baked on a hot plate of 150–200°C for 30 minutes. Photoresist then reflows, shrinks a little bit, and yields rounded channels with slightly higher at the center. A one-minute TMCS vapor treatment is applied before each replication process to prevent adhesion of cured silicone to the photoresist. Molds can be used many times without any significant deterioration in the channel shapes.

Making multiple independently-actuated valves in one device simply requires independent control of the pressure applied to each control line. It is done by connecting each control line to the common port of an external miniature three-way pneumatic valve (LHDA1211111H; The Lee Company, Westbrook, CT), powered by a fast Zener-diode circuit as drawn in Figure 3.3 and controlled by a digital data acquisition card (AT-DIO-32HS; National Instruments, Austin, TX). Regulated external pressure (R-800-30; AirTrol) was provided to the normally closed port, allowing the control channel to be pressurized or vented to atmosphere by switching the state of the miniature three-way valve. In order to speed up the opening time of a microvalve, a vacuum could be applied to the normally open port instead of the normal atmosphere. Therefore, the valve membrane was buckled up into the air control channel at rest position. The swing of the valve membrane between open and closed states were thus nearly doubled if the applied pressure was also 1 atm. Figure 3.4, A to E, shows simple configurations resulting in on-off valves (Fig. 3.4, A and B), a pump (Fig. 3.4C), a grid of valves (Fig. 3.4D), and a switching valve (Fig. 3.4E). Each
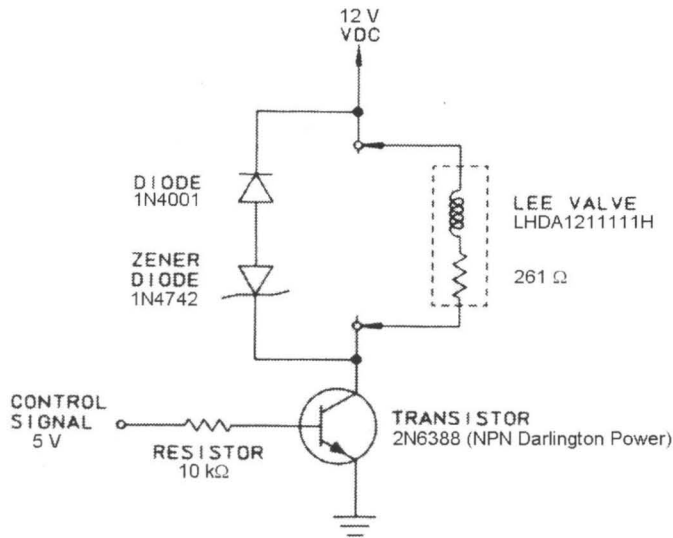
Figure 3.3: Fast Zener-diode driving circuit for an external pneumatic valve. The diode bleeding line is important to prevent high voltage building up at the collector side of the transistor when the valve is switching off. At the same time, the Zener diode is chosen to have a breakdown voltage the same as the supply voltage so as to maintain a negative bias across the pneumatic valve to quickly shut down the current. Therefore, the on and off times become the same: ~ 1.6 ms for LHDA1211111H.
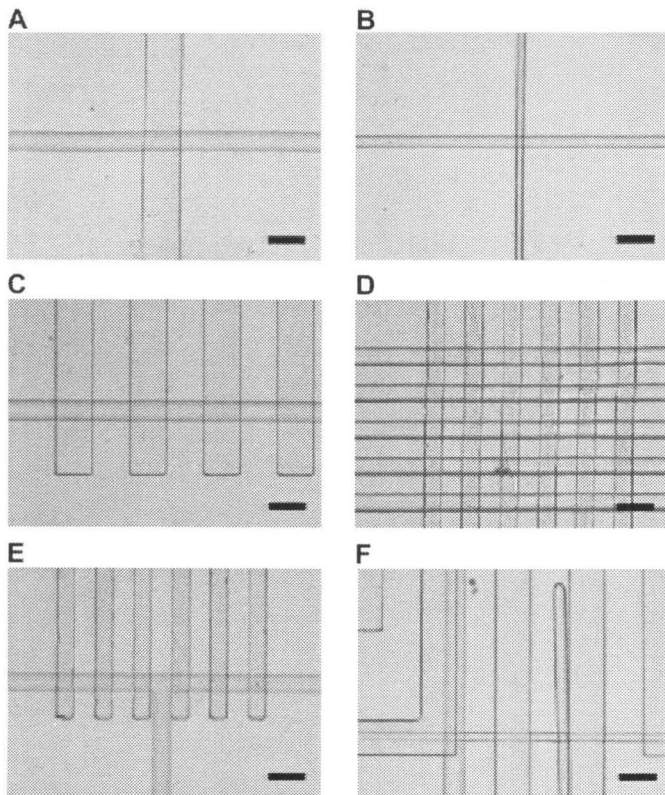
Figure 3.4: Optical micrographs of different valve and pump configurations where control lines are oriented vertically[77]. (A) Simple on-off valve with 200-μm control line and 100-μm flow line ("200×100"). (B) 30×50 on-off valve. (C) Peristaltic pump. Only three of the four control lines shown were used for actuation. (D) Grid of on-off valves. (E) Switching valve. Typically, only the innermost two control lines were used for actuation. (F) Section of the seven-layer test structure mentioned in the text. All scale bars are 200 μm.

control line can actuate multiple valves simultaneously. Because the width of the control lines can be varied and membrane deflection depends strongly on the membrane dimensions, it is possible to have a control line passing over multiple flow channels and actuate only the desired ones. This could eliminate complicated or even multi-layered channel designs when many valves are required in the same chip. In addition, the active element is the roof of the channel itself, so simple on-off valves (and pumps) produced by this technique have truly zero dead volume; switching valves have a dead volume about equal to the active volume of one valve, that is, 100 μm by 100 μm by 10 μm = 100 pl[1]. The dead volume required and the area consumed by the moving membrane are each about two orders of magnitude smaller than any microvalve demonstrated to date[69].

In order to characterize the performance of an elastomeric microvalve with sufficient precision and bandwidth, an epi-fluorescent imaging system was used. The flow channel was filled with a solution of fluorescein isothiocyanate (FITC) in buffer (pH $\geq$ 8) with 0.2% surfactant Tween-20, and the fluorescence of a square area occupying the center half of the channel was monitored through a slit by a photomultiplier tube with 10 kHz bandwidth. Through nearly identical pneumatic connections, the pressure was monitored simultaneously by a Whetstone-bridge pressure sensor (SCC15GD2; SenSym, Milipitas, CA) with an instrumentation amplifier (AD524; Analog Devices, Norwood, MA) circuit. The relation of valve opening versus the applied pressure was thus obtained as shown in Figure 3.5. The response of the valve is almost perfectly linear over a large portion of its range of travel, with minimal hysteresis. Thus, these valves can be used for precise microfluidic metering and flow control. The linearity of the valve response demonstrates that the individual valves are well-modeled as Hooke's law springs. Furthermore, high pressures in the flow channel ("back pressure") can be countered simply by increasing the actuation pressure. Within the experimental range we were able to test (up to 70-kPa back pressure), valve closing was achieved by adding 1.36 times the back pressure to the minimum closing pressure at zero back pressure, as shown in Figure 3.6. The reason that there exists a factor of 1.36 instead of straight 1.0 is more likely due to the deformation of the RTV channels under such a high back pressure.

Monolithic elastomeric valves fabricated as described here can be actuated with surpris-

---

[1]The smallest monolithic microvalve made in our lab is 20 μm by 20 μm by 3 μm = 1.2 pl, which has a elastomeric membrane of 7 μm thick (20:1 RTV)[24].
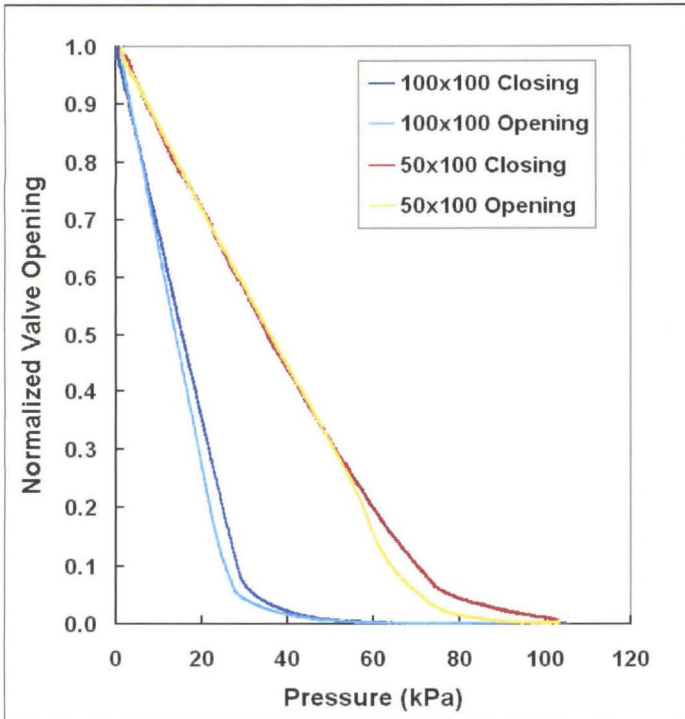
Figure 3.5: Valve opening versus applied pressure. '50×100' indicates a microvalve with 50-μm-wide control channel and a 100-μm-wide fluid channel. 100×50 closing and opening data (not shown) are nearly identical to 50×100 data.
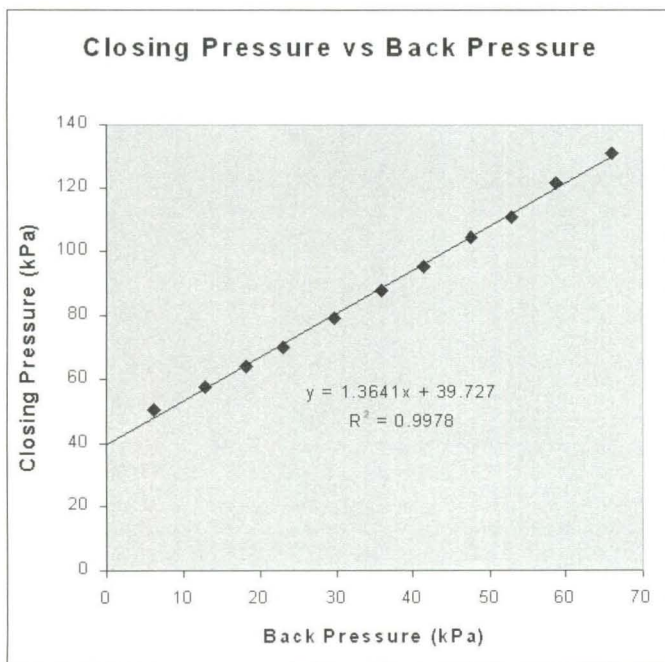

Figure 3.6: Valve fully closing pressures versus various fluid back pressures.

ing speed. The time response for a valve filled with aqueous solution is on the order of 1 ms, as shown in Figure 3.7. The valve runs comfortably at 75 Hz and still opens and closes at 100 Hz although it does not open completely. The valve responds nearly instantaneously to the applied pressure, but applied pressure lags substantially behind the control signal. If one used another actuation method that did not suffer from opening and closing lag, the valve would run at $\sim$ 375 Hz. The spring constant can be adjusted by changing the membrane thickness; this allows optimization for either fast opening or fast closing.

The closing and opening response times of an elastomeric microvalve are affected by many parameters, such as the driving frequency, the switching time of the external pneumatic valve, the length and diameter of the control-line air tubing, the shape and dimension of the valve itself and the viscosity of the flowing fluid. As shown in Figure 3.7, when the control signal turned on, the air pressure started ramping up after a certain delay, $\sim$ 1.6 ms. The delay is mainly due to the actuation time of the external pneumatic valve because sufficient coil current, i.e, energy stored in the magnetic field, has to build up first in order to actuate the internal piston. As the pressure went up, the valve closed correspondingly. The opening session is very similar. However, if a vacuum is not applied, the valve membrane has to bounce back by its own elastic force. Therefore, it tends to have a longer delay because air molecules accumulate inside the control line and its air tubing has to be released so as to lower the air pressure below the minimum closing pressure of the microvalve, $\sim$ 40 kPa for a typical 100 μm by 100 μm by 10 μm valve. A list of dominant parameters and how much they affect the response time is shown on Table 3.2, in which the fluorescence data were fitted by four time parameters: valve closing delay t_{close}, valve closing time constant τ_{close}, valve opening delay t_{open}, and valve opening time constant τ_{open}.

According to Figure 3.7 and Table 3.2, it is obvious that the speed limitation of current RTV microvalves comes mainly from the external pneumatic valve, especially the opening and closing delays. During our experiments, it was also found that that the lengths and diameters of the air tubing used are very important. Narrow and short tubing is preferred at the common port (control-line) whereas wide tubing is preferred at the air supply and air releasing ports. As shown in Table 3.2, response times increased significantly when the control-line tubing was extended to 93 cm. Such a phenomenon could be explained using an RC-circuit argument discussed previously on page 22. The calculations match well with the extra delays observed. In most of our experiments, a 10-cm-long control-line tubing was
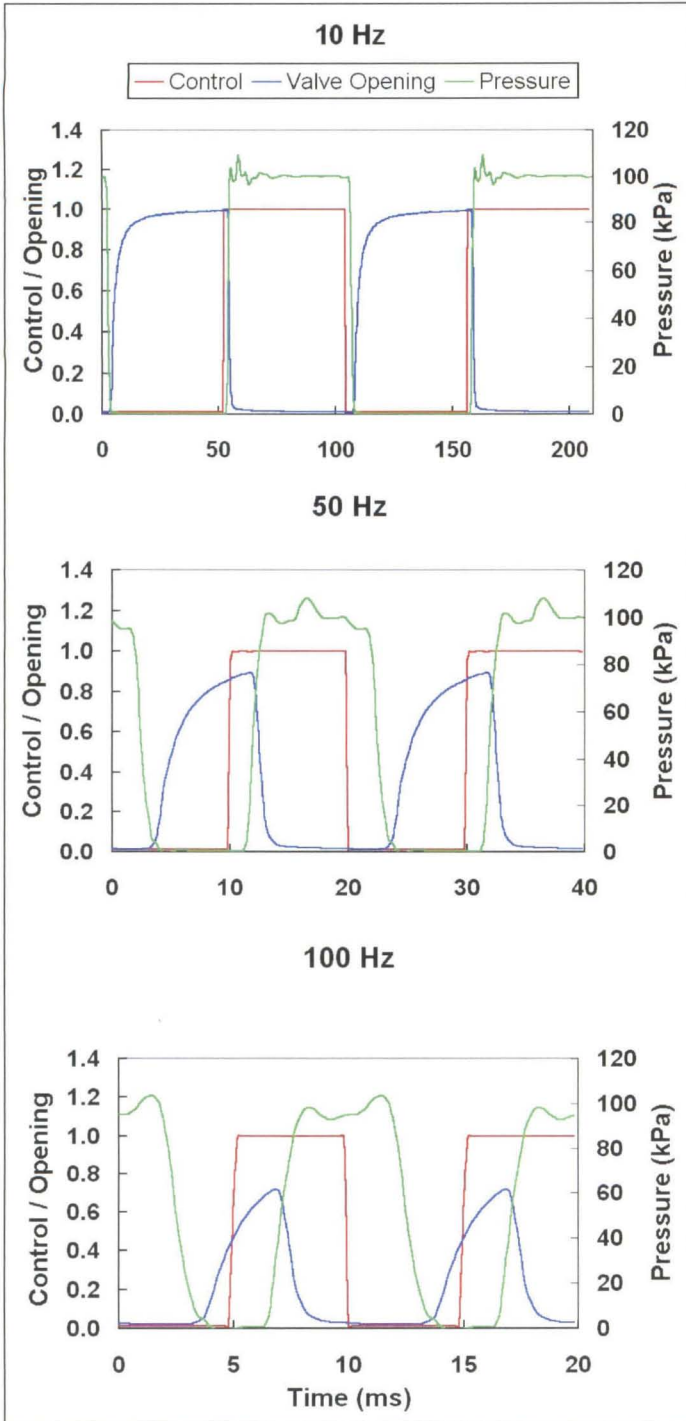
Figure 3.7: Time response of a 100 μm by 100 μm by 10 μm RTV microvalve with a 10-cm-long control-line air tubing connected from the chip to an external pneumatic valve. Two periods of digital control signal, actual air pressure at the end of the tubing, and valve opening are shown here. The pressure applied on the control line is 100 kPa, which is substantially higher than the $\sim$ 40 kPa required to close the valve. Thus, when closing, the valve is pushed closed with a pressure 60 kPa greater than required. When opening, however, the valve is driven back to its rest position only by its own spring force ($\leq$ 40 kPa). Thus, τ_{close} is expected to be smaller than τ_{open}. There is also a lag between the control signal and control pressure response, due to the limitations of the miniature pneumatic valve used to control the pressure. Calling such a lags t and the $1/e$ time constants τ, the values are $t_{\text{open}} = 3.63$ ms, $\tau_{\text{open}} = 1.88$ ms, $t_{\text{close}} = 2.15$ ms, and $\tau_{\text{close}} = 0.51$ ms. If 3τ each are allowed for opening and closing, the valve runs comfortably at 75 Hz when filled with aqueous solution.

	t_{close}	τ_{close}	t_{open}	τ_{open}
Std. Conf.	**2.15**	**0.51**	**3.63**	**1.88**
10 Hz	-0.06	-0.04	-0.07	**+0.63**
100 Hz	**-0.29**	+0.07	+0.09	**-0.22**
50kPa/air, 10 Hz	**+0.25**	**+0.44**	**-1.05**	**+0.83**
50kPa/air, 100 Hz	**+0.15**	**+0.49**	**-1.01**	**-0.13**
100kPa/vacuum, 100Hz	**+0.53**	+0.06	**+0.48**	**-0.51**
93-cm tubing, 10 Hz	**+2.00**	**+7.80**	**+15.54**	**+9.39**
50×100×10 valve	-0.02	**+0.15**	**-0.97**	**-0.28**
100×50×10 valve	**+0.42**	+0.10	**-0.52**	**-0.29**
3× viscosity	-0.07	**+0.16**	**+0.24**	+0.06
10× viscosity	-0.07	**+0.26**	**+0.75**	+0.07
air pressure, 10-cm tubing	**1.61**	**0.48**	**2.01**	**0.58**
air pressure, 0-cm tubing	**1.09**	**0.55**	**1.69**	**0.50**

Table 3.2: Response times (in milliseconds) of RTV microvalves under different conditions. Standard configuration (std. conf.): a 100 μm by 100 μm by 10 μm valve with 30 μm-thick 30:1 RTV valve membrane; cycling frequency: 50Hz; actuation pressures: 100 kPa and normal atmosphere; tubing between the device chip and the common port of the external pneumatic valve: 10-cm long with inner diameter (I.D.) 0.020"; fluid: FITC in aqueous buffer. The bottom two rows show the response times of actuation air pressure measured by a pressure sensor at the end of the same tubing.
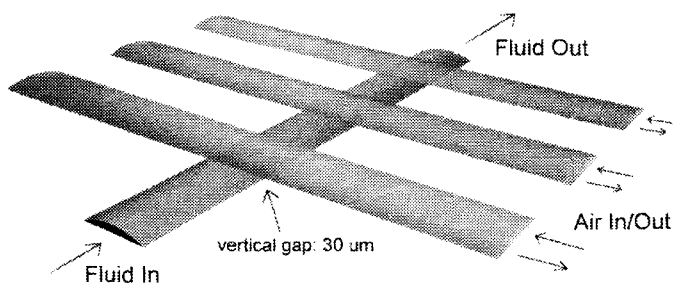
Figure 3.8: A 3-D scale diagram of an elastomeric peristaltic pump. The channels are 100 μm wide and 10 μm high.

used. The response times of actuation air pressure are drawn on Figure 3.7 and listed at the bottom of Table 3.2 for reference.

The other main reason that slows down the valve operation is the weak elastic force of RTV required to bounce back the valve membrane during the opening session. The air pressure has to be lowered to a certain point before the membrane can start moving; therefore, the opening delay was about 1 ms longer than the closing delay. This effect can be alleviated by using a lower actuation pressure, one that is just above the minimum fully-closing pressure. For example, at 50 kPa, the opening delay was reduced significantly to 2.62 ms from its original value of 3.63 ms, even though the closing delay was extended a little bit to 2.30 ms from original value of 2.15 ms. Thus, this low actuation air pressure is preferred when the valve is driven under a 50%–50% duty cycle.

3.4   Peristaltic Micropumps

A peristaltic pump was also fabricated with the same process of multilayer soft lithography, consisting of three valves arranged in a series on a single channel as illustrated in Figure 3.8. Typically, peristalsis was actuated by the pattern 101, 100, 110, 010, 011, 001, where 0 and 1 indicate "valve open" and "valve close," respectively. This pattern is named the "120°" pattern, referring to the phase angle of actuation between the three valves. Other patterns are possible, including 90° and 60° patterns. If the on-off duty cycle is not limited to 50%–50%, a 3-phase pumping pattern can also be used: 101, 110, 011. For all the sequences mentioned here, the fluid is actively pumped to the right, one unit valve volume per cycle. Pumping in the opposite direction can be achieved simply by reversing the pumping sequence. However, according to our tests, the differences in pumping rate at a
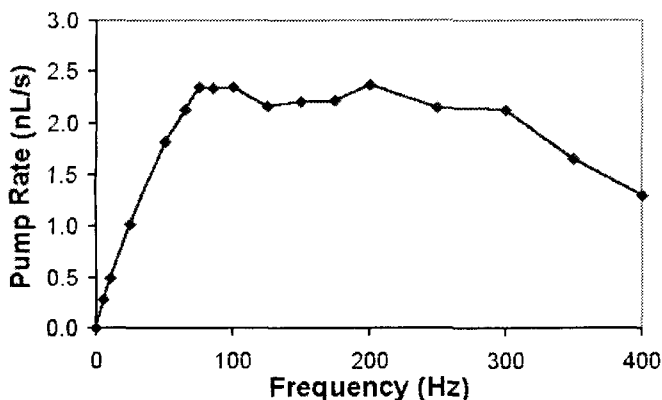
Figure 3.9: Pumping rate of a peristaltic micropump versus various driving frequencies. Dimension of microvalves: 100 μm by 100 μm by 10 μm; applied air pressure: 50 kPa; pumping pattern: 120°, 6-phase.

given frequency of various pumping patterns were minimal ($\leq 20\%$).

Pumping rates were determined by measuring the distance traveled by a column of water in thin tubing (0.5 mm inner diameter); with 100 μm by 100 μm by 10 μm valves, a maximum pumping rate of 2.35 nl/s was obtained as shown in Figure 3.9. Consistent with the previous observations of valve actuation speed, the maximum pumping rate is attained at ~ 75 Hz; above this rate, increasing numbers of pump cycles compete with incomplete valve opening and closing. The pumping rate was nearly constant until above 200 Hz and fell off slowly until 300 Hz. The valves and pumps are also quite durable: we have never observed the elastomer membrane, control channels, or bond to fail. None of the valves in the peristaltic pump described above show any sign of wear or fatigue after more than four million actuations. In addition to their durability, they are also gentle. A solution of *Escherichia coli* cells pumped through a channel and tested for viability showed a 94% survival rate[2].

Pulse waves generated by the pumping cycles in a fluid channel are a common problem for fluidic systems because of the incompressibility of normal liquid solutions. It is especially harmful to the joints. Besides, precise inline fluid-flow control cannot be achieved before this problem is resolved. This phenomenon was also observed at our micropump active region while a buffer containing fluorescent beads was pumped through. However, because of the softness of the RTV silicone, the whole channel serves as a damper. The beads' flow

---

[2]*E. coli* were pumped at 10 Hz through the channel. Samples of known volume were taken from the output well (pumped) and the input well (control), and serial dilution of each were plated on Luria-Bertani agar plates and grown overnight at 37°. Viability was assessed by counting colonies in the control and pumped samples and correcting for sample volumes and dilution.

looked smooth under microscope when it was a few hundred microns above or below the pumping region. Moreover, air cavities can be designed and put before and after the pump region. They can buckle up and down to absorb the pulsed pressure wave and naturally damp it away. This design can easily solve this problem with almost no extra effort.

3.5 Conclusion

Monolithic active valves built as described above have several notable advantages over silicon-based microfluidic valves. Because of the low Young's modulus of silicone rubber, the valves' active area is no larger than the channels themselves; this permits exceptionally low dead volumes. Because of the softness of the membrane, complete valve sealing is easily attained, even in the presence of particulates. The valves close linearly with applied pressure, allowing metering and permitting them to close in spite of high back pressure. Their small size makes them fast, and size and softness both contribute to making them durable. Small size, pneumatic actuation, and the ability to cross channels without actuating them allow a dense integration of microfluidic pumps, valves, mixing chambers, and switch valves in a single, easy-to-fabricate microfluidic chip. The greatest advantage, however, is ease of production. Compared with valves and pumps made with conventional silicon-based micromachining[69, 79, 72] (or even hybrid devices incorporating polymers[22, 27, 87, 89]), monolithic elastomeric valves are simpler and much easier to fabricate.

The use of nontraditional materials gives the multilayer soft lithography method a number of advantages over conventional micromachining, including rapid prototyping, ease of fabrication, and forgiving process parameters. It allows multilayer fabrication without the problems of interlayer adhesion and thermal stress buildup that are endemic to conventional micromachining. This process can be used to construct complex multilayer microfabricated structures such as optical trains and microfluidic valves and pumps. The silicone rubber used here is transparent to visible light, making optical interrogation of microfluidic devices simple. It is also biocompatible — materials in this family are used to fabricate contact lenses. The raw material is inexpensive, especially when compared with single-crystal silicon ($\sim\$.05/cm^3$ versus $\sim\$2.50/cm^3$). Most important, it has a low Young's modulus, which allows actuation even of small area devices. Pneumatically actuated valves and pumps will be useful for a wide variety of fluidic manipulation for lab-on-a-chip applications. In the fu-

ture, it should be possible to design electrically or magnetically actuated valves and pumps that can be used as implantable devices for clinical applications.

Part II

DNA Diagnostics

Chapter 4   Single-Molecular DNA Sizing

Physicists size up DNA molecules :
... As progress towards the microfabri-
cated "lab on a chip" continues, the sim-
ple device reported by the Caltech research-
ers may prove to be one of the critical ele-
ments used repeatedly in its construction.
— Bob Austin, *Physics World*, 12(4), 1999.

4.1   Introduction

Many assays in biology require measurement of the length distribution of DNA molecules in a heterogeneous solution, such as DNA mapping for genomic sequencing, DNA finger-printing for forensic samples, and restriction fragment length polymorphism (RFLP) for disease diagnosis. This measurement is commonly done with gel electrophoresis (Fig. 4.1); the molecules are separated by mobility, from which the lengths are inferred. This method is powerful, yet has some drawbacks. For medium-to-large DNA molecules, the resolution is limited to approximately 10%. Gel electrophoresis is time consuming. It generally takes at least an hour to run the gel, not including the setup time to cast the gel. Furthermore, for large molecules the procedure fails. This problem has been alleviated to some extent by the development of pulsed-field gel electrophoresis[8, 66], but running times can be days.
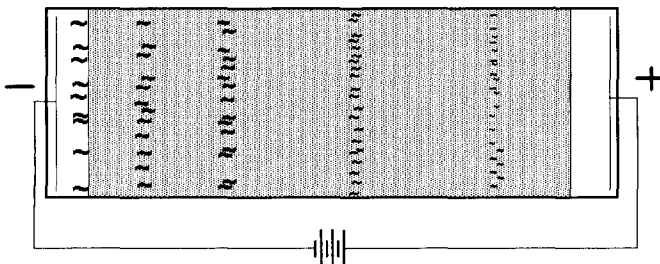

Figure 4.1: DNA gel elec-
trophoresis. DNA molecules are
negatively charged at pH 7–8 be-
cause of their phosphate back-
bones (PO_4^-). They migrate
through a porous gel matrix un-
der an electric field. The small
ones move faster while the big
ones lag behind due to the differ-
ence in their mobility.

With the development of high-affinity intercalating DNA stains[32, 63], it has become possible to directly measure the length of single molecules by quantitating fluorescence. The amount of intercalated dye is proportional to the length of the molecule, so measuring the total fluorescent intensity from a single molecule gives a direct measurement of extremely long DNA molecules because the signal increases with the length of the molecule. This technique has been used with traditional methods of flow cytometry to measure length distributions of DNA molecules[10, 28]. Other groups have imaged restriction enzymes digesting extended single DNA molecules for "optical imaging"[29, 51].

We developed an integrated compact system to size and sort microscopic objects, especially DNA molecules, based on measurement of single-molecule fluorescence using a microfabricated device as described in Chapter 2. It has superior sensitivity, is 100 times faster than pulsed-field gel electrophoresis, and has a resolution that improves with increasing DNA length. Because single-molecule detection is achieved, it generally requires a million times less sample than pulsed-field gel electrophoresis and has comparable resolution for large molecules. Sizing DNA restriction digests and ladders spanning 2–200 kbp was demonstrated. As an example of applications to this system, a protocol for DNA mapping based on bacteria artificial chromosome (BAC) was developed, and matched peaks of fragment lengths of DNA digests between neighboring BAC contigs were shown. In order to facilitate higher screening rate, a multiplex system that can run several samples at the same time was also constructed. Moreover, interesting phenomena were seen under these systems. Clamping effect by intercalating dimers between two end-hybridized DNA molecules was directly observed for the first time.

Here, I would like to discuss detailed design and implementation considerations in order to successfully build such a single-molecule sizing system (SMS), show results of DNA Lambda-HindIII digests and Lambda-ladders, discuss the sources of underlying variations, describe the protocols for BAC fingerprinting, and talk about some interesting facts we found while using this SMS system.

4.2 System Design and Configuration

The idea behind single-molecule DNA sizing systems is intuitive and also straightforward. DNA samples are stained with a fluorescent intercalating dye. The longer the DNA strand,
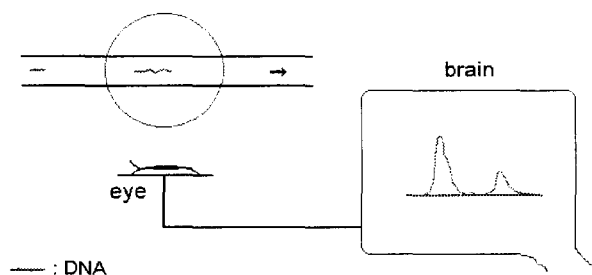
Figure 4.2: Principle of single-molecule DNA sizing. The longer the DNA, the more the fluorescence.

the more dye molecules attach, and the brighter it is when passing through a laser excitation spot, as illustrated in Figure 4.2. DNA molecules flowing through a microfabricated channel can go as fast as the detector can handle. By analyzing the histogram of fluorescent peak heights, the length distribution of DNA samples can be revealed with a computer analysis program in a few minutes of total running time.

However, because the amount of fluorescence from each individual DNA molecule is limited, a highly sensitive epi-fluorescence system has to be constructed. Moreover, in order to compete in speed with conventional gel electrophoresis, the time to examine each DNA molecule has to be kept as short as possible, i.e, to run under a high screening bandwidth, usually $\sim$ 1 kHz. Even though single dye-molecule detection has been demonstrated in many research groups[57], it usually takes several seconds of exposure time to collect enough photons and the variation of intensity measurement between molecules is generally huge, with a typical coefficient of variation (C.V.)[1] around 20% to 50%. For a precise DNA size measurement, such a huge variation is not tolerable. There are two independent parameters to judge the performance of such a system: resolution (precision) and accuracy. The former refers to how well we can separate DNA fragments of close but different lengths, and the latter refers to how accurately we can measure the exact sizes of those DNA molecules. For pulsed-field gel electrophoresis (PFGE), the resolution is around 10%[6], and the accuracy depends strongly on the running condition and how close it is to the lanes of DNA size markers. In general, an accuracy of 2% to 5% could be obtained with a good PFGE setup. For an SMS system, the resolution is comparable, about 8%–15%, and the accuracy within and between runs is usually 1%–2%. With such a similar sizing performance, however, the

---

[1]Coefficient of Variation (CV) $= \dfrac{\text{Standard Deviation } (\sigma)}{\text{Mean } (\mu)}$.

48

Fluorescent Flow Cytometry
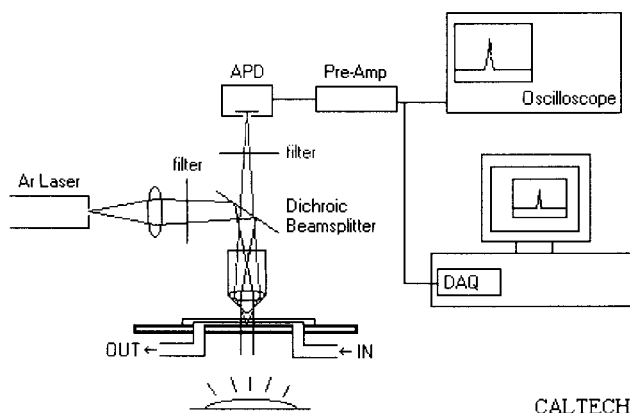
Figure 4.3: Schematic diagram of an SMS system.

running time is significantly reduced from hours and days in PFGE to 10 to 20 minutes in an SMS system. All of these were made possible because of a careful and optimized system design and the right choice of fluorescent DNA intercalating dyes.

4.2.1 Epi-Fluorescence System

A schematic diagram of an SMS system is shown in Figure 4.3. It consists of an excitation laser source, an optical path with a beam expander and steering mirrors, a dichroic filter set, an epi-fluorescence microscope setup, a microfabricated flow-cell device, a sensitive optical detector, and a computer data acquisition and analysis system.

Laser Source

The selection of a laser source strongly depends on the excitation spectrum of the fluorescent dye used. However, typical DNA dyes are usually tuned to match an emitting wavelength of a common laser, such as the 488-nm and 514-nm lines of an argon ion laser or the 532-nm line of a frequency-doubled Nd:YAG laser. A 10-mW 488-nm air-cooled argon ion laser (2214-10SL; Uniphase, San Jose, CA), a 10-mW 532-nm frequency-doubled Nd:YAG laser (BWT-10; B&W Tek, Newark, DE) and a fiber-coupled 2-W water-cooled argon ion laser (Innova 70; Coherent, Santa Clara, CA) have all been tested in our lab. The 488-nm laser was used to excite dye YOYO-1 (Y-3601; Molecular Probes, Eugene, OR), PicoGreen (P-7581; Molecular Probes) and the other blue/green fluorescent dyes, whereas the 532-nm

laser was mainly used for dye POPO-3 (P-3584; Molecular Probes).

In addition to the laser emission wavelength, the most important criterion for a good laser source is its 'stability': both short-term rms noise and long-term drift. The former would add into the variation of fluorescence measurement and thus reduce the sizing resolution, and the later affects the accuracy of absolute size measurement within several runs. In general, we would like the rms noise to be below 1% and the drift to be as small as possible. A power monitoring setup (a beam splitter + a photodetector) could be inserted into the light path so as to be used as a normalization factor to cancel out the fluctuations in fluorescence measurement. However, since it would be very costly to make identical detectors in order to match the frequency responses of this monitoring photodetector and the final sensitive avalanche photodiode (APD) or photomultiplier tube (PMT), this method is impractical in canceling out the rms noise, especially when it is already low ($\leq 1\%$). Nevertheless, this is a good way to keep measurement between runs consistent, particularly when it spans several days. In our experience, a fiber-coupled laser source is actually a bad idea because the mechanical and thermal instability of fiber coupling causes the rms noise $\sim 1.2\%$ in comparison to $\sim 0.5\%$ from the direct-illuminating 10-mW argon ion laser. An increase of $\sim 1\%$ in the coefficient of variation of fluorescent measurement was observed. It could be reduced by merely about 0.1%–0.2% when a power monitoring scheme described above was installed. Therefore, choosing a laser with high stability is the most important issue once the excitation wavelength is decided.

The next concern about a laser source is its output power. Generally speaking, the higher the better. Figure 4.4 shows the dependence of the fluorescent peak heights of lambda-phage DNA molecules (49 kps long) at various laser excitation powers. Even though the response is no longer linear when the power is above 20 mW, saturation of fluorescence emission due to photobleaching of dye molecules has not been reached even at a laser power of 90 mW. It is obvious that the saturation laser power depends on the flow rate of DNA molecules, i.e, the sizing speed. The faster the DNA flows, the higher the laser power could be applied before limitation due to photobleaching shows up.

Optical Train and Epi-Fluorescence Microscope

The optical path of an SMS system consists of a pair of lenses for beam expansion, two dielectric mirrors for beam steering, a third convex lens to refocus the laser beam to the back
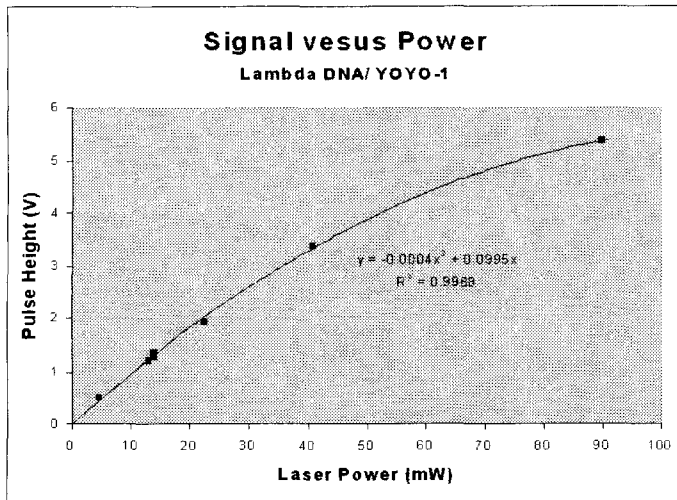
Figure 4.4: Fluorescence of lambda DNA molecules stained with YOYO-1 at various laser powers. Fiber-coupled 488-nm Coherent argon laser was used. Power was measured at the output of the fiber. APD bandwidth: 1 kHz. Buffer and DNA flow speed in the channel: ~ 2 mm/s.

focal plane of an objective lens, and a dichroic filter set to give setting of an epi-fluorescent illumination, as shown at the center part of Figure 4.3. A microfabricated flow-cell device sits on a microscope stage with the detection channel focused and imaged onto a CCD camera (Philips FTM800 or Marshall V-1055-BNC) through the same objective lens. A white back illumination light is used to align the channel to an alignment mark on the screen of the CCD monitor. However, this back light and the CCD camera are switched off or away when the actual flow cytometry measurement starts, where laser excitation and APD/PMT detection are used.

The three-lens optical setup (the beam expander and the third condenser lens) makes the laser alignment much easier. Besides, by fine tuning the distance between the two beam expansion lenses, we could change the ratio of beam expansion and thus control the size of the final laser illumination spot. The third convex lens is used to refocus the expanded parallel laser light to the back focal plane of the objective lens, which then yields a wide illumination spot onto the microfabricated device, typically 30 μm in full-width half-maximum (FWHM) as measured using a fluorescent FITC solution (0.4 mg/ml) and a calibrated CCD monitor. Because of the diffractive nature of laser light (EM_{00} mode), the illumination profile is actually a Gaussian with a flat top at the center. For a channel of 5 μm in width and centered perfectly in the laser excitation region, the maximum difference of laser intensity between the center of the channel and the edge of the channel is 1.9%. Yet, due to a parabolic flow profile, most of the DNA molecules would actually go through

Channel width (μm)	Max. diff.	Average C.V.
0	0.00%	0.00%
1	0.08%	0.02%
2	0.31%	0.07%
3	0.69%	0.16%
4	1.22%	0.26%
5	1.91%	0.41%
6	2.73%	0.59%
7	3.70%	0.80%
8	4.81%	1.05%
9	6.05%	1.32%
10	7.41%	1.63%

Table 4.1: Average intensity variation due to a Gaussian illumination profile with a 30-μm FWHM. Max. diff. represents the maximum intensity difference between the center and the edge of the channel of given width. Parabolic flow profile is assumed and is used as the weighting factor when calculating the average coefficient of variation (C.V.) of the excitation intensity. For different FWHM, the channel width should be adjusted proportionally.

the center of the channel where the laser illumination is more uniform. Therefore, the real variation of fluorescence measurement due to this excitation nonuniformity is much less than this maximum deviation. Using a parabolic function as a weighting factor with zeros at the edges of the channel, the coefficient of variation caused by this effect is calculated and listed in Table 4.1 for channels of different widths. It matches with our experimental tests very well. Nevertheless, this variation affects the final resolution of DNA sizing, so a wider illumination spot and a narrower channel are always preferred.

A dichroic filter set is the heart of an epi-fluorescent setup, in which a dichroic filter passes light of a wavelength longer than its cutoff edge but reflects any light of shorter wavelengths. As shown in Figure 4.3, the laser light is reflected and sent into the objective lens by the dichroic because its wavelength is shorter than the cutoff edge. The fluorescence signal that has a longer wavelength would then pass the dichroic, while all the scattered or reflected laser lights are blocked. Yet, the discrimination ratio of a dichroic filter is usually no more than 100 to 1. A second bandpass filter should be added right in front of the fluorescence photodetector, an APD or a PMT, in order to further filter out any leaked laser illumination and ambient scattered light. Because most fluorescent dyes have broad emission spectra at room temperature, a bandpass filter with a wide passband would be normally favored. However, more background fluorescence and scattered laser light may also be able to pass through it. Therefore, a compromise should be sought in order to achieve the highest signal-to-noise ratio. Table 4.2 shows how much fluorescence signal

Dichroic Filter	Bandpass Filter	Fluorescence Collected
500DCLP	D510/20	19.64%
500DCLP	D525/40	36.32%
500DCLP	D535/50	34.84%
500DCLP	D535/60	47.19%
500DCLP	D550/100	59.10%
505DCLP	D510/20	15.14%
505DCLP	D525/40	33.49%
505DCLP	D535/50	34.49%
505DCLP	D535/60	44.77%
505DCLP	D550/100	53.62%

Table 4.2: Percentage of YOYO-1 fluorescence collected through various dichroic filter sets. 500DCLP means a dichroic with a cutoff edge at 500 nm. D510/20 represents a bandpass filter centered at 510 nm with a passband of 20 nm wide. Data of YOYO-1 emission spectrum are obtained from Molecular Probes. Data of filter characteristics are given by Chroma Technology.

from DNA intercalating dye, YOYO-1, is actually collected through various combinations of dichroic and bandpass filters (Chroma Technology, Brattleboro, VT). Even though a D550/100 bandpass filter can pass more fluorescence signal, the background level is about five times higher than a D535/50 when a 500DCLP dichroic is used. Therefore, a D535/50 with a 500DCLP is the most common filter set used in our SMS systems.

Optical Detection

There are two choices of sensitive photodetectors: avalanche photodiodes (APD) and photo-multiplier tubes (PMT). Both of them have an internal gain of photoelectrons with similar mechanisms. A high voltage bias is applied between the photoelectron generation cathode, a PIN junction in an APD and a photosensitive coating in a PMT, and the final electron collection anode. When electrons go through such a high electric field, they quickly accumu-late a lot of kinetic energy. In an APD, the electrons hit the lattice, knock more electrons out from the valence band into the conduction band, and the process goes on again and again until they reach the collection electrode at the end. It is just like the event of a snow avalanche. In a PMT, it is very similar: Free electrons are moving in a vacuum under the same high voltage bias; every time they hit a dynode which is coated with a material of low work function, more electrons are generated. This event cascades for several stages until the final collection anode is reached. Usually, an internal gain of a few hundred can be obtained in a APD whereas a huge gain of 10^5 to 10^7 is commonly achieved in a PMT.

For an accurate single-molecule sizing system, a detector with large detection area is needed. It does not only collect more photons but it also increases the depth of focus[3].

$$\text{DOF}_{\text{tot}} = \frac{\lambda n}{\text{NA}^2} + \frac{n}{M\text{NA}}e, \tag{4.1}$$

where DOF, depth of focus, is defined as $\frac{1}{4}$ of the axial distance between the first minima above and below focus of the diffraction image of a small pinhole. λ is the wavelength of the light, n is the refractive index of the medium, NA is the numerical aperture of the objective lens, M is the magnification, and e is the smallest distance resolved by the detector, which is proportional to the size of the detection area in this case. For an objective lens with a high numerical aperture (NA), more light would be collected (in proportion to $(\text{NA})^2$). However, the depth of focus also becomes very small as given in the first term of Eq. 4.1. It could be overcome with a large-area detector because it still collects the light signal even when the object is out of the focus plane, as indicated in the second term of Eq. 4.1. The larger the detector, the more the depth of focus, and the less the variation when molecules are flowing through the channel at different vertical positions.

Before large-area avalanche photodiodes (LAAPD) were first demonstrated in research laboratories in the late 1980s, APD were usually small, with diameters of 300-μm or less[40]. They were limited by the massive dark noise from both bulk and surface leakage current. Two key techniques came along to make large-area APD available: neutron-transmutated silicon and special passivation of the beveled edges. Instead of doping the silicon to produce an n-type avalanche layer in the conventional manner, neutron bombardment was used to transmutate some of the silicon atoms into phosphorous atoms through β-decay. Silicon prepared in this manner has excellent doping uniformity and a low number of lattice defects. As to beveling the edge, the field strength is reduced at its highest point, PN junction, and extended into the n-type avalanche region. Leakage due to edge breakdown at the junction is significantly reduced while a more uniform avalanche breakdown is obtained. With these techniques, LAAPD became commercially available from Advanced Photonix in the early 1990s. A comparison between an LAAPD and a PMT is given in Table 4.3. Even though a PMT has a very high internal gain and thus can operate with a high bandwidth, an APD has a much better uniformity in its spatial response. It is actually important in this case because we would like molecules flowing at different lateral positions to give the same

	LAAPD	PMT
Quantum Efficiency	**70%–90%**	5%-20%
Spectral Response	**∼ 600 nm**	∼ 200 nm
Internal Gain	10^2	10^6
Operating Bandwidth	lower	**higher**
Spatial Uniformity	**±1%**	±5%
Size	**small**	big
T.E. Cooled	**easy**	hard
Magnetic Field	**immune**	needs shielding
Lifetime	**longer**	shorter
Multi-Channel	N/A	**Available**

Table 4.3: Typical characteristics of a large-area avalanche photodiode (LAAPD) versus a photomultiplier tube (PMT).

amount of signal. In addition, an APD is generally small and can be cooled easily with a thermoelectric cooler to reduce its dark current, whereas a big housing would be required in order to cool a PMT down. Therefore, selection between these two detectors should be done carefully based on the intensity of the signal, the desired operating bandwidth, the variation over the width of the channel, and also the space and the cost.

In our labs, a TE-cooled 5-mm LAAPD (SD 197-70-74-520; Advanced Photonix, Camarillo, CA), a side-on PMT assembly (H957-08; Hamamatsu, Bridgewater, NJ) and a multi-channel PMT (R5900U-00-L16; Hamamatsu) were built and tested in our SMS systems. Working with Charles Spence through three generations, a quiet and highly sensitive LAAPD detector was built. It was cooled to $-40°$C with a two-stage thermoelectric cooler (6320/157/040C; ITI, Chelmsford, MA), which reduced the dark current of the detector from 50 nA to 90 pA. The detector was reverse-biased typically at 2,400 V with an ultra quiet high-voltage power supply (PMT-30CN-3; Bertan, Hicksville, NY), giving an internal gain of 300. A transimpedance amplifier (OPA128; Burr-Brown, Tucson, AZ) converted the photocurrent to a voltage at a gain of 100 mV/nA (100 MΩ). A second stage amplifier (OP-27; Analog Devices, Norwood, MA) provided additional voltage gain of 10. A complete circuit diagram is shown in Figure 4.5. A negative bias based on a voltage regulator (LM317;National Semiconductor, Santa Clara, CA) and an adjustable voltage divider was added in later at the second stage. A constant output bias of 0 to -8 V could be set in order to cancel the background and thus preserve the whole dynamic range (10 V) for real pulse signals. A picture of the two-stage pre-amplifier and the output bias circuit is shown
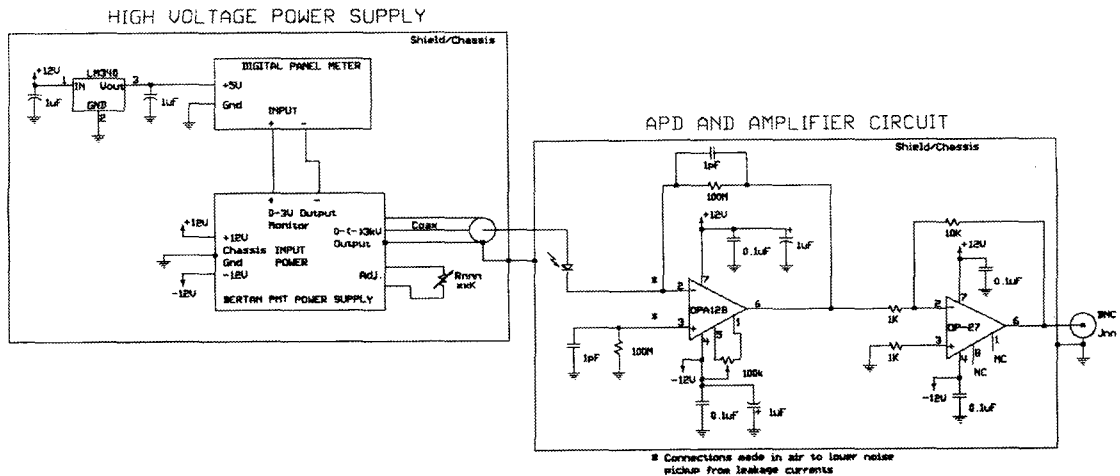
Figure 4.5: Circuit diagrams of the high-voltage bias and pre-amplifier of an LAAPD. The Bertan PMT-series gives a stable high-voltage bias with a very low p-p noise ($\leq$ 2 ppm). For the pre-amplifier, in addition to a good transimpedance operational amplifier, such as OPA128, resistors are very important. They have to be at least metal thin-films with a low thermal current noise. The pre-amplifier was built right on top of the APD and shielded together by the metal case to prevent any 60-HZ AC-noise pick-up.

in Figure 4.6. After pre-amplification, the signal was filtered by an RC lowpass filter with a corner frequency of 1.6 kHz, and then digitized at 5 kHz by a NI-DAQ card (Lab-PC-1200; National Instruments, Austin, TX) on a personal computer running LabVIEW. As to the side-on PMT assembly H957-08, only a 15-V DC power supply is needed since it has a built-in adjustable high-voltage power supply. The signal was filtered with the same RC lowpass filter and digitized with the same instruments describe above. The multi-channel PMT was constructed in order to screen multiple samples at the same time. Further discussion would be given in section 4.2.4.

The sensitivity of the LAAPD and the side-on PMT used in our lab is calculated and listed in Table 4.4. Even though the PMT gives higher signal when the emission wavelength is around 500 nm, it is noisier too. A lot of sharp spikes could be seen constantly at its output on a oscilloscope. Therefore, judging by the final signal-to-noise ratios, the cooled large-area APD is about twice as good as the side-on PMT assembly. Therefore, most of data shown in this thesis were taken with the LAAPD unless otherwise mentioned.
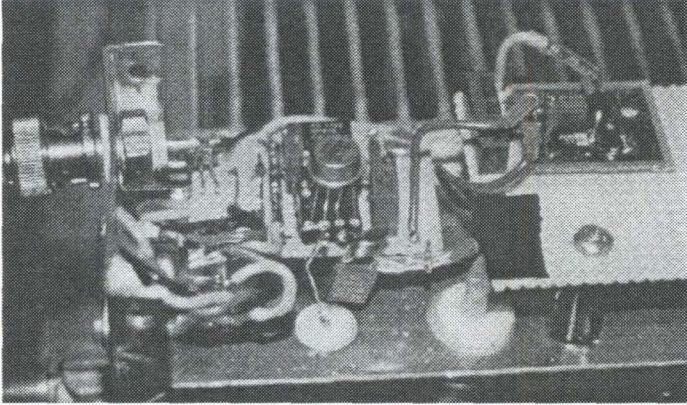
Figure 4.6: A picture of the LAAPD pre-amplifier with an output bias circuit. Center to left-hand side is the pre-amplifier based on OPA128. The small circuit on the right-hand side is the output bias circuit. The bottom two Teflon rings are high-voltage and signal fit-through for the LAAPD located in the lower desiccated chamber. Heat sink of the TE cooler can also be seen.

Detector	λ (nm)	Q. E.	Sensitivity (A/W)	Output (V/W)
APD	500	86.00%	0.347	1.73×10^{11}
	550	88.00%	0.390	1.95×10^{11}
	600	87.00%	0.421	2.22×10^{11}
PMT	500	15.00%	0.060	6.65×10^{11}
	550	7.50%	0.033	3.66×10^{11}
	600	3.20%	0.015	1.70×10^{11}

Table 4.4: Comparison of the LAAPD and the side-on PMT used in our lab. Both are assumed to operate at highest bias voltages: -2,450 V for LAAPD and -900 V for PMT. The LAAPD has an internal gain of 500 at this voltage, whereas the PMT has an internal gain of 1.1×10^7.

4.2.2 Fluorescent Dyes

In addition to a delicate optical system, a bright and stable fluorescent DNA stain is also the key to make fluorescent single-molecule DNA sizing possible. YOYO-1 and TOTO-1, reported by Glazer et al. in 1992[63], are two very bright cyanine DNA stains, yielding more than ten times the fluorescence of the conventional DNA dye, ethidium bromide. Moreover, they are engineered to be intercalating dimers, which have two arms of independent fluorescent cyanine monomers to stick into the grooves of double-stranded DNA (dsDNA). The binding coefficients to dsDNA are greatly enhanced by several orders of magnitude in comparison to their parent monomer compounds (Table 4.5). This makes the stained DNA complexes extremely stable. In addition to the superior brightness and stability, the fluorescence of dye molecules increases by more than 1000 fold while binding a nucleic acid. With high affinity to DNA and low fluorescence in an unbound state, the fluorescent background from free dye molecules in solution is significantly reduced. Similar cyanine intercalating dimers tuned to different excitation and emission wavelengths showed up later, such as POPO-3 and BOBO-3. Together with other new bright intercalating monomer dyes, PicoGreen, YO-PRO-1 and TO-PRO-1, they are all commercially available through Molecular Probes now[32].

Table 4.5 gives a list of important characteristics of common DNA stains, including their absorption and emission maxima, extinction coefficients and quantum efficiency. DNA complexes stained with YOYO-1, YO-PRO-1 and PicoGreen can be excited with a 488-nm argon ion laser, while those stained with TOTO-1 and TO-PRO-1 can be excited with a 514-nm argon ion laser. For DNA stained with JOJO-1, POPO-3, JO-PRO-1 and PO-PRO-3, a frequency-doubled Nd:YAG laser emitting at 532 nm can be used as the laser excitation source. Once excited by a laser, the fluorescence intensity of a stained DNA molecule is determined by the number of dye molecules on it, the extinction coefficient (absorption cross-section) ϵ and the quantum yield efficiency QE of the dye used. The product of these three decides the final peak heights of fluorescent pulses obtained on the detector. When an intercalating dimer dye is used, a maximum staining ratio of one dye molecule per five base pairs is commonly achievable[2]. For a monomer dye, a 1:2 dye:base pair ratio is theoretically

---

[2]Some dimer dyes were found to exhibit two distinct binding modes: at low dye:base-pair ratios, the binding mode appears to consist primarily of intercalation; at high dye:base pair ratios, a second mode involving external binding begins to contribute[42].

Dye	MW^a	Abs/Em^b	ϵ_{max}^{c}	QE^d	FE^e	BC^f
YOYO-1	1271	491/509	98,900	0.52	3,200[63]	6.0×10^{8}[30]
TOTO-1	1303	514/533	117,000	0.34	1,100[63]	1.1×10^{9}[30]
JOJO-1	1273	529/545	171,400	0.44		
POPO-3	1223	534/572	146,400	0.46		
BOBO-3	1255	570/604	147,800	0.39		
EthD-1	857	528/617	7,000	0.08	35[63]	2×10^{8}
PicoGreen		502/523	70,000	0.53	1,980[70]	
YO-PRO-1	629	491/509	52,000	0.44	700[63]	
TO-PRO-1	645	515/531	62,800	0.25	18,900[63]	3.2×10^{5}[58]
JO-PRO-1	630	530/546	94,400	0.38		
PO-PRO-3	605	539/567	87,900	0.57		
Hoechst 33258	624	352/461	40,000	0.59	95[70]	
Ethidium Bromide	394	518/605	5,200	0.15	21[30]	1.5×10^{5}

^{a}Molecular weight (g/mol).

^{b}Absorption and emission maxima (nm).

^{c}Extinction coefficient ($\text{cm}^{-1}\text{M}^{-1}$) measured at the absorption maximum.

^{d}Quantum efficiency of fluorescence yield.

^{e}Fluorescence enhancement when bound to dsDNA ($F_{\text{bound}}/F_{\text{free}}$).

^{f}DNA binding coefficient $= \frac{[\text{DNA}_{bs}\text{-Dye}]}{[\text{DNA}_{bs}][\text{Dye}]}$ (M^{-1}), where [DNA_{bs}] represents the concentration of available DNA binding sites.

Table 4.5: Spectral characteristics of common nucleic acid stains. Dyes on the top portion are dimers whereas those on the bottom portion are monomers. Data are taken from [32] or otherwise as noted. Abs, Em, ϵ and QE are determined for DNA complexes in 10 mM Tris, 1 mM EDTA, 50 mM NaCl, pH 7.4.

possible. However, because of the low binding coefficient, a high concentration of dye molecules is needed, which would yield a very high fluorescent background. For example, if a ratio of 10:1 [DNA$_{bs}$-Dye]:[DNA$_{bs}$] is desired for TO-PRO-1, the concentration of dye molecules would be 31 μMaccording to the binding coefficient from Table 4.5. It is about 1000 times higher than the concentration used for YOYO-stained DNA. In my experience, TO-PRO-1 suffices for large DNA molecules, such as lambda-phase DNA. DNA molecules of 5 kbp or less were lost in the fluorescence background. Nevertheless, the 488-nm line was used in this test, and for a laser illumination of 514 nm, a better result would be expected. As to PicoGreen, the best monomer dye up to now, the dye concentration that yields the best sensitivity is around 0.8 μM[70]. Even though it is a trade secret, an abnormally high binding coefficient could be anticipated, 10^6–10^7 M^{-1}. Following the standard staining protocol for PicoGreen, the fluorescent signal obtained is about one quarter of a YOYO-stained sample. However, since PicoGreen is a monomer dye, the staining process is much faster: Only 10 minutes of incubation time is required after DNA-dye mixing. As to YOYO-1 staining, it takes 2 to 4 hours at least, the bottleneck for the whole procedure of single-molecule DNA sizing.

To get a clearer picture, let's calculate the amount of fluorescence signal we would expect to get from a single YOYO-stained lambda-phage DNA molecule. We will use the fundamental equation of light absorption:

$$\frac{dI}{I} = -\epsilon\, c\, dx, \tag{4.2}$$

where I is the light intensity, ϵ is the absorption coefficient, c is the concentration of the dye molecules (in mol per unit volume) and x is the distance measurement along the light path. Let A denote the area of light cross-section. The number of dye molecules dN inside this thin slab of absorption medium is then $c\, N_A\, A\, dx$, where N_A is the Avogadro's number (6.022×10^{23} /mol). The power of light absorbed dP_{abs} equals $-A\, dI$. Supposing that we are still in the linear absorption regime of these dye molecules (no quenching effect from nearby dye molecules), the amount of light absorbed by each individual dye molecule would be

$$\frac{P_{\text{abs}}}{N} = \frac{\epsilon\, I}{N_A}. \tag{4.3}$$

Therefore, the photon emission rate r_{em} by a single dye molecule under an illumination intensity I_{ex} ($= I$ in the above) is:

$$r_{em} = \frac{QE\,\epsilon\,I_{ex}}{N_A\,h\nu_{ex}}, \tag{4.4}$$

where QE is the quantum efficiency of fluorescence yield of this dye as listed in Table 4.5 and $h\nu_{ex}$ is the energy of an individual excitation photon.

Assume 5-mW 488-nm laser excitation of a Gaussian profile with 30 μm FWHM is used[3]. The peak excitation intensity I_{ex} over a channel of 5 μm wide under a parabolic flow profile is then 4.88×10^6 W/m^2. QE is 0.52 and ϵ equals $0.98\,\epsilon_{max} = 9.69 \times 10^3$ m^2/mol. Using Eq. 4.4, we can calculate the photon emission rate per dye molecule r_{em} to be '1.00×10^5 photons/sec'. Typically, fluorophores have an emission half lifetime of about ten thousand photons[4]; that is, the half lifetime of YOYO-1 molecules under this illumination condition would be ~ 100 ms. This matches well with our experience[5]. Typically, the fluid flow rate through a HCl-treated RTV microchannel is about 3 mm/s under the pull of the capillary action. This means that the time for a YOYO-stained DNA molecule to flow through the excitation spot of 30 μm FWHM is approximately 10 ms, ten times less than the half lifetime of dye molecules. Therefore, we can assume that all the dye molecules are still active when the DNA molecule passes through the excitation maximum, i.e, the peak of the fluorescence pulse shown on the detector. Or, more accurately, the fraction of active dye equals $(\frac{1}{2})^{\frac{1}{20}} = 97\%$.

For a lambda-phage DNA (48,502 base pairs long) stained at the highest stoichiometric dye:bp ratio of 1:5, the fluorescence peak is expected to be 9.70×10^8 photons/sec according to the unit r_{em} calculated above. When an oil-immersion objective lens of NA 1.4 is used, fluorescent light within an angle of $\theta = \sin^{-1}(\frac{NA}{n})$ to the z-axis is collected, where n is the index of refraction of the glass medium, 1.515. So, $\theta = 1.18$ rad, which gives a solid angle of $\Omega = 2\pi(1 - \cos\theta) = 3.88$ that corresponds to 30% of the whole solid angle, 4π. Using a dichroic filter 500DCLP and a bandpass emission filter D535/50 together with

---

[3]When the argon ion laser is operating at 10 mW, the final power output from the objective lens after passing through all the optical components is about 5 mW.

[4]After emitting certain amount of fluorescent photons, fluorophores *photobleach*. Usually it is due to oxidation y free radicals in the solution since they were in an excited state for about half of the time.

[5]The actual half lifetime of a YOYO-stained DNA molecule under this condition is about 300 ms. The calculation above uses the peak intensity. The average intensity as a molecule going through the Gaussian illumination is only about half of that value.
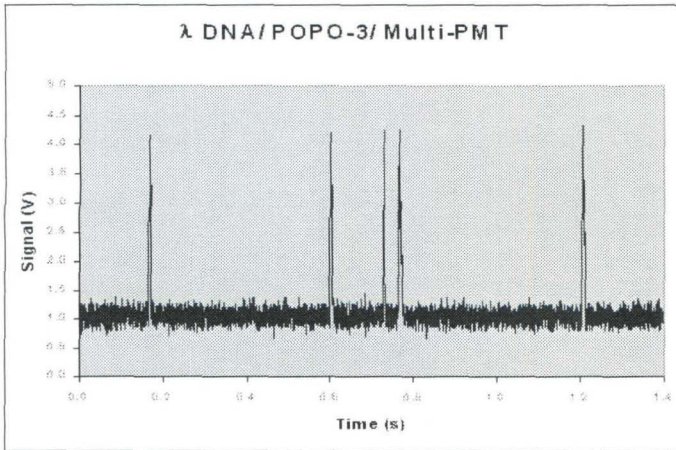
Figure 4.7: Pulses of fluorescent-labeled DNA molecules on an SMS system. A sample containing uniform lambda-phage DNA stained with POPO-3 was used. Fluorescence data was monitored by a multi-channel PMT. However, only one channel was used here.

the data given in Table 4.2, the rate of fluorescence photons that reach the surface of the photodetector is 1.04×10^8 /sec. Supposing the LAAPD discussed in section 4.2.1 is used as the photodetector with a photoelectron quantum efficiency of 86%, an internal gain of 300 (when biased at -2,400 V), and a transimpedance 1GΩ after the two-stage pre-amplification, the voltage peak of the fluorescent pulse should then be 4.31 V. This is very close to the value actually obtained in a real SMS system (see Results).

4.2.3 Computer Data Acquisition and Analysis

A simple threshold algorithm is used to identify fluorescent pulses of DNA molecules and also to determine their characteristics, such as peak heights and widths. Initially, the voltage data from the sensitive photodetector, an LAAPD or a PMT, are lowpass-filtered by a passive RC filter of a corner frequency 1.6 kHz in order to cut off any high-frequency noises. Monitored by an oscilloscope, the analog filtered signal is fed into a computer through a data acquisition card (Lab-PC-1200; National Instruments, Austin, TX) at 5,000 kHz using a LabVIEW program. This digitization rate is chosen to be more than twice of the lowpass cut-off frequency so as to minimize the aliasing effect: noise at higher frequency is folded into the low-frequency passband due to the discrete-time sampling. A typical trace of fluorescence signal containing pulses of DNA molecules is shown in Figure 4.7. After a total running time of 10 minutes to an hour, the data were then analyzed by a C++ program to obtain characteristics of all fluorescence pulses using a threshold algorithm. First, the data are smoothed again by a digital lowpass filter, a Butterworth filter of order 10 with a typical

cut-off frequency set at 300 Hz. A baseline (background level) is calculated[6] and voltage points above certain threshold plus the baseline are considered as the beginnings and the ends of pulses. The maximum voltage (minus the baseline) within a pulse is taken as the peak height of this pulse. The width of a pulse, full-width half-maximum, is also calculated by the program. Because of a parabolic flow profile, DNA molecules were not flowing at the same speed. Thus, the width of a pulse simply tells us where the DNA molecule was flowing through in the microfabricated channel. However, pulses of very short widths (APD or PMT breakdowns) or of very long widths (photobleached) are discarded. After the pulse analysis by the C++ program, all the results are ported into an Excel worksheet. A histogram of pulse peak heights is generated and plotted using a VBA macro program. Bands of DNA molecules of different sizes could be seen clearly, such as Fig. 4.10 and Fig. 4.12 shown in Section 4.3.

4.2.4 Multiplex System

Even though the SMS system described above demonstrated outstanding performance in terms of the running time, 10 to 20 minutes compared to hours or days for gel electrophoresis, a multiplex system that can run several samples at the same time could increase the screening rate even more. This would be of great help for high-throughput DNA sizing applications such as genomic projects of chromosome scales. For conventional flow cytometry, such a multiplex system is difficult because of the size and complexity of glass capillaries used. However, by using microfabrication, devices with multiple channels can easily be made. Since all channels could fit into the same field of view of a single objective lens, there is no need for any significant modification of the original SMS system except for the photodetector, where a multi-channel version must be incorporated. Such a multiplex SMS system was actually built and tested in our lab (Fig. 4.8). Modifications of the flow-cell devices and the photodetector are described as follows.

A design of a multi-channel flow-cell device is shown in Figure 4.9. Since there is no need for sorting in this case, only straight channels with input and output sample wells were incorporated into it. Each individual channel in the detection region is 3 μm wide with 7 μm

---

[6]Since part of the background light consists of fluorescent signal from various optical components, RTV and dye molecules adsorbed on the surface of the channel, the background voltage level tends to decline slightly as time goes on because of photobleaching. A slow feedback mechanism is implemented in the program to adjust the background level accordingly.
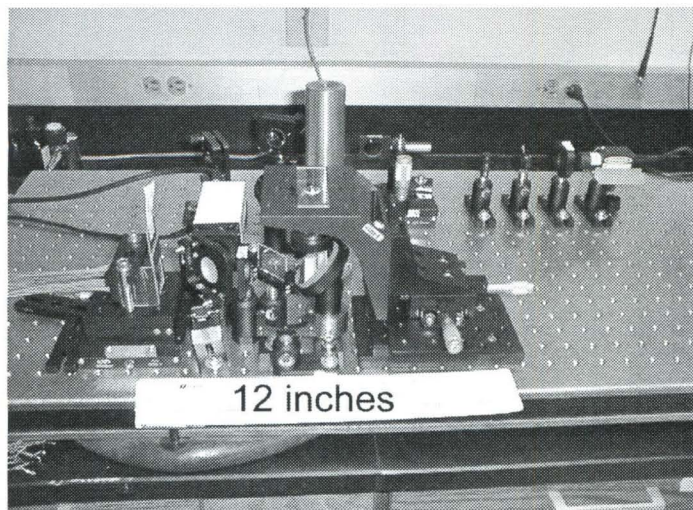
Figure 4.8: A compact multiplex SMS system. A small 532-nm frequency-double Nd:YAG laser is shown at the top right corner. The multi-anode PMT detector is placed at the left end with a manual shutter in the front. The size of the whole system is about 1' by 1.5' by 0.5'.
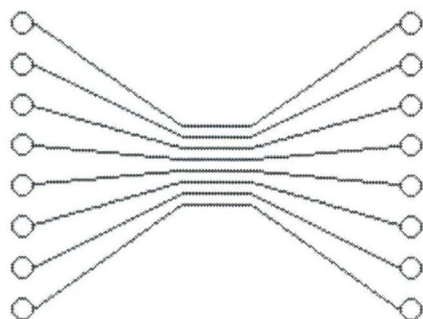

Figure 4.9: Design of a multi-channel flow-cell device.

spacing in-between. Thus, the width of eight channels in parallel is only 73 μm total, which is less than the field of view of an 100× oil-immersion objective lens (170 μm). The size of laser illumination can also be adjusted accordingly with a larger beam expansion ratio (a 6-mm concave and a 40-mm or higher convex lenses). Silicon master molds with this multiple-channel pattern were fabricated and RTV replica were made successfully. Yet, the yield of devices with all eight channels working was not high because it was very difficult to keep those long and narrow channels well-defined and clean at the same time without using any clean-room facility. Buffer containing DNA samples could flow through these channels once they are treated by our HCl hydrophilic treatment.

As for the photodetector, since there is no multi-channel APD available in the market, multi-channel PMTs were thus the only choices. Fortunately, Hamamatsu Photonics offers an ideal selection: a multi-anode PMT (R5900U-00-L16) with 16 independent rectangular PMT windows in parallel, each 1 mm apart. After magnification of 100× by the objective lens, the channels in a microfabricated device (10 μm apart) match perfectly with each linear PMT channel. A housing with optical mounting trenches was carefully machined from black Delrin and almost no light leakage could be detected from all directions. A quiet high-voltage supply (PMT-10CN-3; Bertan) was used to power the PMT, and a multi-channel pre-amplification circuit based on quad operational amplifiers (OPA4134; Burr-Brown, Tucson, AZ) with build-in lowpass RC filters (1.6 kHz corner frequency) was also built. Little crosstalk was observed even between the nearest input channels. The computer program was also modified to facilitate analysis of the measured multi-channel data sets. An example of signal traces obtained with this multi-anode PMT setup is shown in Figure 4.7.

Even though such a multiplex system was successfully built, its sizing resolution is not as good as the single-channel version. This is due to the spatial nonuniformity of PMT responses, $\sim$ 10% difference between the center and the edges. Despite of the catalog specification, the actual nonuniformity of PMT responses was revealed when running 1 μm fluorescent beads 90° across all the channels. Since the microfabricated channels are only 3 μm wide and most of DNA molecules flow through the center, an actual reduction of resolution is not as significant. However, an $\sim$ 2% increase of the coefficient of variation was observed. Therefore, the best system and configuration to use should depend on the applications, trading between speed and resolution.
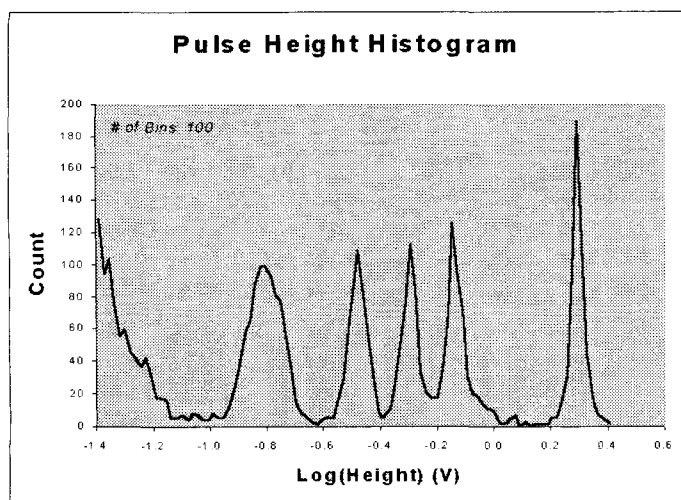
Figure 4.10: Histogram of HindIII digest of λ DNA. The peaks represent (from right to left) fragments of 23 kbp, 9.4 kbp, 6.7 kbp, 4.4 kbp, and an unresolved combination of 2.3 kbp and 2.0 kbp.

4.3 Results

4.3.1 Lambda-HindIII digests and Lambda Ladders

To test the utility of the SMS system for screening restriction digests, we analyzed a HindIII digest of lambda-phage DNA. λ DNA (25250010; Gibco, Rockville, MD) was digested with HindIII restriction enzyme (15207012; Gibco): 10 μl SuRE/Cut 10× Buffer B, 80 μl DI water, 2 μl HindIII endonuclease (20 units) and 8 μl λ DNA of 0.5 μg/μl, incubated at 37°C for an hour. Then, it was diluted and stained with the intercalating dye YOYO-1 according to a procedure similar to the one given in Appendix B.2: λ-HindIII digest of 50 pg/μl (10.5 pM of DNA molecules) was stained in a STE buffer containing 20 nM YOYO-1, at a stoichiometry of one dye molecule per four base pairs. After incubation at 50° for 4 hours, the stained DNA sample was diluted by 50 times in the running buffer (Appendix B.2). It was then introduced into a microfabricated flow-cell device, and fluorescence was collected by an epi-fluorescence setup and monitored with a large-area avalanche photodiode using an SMS system described in Section 4.2.1. Figure 4.10 shows a histogram of the observed peak heights. After collection of data for 10 minutes, the major fragments are clearly resolved. The 2- and 2.3-kbp pieces are not resolved from each other, but are well above the noise floor of the system. For larger fragments, the resolution[7] is on the order of 10% and improves with the length of the molecule (Fig. 4.11). A notable feature of this measurement is that it

---

[7] *Resolution* is defined as two times the coefficient of variation (2 × C.V.).
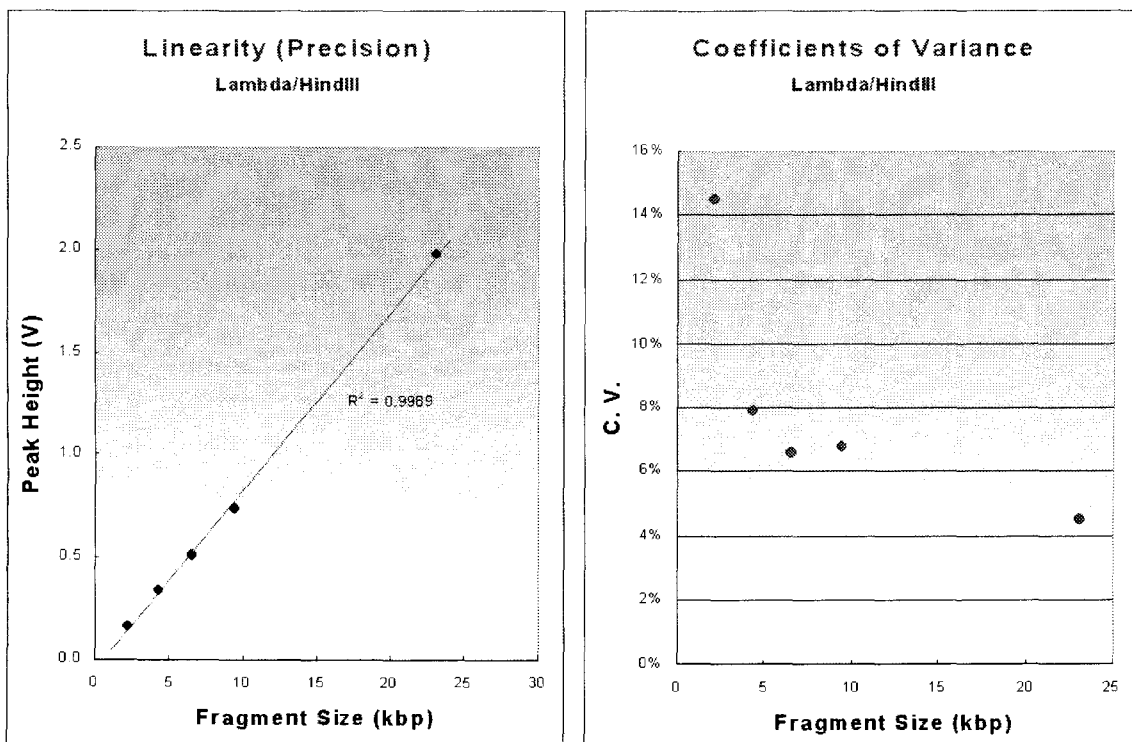
Figure 4.11: Precision and resolution of λ–HindIII digest. The histogram of Fig. 4.10 was fit with 5 Gaussians to estimate the precision and resolution of the measurement. (*Left*) The known sizes of the restriction fragments are compared with the fitted peak locations. The measurements are linear with a precision of 1%–2%. (*Right*) The widths of the peaks determine the resolution of the measurement. The coefficient of variation is the peak's standard deviation divided by its mean height and is an indication of the fractional resolution. Resolution improves with longer molecules. In both graphs, the error bars are smaller than the size of the data point symbols.
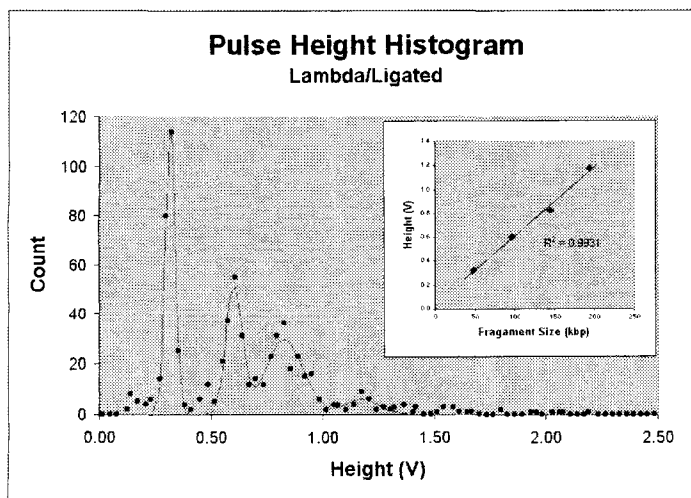
Figure 4.12: Analysis of λ ladder. To test the upper length limit of the device, a λ ladder was analyzed. Peaks corresponding to 50, 100, 150, 200 kbp can clearly be resolved. (*Inset*) The peak height measurement is linear even out to 200 kpb.

requires very small amounts of sample: 28 femtograms of DNA, or about 3,000 molecules, were analyzed.

The detection volume for the single-molecule DNA sizing (SMS) devices is typically 375 femtoliters, more than an order of magnitude smaller than what has been achieved so far with conventional flow cytometry. This small detection volume reduces the background signal proportionally. Furthermore, the geometry of the microfabricated devices allows the use of a high numerical aperture objective for efficient collection of the fluorescent light. DNA fragments of 2 kbp in size, containing ∼400 fluorophores, were easily measured. The noise floor of the histogram for the λ-HindIII digest indicates that the current sensitivity of the system is approximately 1 kbp.

To determine the upper length limit of analysis in the device, we analyzed λ DNA ladders made by ligation of λ-phage DNA with the T4 DNA ligase (M0202S; New England Biolabs): 20 μl λ DNA of 0.5 μg/μl, 2.5 μl of 10× T4 ligase buffer and 2 μl T4 DNA ligase (800 units), incubated at 16°C for 4 hours. After staining (Appendix B.2) and dilution, the ladder was introduced into the device and molecules with up to 200 kbp could be identified (Fig. 4.12). The upper limit is determined solely by the geometry of the optical setup and does not represent an inherent limitation of the technology. As with the λ-HindIII digest, about 3,000 molecules were analyzed in 10 minutes.

These two examples show that the SMS system can be used for rapid sizing of DNA molecules ranging from 2 to 200 kpb. The operating time of 10 minutes is independent of
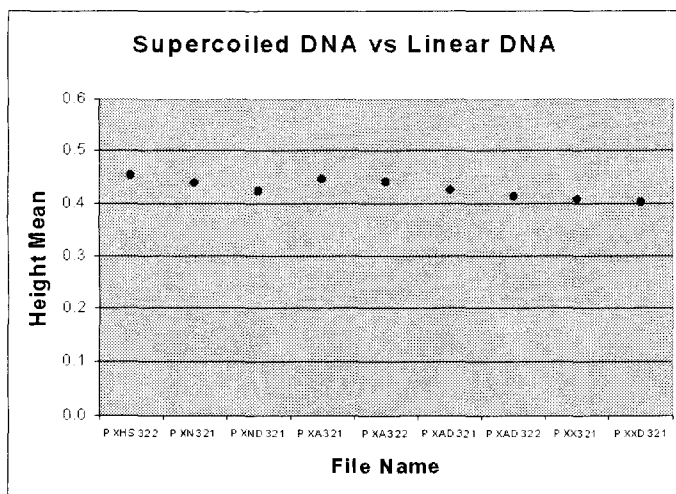
Figure 4.13: Fluorescence of supercoiled DNA versus linear DNA. Prefix *PX* in the file names stands for ϕX174 DNA, the template DNA used here. Both *HS* and *N* following *PX* stand for supercoiled DNA samples, while *A* stands for linearized DNA digested by Ava II and *X* stands also for linearized DNA but digested by Xho I.

the size of the DNA molecules measured and represents a significant improvement over gel electrophoresis in terms of the running and analysis time. DNA molecules of 1 kbp could also be detected because the signal heights stand just above the end of the noise floor. For DNA molecules more than 200 base pairs long, the magnification of the objective lens should be reduced from current $60\times$ or $100\times$ to below $40\times$. The size of the channel can also be made wider, such as 10 μm. Moreover, the width of the channel should be kept uniform from the beginning to the end of the fluorescence detection to prevent stretching of long DNA molecules due to the gradient of flow speed, which occurs at the triangular region of current design (Fig. 2.1).

4.3.2 Linear and Supercoiled DNA

An interesting question that has not been answered yet is whether DNA supercoiling would hinder the access of intercalating dye molecules, i. e, what is the difference in fluorescence intensities of a supercoiled DNA molecule and a linear DNA molecule of the same length. This is also an important question aor an SMS system in order to give a correct size measurement even when the DNA samples are supercoiled. To check this, supercoiled circular 5.4-kbp DNA, ϕX174 (25260-027; Gibco), was used. An original supercoiled form and two linearized forms made by one-cut digestion of restriction endonucleases, Ava II and Xho I, were stained with YOYO-1 and run under the SMS system. The results are shown in Figure 4.13. Obviously, all three forms gave almost the same fluorescence signatures within

the range of measurement errors (C.V. is about 8% here.) Therefore, the effect of DNA supercoiling is not significant for fluorescence single-molecule sizing using intercalating dye YOYO-1.

4.3.3 Bacteria Artificial Chromosomes

For the analysis of complex genomes, the construction of representative large insert DNA libraries is critical. Such a task is predominantly done using a yeast artificial chromosome (YAC) system, where chromosomes are first partially digested, connected with a vector to form circular plasmids, introduced into yeast hosts and replicated millions of times in each yeast colony. Despite the success of YACs, many problems have been described including: chimerism, tedious steps in library construction and low yields of YAC insert DNA. Recently an *E. coli*–based system was developed, the bacterial artificial chromosome (BAC) system, which offers many advantages over YACs[68]. Many BAC libraries have thereafter been constructed[55, 83] and are a basis of large-scale genome sequencing[80].

In order to guarantee complete representation of the chromosomes, these libraries are usually constructed with a high redundancy, a 4 to 7 fold coverage of the original genome. The length of a partially-digested fragment in a BAC library is generally around 50 kbp to 300 kbp, with an average of 110 kbp to 140 kbp. So, for a BAC library of a 100-Mbp chromosome with 5-fold coverage, the number of bacteria clones would be around 4,000, which is still a large number for a fast sequencing facility nowadays[8]. Therefore, it is always preferable to obtain a physical map of contig relations between the BAC clones in advance. With this information, a significantly smaller number of BAC clones could be selected for further sequencing while still covering the original chromosome genome. This in turn saves a lot of time, labor and costs. Moreover, such contig information is also very valuable in the final phase of genomic sequence assembly when a 'shotgun' method is employed.

Physical maps of BAC clones are generally compiled through multiple-complete-digest restriction fragment mapping[7, 51, 82]. By comparing fragment-length distributions of digested BAC clones, contigs that overlap with each other can be revealed (Fig. 4.14). The relations between all BAC clones is then obtained, i.e, the physical map is created. Because of the right dynamic range and the rapid sizing speed, SMS systems become very suit-

---

[8]Each selected seed BAC should be further digested to form a small M13 or plasmid library of about 3,000 clones. Then, complete automatic sequencing is carried out for these clones and the results are reassembled to recover the original BAC sequence[80].
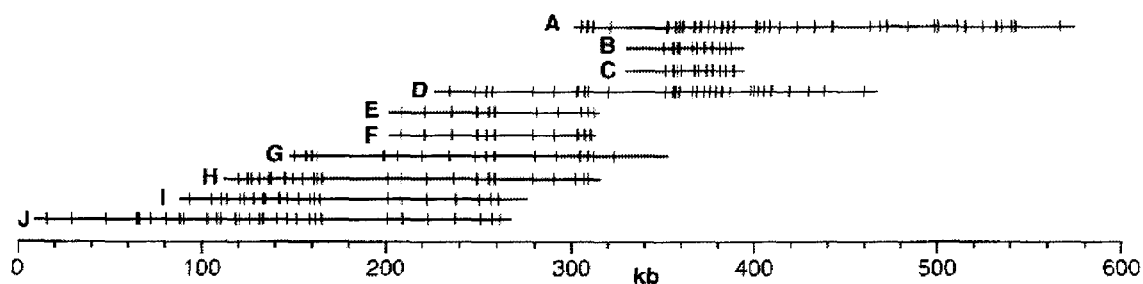
Figure 4.14: Illustration of DNA mapping based on sizing of restriction fragments. BAC clones which have many restriction fragments of the same lengths can be considered as contig candidates. The real relation between them can be obtained after enough sizing information is collected. [7].

able to generate contig mapping of BAC libraries fast. Working with Prof. Melvin Simon and postdoc Sang-dun Choi at Caltech, a protocol for BAC mapping in SMS was devised. Moreover, matching restriction-fragment peaks of BAC contigs were obtained on the SMS system.

The protocol of DNA mapping on SMS consists of six steps: DNA mini-prep, plasmid-safe enzyme treatment, restriction digestion, dye staining, fluorescent single-molecule sizing and final computer analysis. First, *E. coli* BAC clones were grown in a liquid LB broth and the plasmids containing part of Human Chromosome 22 were extracted by a DNA mini-prep procedure based on phenol/chloroform extraction and IPA precipitation. Then, the DNA samples were treated with a plasmid-safe DNase (E3101K; Epicentre, Madison, WS) to get rid of any contamination of linear DNA residues of *E. coli* chromosomes. This step is important. Otherwise, small digested chromosome contaminants would show up as a background in the sensitive SMS runs. After clean-up, the plasmid samples were digested with 4-bp cutters, such as Hind III, Xho I or EcoR I. Then, they were stained with YOYO-1 according to the standard procedure and run through the SMS system. Results of three known BAC contigs are shown in Figure 4.15. Matching fragment peaks were consistent with the results obtained from agarose gel electrophoresis. Because all six runs were taken sequentially, the stability of the SMS can also be seen here.

Even though a successful protocol of BAC DNA mapping has been worked out and accurate sizing results were obtained by the SMS system, the resolution of SMS, which is comparable to pulsed-field gel electrophoresis (PFGE), cannot compete with agarose gel
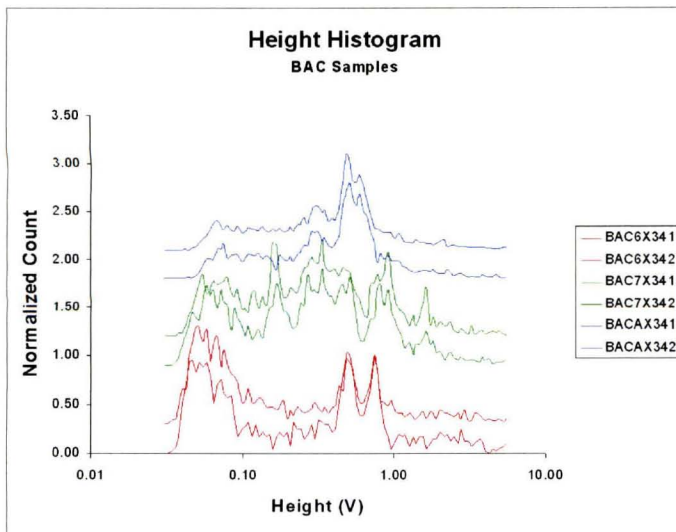
Height Histogram
BAC Samples

Figure 4.15: Restriction mapping of three BAC contigs under an SMS system. BAC clones, 6, 7, and A, digested by restriction endonuclease Xho I were used. Two SMS runs were taken for each sample. There is a matched peak of DNA fragment lengths between 6 and A, and another one between 7 and A, the same as the results from agarose gel electrophoresis.

electrophoresis for 1– to 10–kbp DNA molecules. The latter is about $2\times$ better than SMS. Although SMS is faster in a single run, more digest results would be needed to complete the BAC physical mapping of $\sim$ 4,000 clones. Further improvement is thus necessary for such a task. Nevertheless, for digest mapping of DNA molecules larger than 10 kbp, SMS is surely the better choice because this is close to the limit of the sizing range of agarose gel electrophoresis, where slow PFGE is used conventionally.

4.3.4 Rapid Molecular Fingerprinting

In addition to staining DNA molecules with some intercalating dye so as to obtain the size measurement, we can actually generate fluorescent strands of DNA molecules using in-situ DNA polymerase transcription with the presence of fluorescently labeled single nucleotides. Samples containing regular non-fluorescent DNA molecules are mixed with DNA polymerase, primers which target the regions we are interested in, and single nucleotides covalently attached with fluorophores, such as fluorescein-dNTP, Cy3-dNTP and Cy5-dNTP. The mixture is heated to denature the double-stranded DNA molecules and then cooled down to the right temperature for primers to anneal (hybridize) onto desired regions with complementary DNA sequences. Then, in-situ transcription (copying) of those primed DNA molecules is carried out by DNA polymerase reaction. Because of the presence of fluorescently-labeled single nucleotides, the transcribed DNA products fluoresce brightly by

themselves when excited with the right laser beam. Furthermore, by trimming the products with some restriction enzymes or by doing PCR with a pair of forward and reverse primers, fluorescent DNA molecules of fixed lengths representing the original non-fluorescent DNA templates in the samples are created. We can then run them through the single-molecule sizing system and quickly obtain the important sizing information. There is no need to wait for dye staining in this process.

This method has very important advantages and also tremendous possibilities for applications associated with it. Because primers are used, only specific regions of the DNA templates in the sample are actually copied and become fluorescent. Therefore, we can ignore the large non-fluorescent DNA background in SMS runs while pulling out the important fingerprinting information we would like to obtain. This is thus a very good substitute for the famous fingerprinting protocol — the Southern blot, where DNA molecules are differentiated first according to their sizes by gel electrophoresis, transferred onto a nylon member after an overnight process, and then hybridized against radioactively labeled or fluorescently labeled primers to pull out the same size information of interested regions. Because of the complexity of the transfer process, it is very hard to modify the Southern blot to be compatible with current lab-on-a-chip techniques. On the other hand, every step described above in this new method could be easily incorporated into a single microfabricated device. All we need are an on-chip transcription chamber, an exterior thermoelectric heater, some flow control mechanisms (such as the microvalves described in Chapter 3), and a sizing flow-cell channel. Therefore, we could anticipate that such a device would be demonstrated in the near future. Many applications can be simplified and done automatically in this system, such as DNA fingerprinting of human forensic samples based on VNTR[37, 56] and disease diagnosis based on RFLP[71]. All of them are closely related to genetic studies and our daily lives.

To quickly test the ideas, a simple protocol was worked out and molecular fingerprinting between λ-phage and T7-phage DNA molecules was demonstrated on the SMS system within 4 hours of total working time. First, samples containing either λ or T7 DNA are transcribed by Taq polymerase (ELONGASE 10480010; Gibco) in the presence of primers specific to T7 genome and a mixture of four different kinds of dNTPs, with two thirds of dATP substituted by fluorescein-dATP (NEL465; NEN) (see Appendix B.3). After denaturing (94°C) and primer annealing (55°C), the DNA extension was carried over at 68°C for an
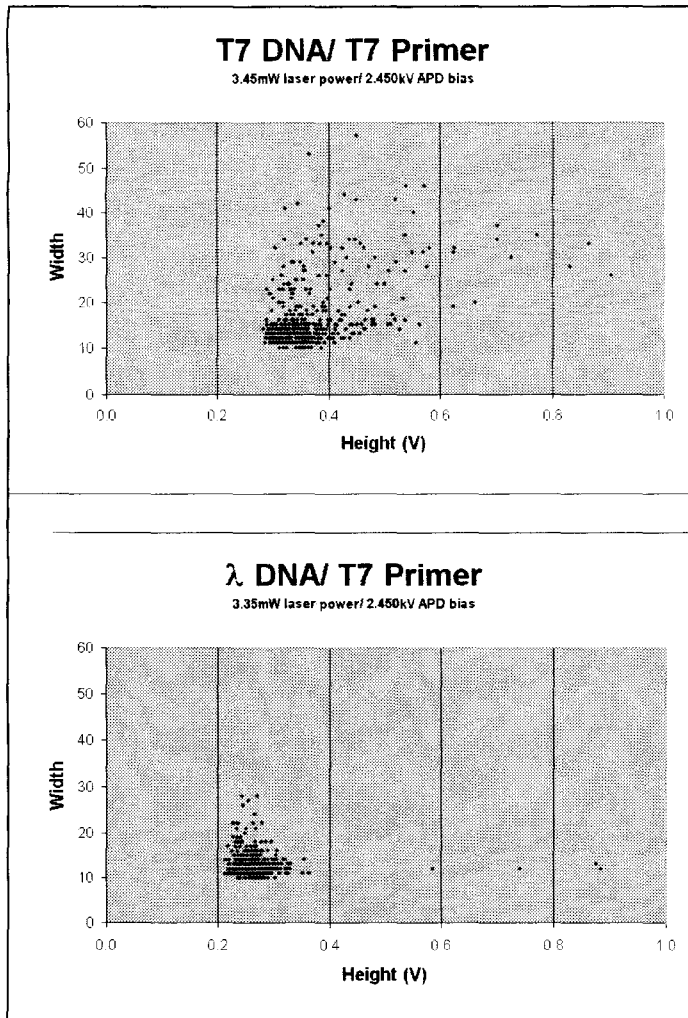
Figure 4.16: SMS molecular fingerprinting of λ and T7 DNA using T7 primers. The top T7 DNA with T7 primers shows a lot of long fluorescent DNA molecules, whereas the bottom λ DNA with T7 primers shows very few fluorescent DNA molecules except some fluorescent background.

hour. Then, unused fluorescent single nucleotides in solution were extracted using a floating-membrane dialysis method for an hour. Standard spin-column purification kits can also be used to speed up this process. However, since the template DNA, λ and T7, here are quite long, dialysis was thus chosen in this case. After purification, samples were diluted to about 100 fM of fluorescently-labeled DNA molecules and run through the SMS system. Two examples of the results, one with λ DNA and the other with T7 DNA, are shown in Figure 4.16. Clearly, there are much long fluorescent DNA molecules in the λ DNA sample than the target T7 DNA sample. Fluorescently-labeled DNA molecules were not of the same size here because restriction enzyme cutting was not employed for these experiments. However, it is actually not necessary in this case, where we just want to determine the

Figure 4.17: Summary of SMS molecular diagnostics of several control (λ-DNA) and target (T7-DNA) samples. A fixed fluorescent threshold was applied and molecules with fluorescence intensities above this threshold level were counted and plotted here.
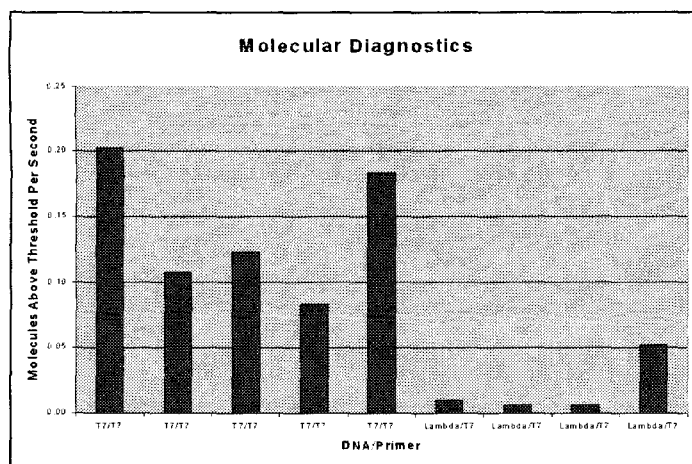
existence of T7 DNA molecules in the sample. For the purpose of a simple human/animal pathogen diagnosis, a threshold algorithm would be very suitable: A voltage threshold can be set to count the number of molecules exceeding a fixed fluorescent level. For example, five T7-DNA target samples and four λ-DNA control samples were measured under the process described above. Then, the number of molecule above a certain threshold in the SMS runs were counted and shown in Figure 4.17. All samples containing target T7 DNA were clearly identified. Only one λ DNA sample shows a near false-positive result.

In summary, prototype work of molecular fingerprinting based on SMS was demonstrated and a general protocol is given on Appendix B.3. However, for more complicate fingerprinting processes, optimized protocols could be developed easily by groups who are interested in using this new rapid fingerprinting method.

4.3.5 Polarization Dependence

In addition to the dichroic filter set which influences the fluorescent signal intensity, 'polarization' of the laser beam turns out to be the most important factor in determining SMS performance[1]. It affects not only the signal height, but also the variance significantly. With the measurement done by Shuli Eyal on our new SMS system, the dependence of peak height and C.V. of Lambda-phage DNA measurement at different angles of laser polarization to the channel axis is shown in Figure 4.18. The highest signal and lowest variation was obtained when the laser polarization is perpendicular to the channel and the flow directions. On the other hand, if the polarization is off by 90°, a huge C.V. of 15%–20% was observed.
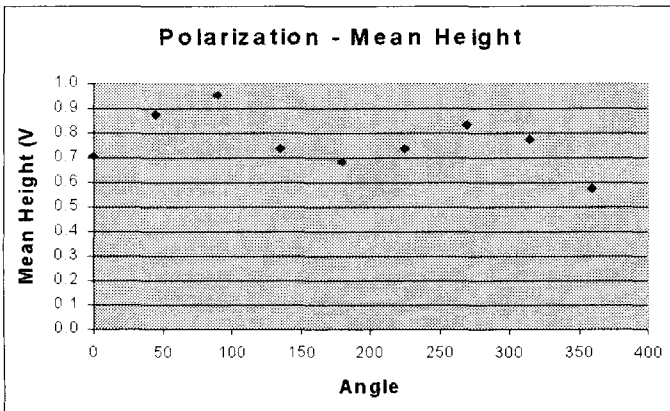
(a).
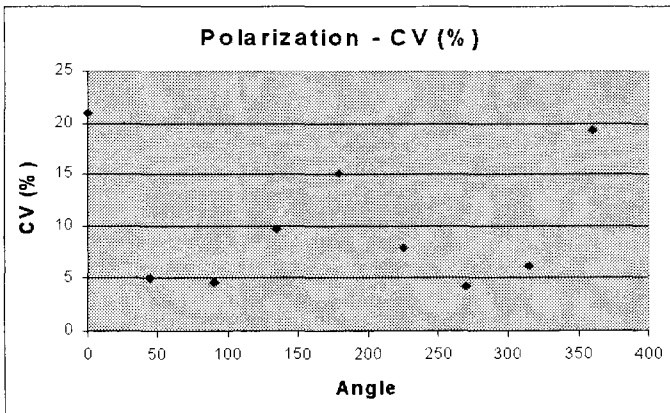
(b).

Figure 4.18: Effects of laser polarization in an SMS system. The Angle here is the angle of the laser polarization to the longitudinal axis of the flow channel. λ DNA samples were used for this test.

This could be explained by the polarizability of the intercalating dye molecules. Each chromophore (arm) of these cyanine dyes has an electron donor and an electron acceptor. Because of the flat benzene ring substructures, they orient perpendicularly to the axis of DNA molecules when sticking into it. However, as the DNA molecules flowed through the channel, they were stretched by the velocity gradient and thus in parallel to the flow direction, i.e, the channel longitudinal axis. Therefore, those stained dye molecules were also mostly oriented around 90° relative to the channel axis. When the laser is polarized in the same direction, the excitation becomes more efficient and it is much less susceptible to the rotation and the exact orientation of those dye molecules. Such a phenomenon becomes more perceivable when the DNA molecules are long, such as the λ DNA molecules used here. Therefore, for all runs of single-molecule DNA sizing, the laser polarization is set to be in a perpendicular direction to the channel axis.

Two results are worth mentioning here. One is that this effect was not seen for fluorescent beads, which is obvious. The other is that the relative angle of the laser polarization to the dichroic filter, dielectric mirrors and so on has almost no effect on the overall signal strength and variation. Only the angle of final laser illumination and the channel axis matters.

4.3.6   Intermolecular DNA Cross-Linking by Intercalating Dimers

Intermolecular cross-linking of DNA molecules through bifunctional intercalators, such as antibiotic Luzopeptin and fluorescent dimer dyes TOTO-1, YOYO-1 and EthD-1, has been reported for many years[9, 35]. It was mainly inferred from the observation of double-band formation in gel electrophoresis when the concentrations of DNA molecules and intercalators were both high at the staining process. Therefore, the intermolecular cross-linking of DNA was hypothesized and underlying mechanisms were proposed. With the power of SMS systems, we were able to verify this directly for the first time in a single-molecular scale. According to the experimental results, a strong clamping effect of two hybridized DNA molecules by the intercalators right at the hybridization region was more likely the main cause of this double-band formation in SMS runs.

Basically, there are two different kinds of intermolecular cross-linking of DNA through the intercalators, as shown in Figure 4.19. The first kind of DNA cross-linking refers to the type I binding mode when the two chromophores (arms) of an intercalator bind onto the same strand of DNA and it happens to be at the hybridization region of two DNA molecules.
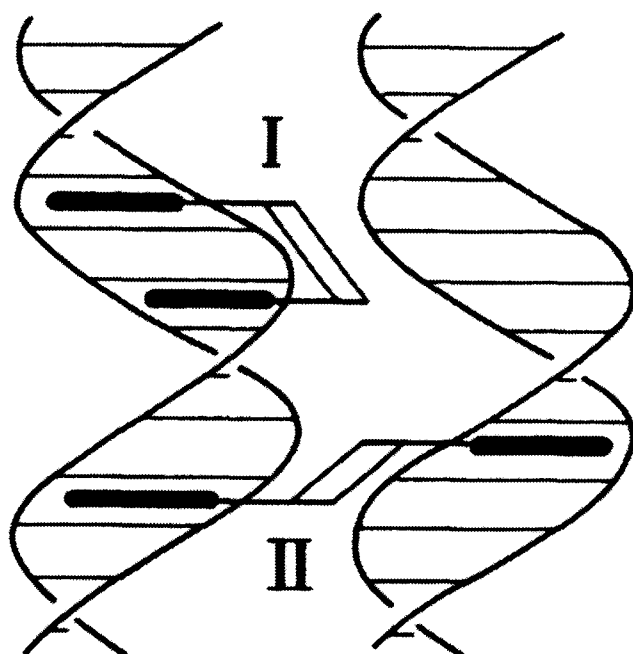
Figure 4.19: Binding modes of DNA intercalators. In type I intercalation, the two intercalative chromophores intercalate with the same DNA or two hybridized DNA molecules, intermolecular cross-linking of the first kind. In type II intercalation, the two chromophores intercalate with two separate DNA molecules, intermolecular cross-linking of the second kind. [35].

The second kind of DNA cross-linking refers to the type II binding mode when the two chromophores intercalate with two separate DNA molecules, where a simple intermolecular cross-linking of unrelated DNA molecules was formed. In addition to hybridization, the other difference between this two kinds is their binding coefficients. The bis-intercalating of the first kind has a high binding coefficient as the dimer itself, whereas the binding coefficient of the second kind is similar to its monomer chromophore, about 1000 times less than the dimer (see Table 4.5). Therefore, the cross-linked DNA molecules of the first kind are more likely to survive when the dye concentration in solution is reduced later after staining, which is common in most running conditions, both SMS and gel electrophoresis.

Staining λ DNA molecules with YOYO-1 at a concentration of more than ten times higher than normal ($\sim$0.2nM λ DNA and 2.5μM YOYO-1), the SMS results showed clearly a second group of DNA molecules who had fluorescence intensity exactly twice of normal λ DNA molecules (Fig. 4.20). Since there was no enzyme involved in this cross-linking process, the quality of λ DNA was preserved. Therefore, the result here looks much cleaner in comparison to the result of λ-ladder shown previously in Figure 4.12.

This cross-linking effect is actually very strong. After staining (50°C for 2 hours), the
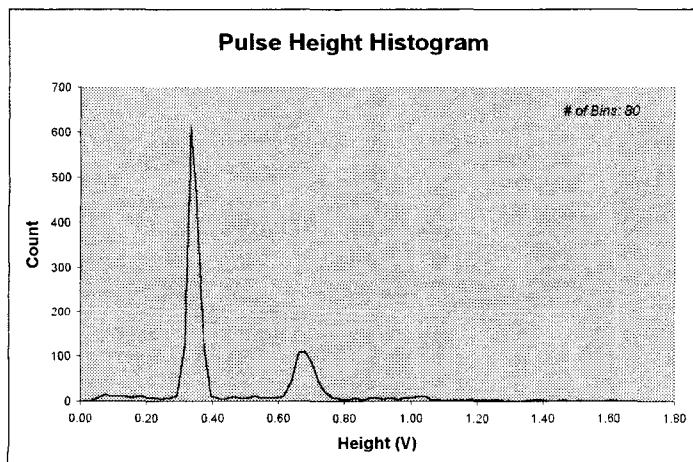
Figure 4.20: Direct observation of intermolecular cross-linking of λ DNA molecules by fluorescent intercalating dye YOYO-1. The first group is normal stained λ DNA molecules. The second group contains cross-linked λ DNA doublets, which has exactly twice of the fluorescence.

sample was diluted in STE buffer to normal staining condition (15 pM) and stored at 4°C overnight. Later, before being introduced into a microfabricated device for the SMS test, it was diluted again by 20 times with a final dye concentration of only 2 pM. However, the cross-linked DNA molecules remained in contact through the whole dilution process. We could even heat the overnight sample at 65°C for 10 min, that normally would separate any hybridized DNA molecules. However, in this case, the concentration of DNA molecules remained the same after heating, and the DNA doublets could still be seen clearly under an epi-fluorescence microscope. With such a low concentration of free dye molecules and a long waiting time, it is more likely that cross-linked DNA molecules of the first kind play a more important role than those of the second kind.

A common practice for general SMS staining is to preheat the DNA sample at 65°C for 10 minutes before mixing with the staining dye solution (Appendix B.2). Otherwise, those hybridized DNA molecules would show up and mess up the actual bands of DNA fragments which we would like to get. With much lower DNA and dye concentration during the staining process than the special one described above, the probability of intermolecular DNA cross-linking of the second kind is significantly reduced. Moreover, in our experience, the preheating treatment actually works well in the way to eliminate those undesired bands, which should only be effective to prevent the DNA cross-linking of the first kind. Therefore, we can conclude that the clamping effect of hybridized DNA molecules by fluorescent intercalating dyes is the dominant source of double-band formation in SMS systems. However, for those where concentrations of DNA molecules and intercalators are both relatively high,

further investigation should be made if necessary[9].

4.4   Conclusion

We have shown that the SMS systems can be used for rapid, efficient sizing of DNA molecules ranging from 2 to 200 kbp. The typical operating time of 10 min is independent of the size of the DNA molecules being sorted and represents a significant improvement over gel electrophoresis. Furthermore, the devices require only tens of femtograms of DNA to operate, making it possible to envision future applications in which an SMS system obviates the need for PCR.

By directly measuring length via fluorescent dye intercalation, SMS systems allow an absolute measurement of length, which eliminates the need for sizing standard in each run. Finally, for gel electrophoresis, the resolution decreases as the molecules being analyzed become longer. SMS has the opposite property: the longer the molecules, the better the signal to noise, and the fewer fluctuations because of the statistics of dye binding (Fig. 4.10). For the longest molecules in the lambda ladder (Fig. 4.12), the SMS resolution begins to degrade as a result of the optical setup: the molecules become bigger (or longer) than the region illuminated by the laser beam used to excite fluorescence. This problem can be easily remedied in the future, as applications require. The ultimate sizing limit probably will be determined by the ability of DNA molecules to survive fluid shear forces in the device.

Because the devices are microfabricated, additional features could be added directly to the chip. One example is the multiplex system described in Section 4.2.4, where multiple channels were designed and incorporated into the device easily. Moreover, one can envision future SMS devices with cascaded T channels capable of sorting fragments according to size and then recutting the individual fragments with different enzymes for ordered mapping, something that is not possible with electrophoretic or optical mapping techniques (Fig. 4.21). Furthermore, because the detection system is all solid state and does not in principle require imaging optics, it should be possible to build an integrated SMS device with semiconductor laser excitation and detection on a single chip.

---

[9]A way to check the relative weight of these two different kinds of DNA cross-linking mechanisms is to use Mung Bean nuclease, an enzyme that will chop off all the sticky single-stranded overhangs at the ends of DNA molecules. Therefore DNA cross-linking of the first kind could be totally eliminated. A complete experimental tests based on this are currently on the way for λ DNA in our lab.

waste   DNA sample
detection
digestion
area
waste
restriction enzyme
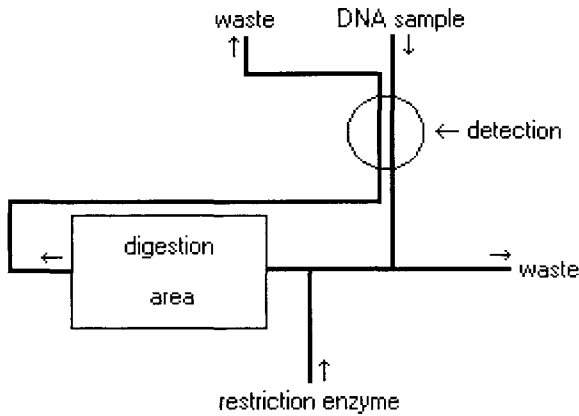
Figure 4.21: Sequential digestion on a single device.

As a demonstration of the real power of SMS, prototype work of two important applications using SMS systems were devised: DNA mapping of BAC libraries and molecular DNA fingerprinting. The former is essential to many genomic projects and the latter gives a fast DNA molecular typing without the need of PCR. Restriction fragment length polymorphism (RFLP), which is used commonly in biological studies and disease diagnosis[71], can also be easily incorporated into this SMS system because it is actually part of the BAC DNA mapping. With a significant breakthrough of speed and quantity for a fundamental tool — DNA sizing, enormous amount of possible applications in biological studies and hospital diagnosis could thus be anticipated.

Chapter 5 Multiple Disease Diagnosis on a Single Chip

5.1 Introduction

We experience various diseases in our daily lives, which may be caused by genetic inheritance, infectious transmission, accidents, or mental malfunctions. Diagnosis of the sources, types and cures of the diseases we have are usually made by doctors based on the symptoms and the results of some simple tests and observations. However, since there are so many similar diseases, further diagnoses are generally required to precisely differentiate them, especially for those with infectious or genetic roots, such as HIV, tuberculosis, hepatitis and human BRCA1 breast cancer. Conventionally, these are done mostly through bacterial cultures and antibody/antigen reactions[49]. Recently, DNA restriction fragment length polymorphism (RFLP) diagnosis has also become available for mutation-intense diseases, such as tuberculosis[71], the second largest infectious disease in the World[1], which kills more than 2 million people a year[73]. Nevertheless, all the diagnostic procedures are generally done by lab technicians using test tubes or petri dishes, in which significant amounts of sample volumes are required. Moreover, these procedures require a lot of human attention and become very labor-intense when multiple disease diagnostics are required.

State-of-the-art DNA chips, pioneered by Affymetrix[11, 46] and other research groups[65], have shown promising results for multiple disease diagnoses on a tiny chip[61]. An array of various DNA hybridization probes is laid down on the substrate. They are designed to react only with specific target DNA fragments from chosen disease entities. Nevertheless, hundreds of microliters to a few milliliters of samples are still required to cover the whole chip. In addition, since the diffusion constant of DNA fragments is small, $\sim 10^{-7}$ cm^2/s for 1-kbp DNA fragments[2], it takes a long time for target DNA molecules to find the right hybridization spots[2]. Therefore, many target DNAs are actually lost during this

---

[1]Next to the Acquired Immune Deficiency Syndrome (AIDS).

[2]Diffusion length $l = \sqrt{Dt}$, where D is the diffusion constant and t is the time. Let D be 10^{-7} cm^2/s for a typical 1-kbp DNA and t be an hour. Then, the diffusion length l would be 0.19 mm. So, if only passive

process. Usually, PCR amplification is thus required to obtain enough DNA sample, which complicates the process and gives new sources of possible errors.

On the other hand, several techniques are currently being developed towards the goal of an integrated fluidic lab-on-a-chip[25, 39, 44, 77, 81, 84]. They offer us the possibility to automatically manipulate small volumes of biological samples on a small device, where reactions and diagnoses could be carried out. Among them, monolithic microvalves and micropumps made from silicone elastomer as described in Chapter 3 have great potential because of their simplicity, robustness, easy fabrication and low cost. Therefore, instead of a passive DNA hybridization chip, a better approach is to use these microfluidic devices to *actively* pump solutions of target DNA over a set of anchored pathogenic probes in order to ensure that all of the target DNA is exposed to each of the probes. This would provide increased sensitivity as well as decreasing the amount of time needed for hybridization. Chips with high sensitivity would also be useful for measuring single cell gene expression. This higher sensitivity may eliminate the need for PCR in many cases of pathogen detection and therefore make it possible to do multiple disease diagnosis with one integrated lab-on-a-chip.

Making such chips requires a number of important technological advances in the current state of the art of microfluidics. First, one needs to be able to fabricate microfluidic devices in a way that is compatible with the delicate surface chemistry required to anchor or synthesize DNA probes on a chip. Second, one must be able to effect the desired patterning or surface chemistry. Third, one must be able to manipulate small amounts of material and perform the necessary biochemical reactions on chip. Finally, one needs to be able to pump the targets over the probes.

The first two issues we have addressed by using "soft lithography", which in part refers to the notion of fabricating channel systems out of soft elastomeric materials using replication molding techniques[86]. We have found that elastomeric devices provide a number of important advantages over conventional micromachining, such as ease of fabrication, room temperature sealing of devices to glass substrates, good optical properties, and low materials cost, especially compared to single crystal silicon. Microfluidic networks fabricated in such a manner can easily be sealed to substrates with delicate surface chemistry (Chapter 2).

---

diffusion is used, each hybridization spot can only cover an area of about 0.4 mm in diameter. Even after a day, 24 hours, only target samples in an area of ~ 2 mm in diameter can possibly reach a specific probe to give a positive signal. This is an extremely slow process for large molecules like DNA.

Another aspect of soft lithography we have taken advantage of is the ability to chemically pattern surfaces using fluid flow[19, 38]. The third and final issues we have addressed by developing a multilayer fabrication process in silicone elastomer[77]. This multilayer process allows easy fabrication of devices with moving parts, including microfluidic valves and pumps (Chapter 3).

Here I would like to describe our design of an active multiple disease diagnosis lab-on-a-chip device. Then, new experimental results of its building components are shown. One is that we chemically patterned surfaces with biotin/avidin and DNA using fluidic networks in a way that is compatible with further fluidic processing. The other is to show how pumps can be incorporated into an integrated device to both meter reagents and pump fluid in a closed loop. Fast inline mixing and rotary pumping were demonstrated to overcome the slow hybridization process. Rotary flow in a closed loop cannot be achieved by electrophoresis or electroosmotic flow used in most common lab-on-a-chips because of the existence of two electric polarities. Finally, a model system was successfully built, where avidin coated 1-μm beads were captured onto the bottom biotin spots within 4 minutes when the pump was turned on. In contrast, when we simply relied on passive diffusion, only beads very local to the reaction spots were captured even after hours of waiting time.

5.2 Device Design and Fabrication

Multilayer soft lithography is a process recently developed in our lab in order to make 3-D monolithic elastomer devices with a combination of air and fluid channels (Chapter 3). When an air channel passes above another fluid channel, the thin membrane between these two channels becomes a valve. By applying air pressure in the air channel, the membrane collapses and stops the fluid flow. Releasing the pressure then reopens this valve. Three valves in series become a peristaltic pump when an appropriate on/off air pressures are applied in a sequence. For example, 100, 110, 010, 011, 001, 101 pumps water to the right, where 1 and 0 represent closed or open valves respectively. A schematic diagram is shown in Figure 3.8. A brief description of the fabrication process follows.

Air and fluid mother molds were fabricated on silicon wafers by photolithography. Photoresist (Shipley SJR 5740) was spun onto the silicon substrate at spin rates corresponding to the desired channel heights. After photolithography, intrusive channels made of photore-

sist were formed. Fluid channel molds were baked on a hot plate of 200°C for 30 minutes so that the photoresist could reflow and form a rounded shape, which is important for complete valve closure[77]. A one-minute trimethylchlorosilane (TMCS) vapor treatment was applied to these molds before each RTV replication process to prevent adhesion of cured RTV to the photoresist. With this protective coating, molds can be reused many times.

30:1 GE-RTV 615A:615B was spun on a fluid channel mold at 2,000 RPM, which covers the photoresist channel and leaves a thin membrane on top of it. At the same time, 3:1 GE-RTV 615A:615B was poured onto an air channel mold. After baking both in an oven of 80°C for 20 minutes, the block of 3:1 RTV with air channels at the bottom was peeled off from the second mold. Air supply through-holes were punched. Aligned to the fluid pattern under a microscope, it was then pressed against the thin 30:1 RTV on the first mold. A post-bake of an hour at 80°C made the two silicone pieces chemically bond to each other. After it was peeled it off from the mold and the fluid through-holes were punched, the monolithic RTV device could seal hermetically to a glass cover slip. In practice, this glass cover slip was chemically patterned in advance, as we will describe in Section 5.3.1, to make an active diagnostic chip. If high-resolution transparency photomasks were used (minimum feature size: ∼ 10 μm), the whole process from the design to the final products can be accomplished in one day.

A design of a multiple disease diagnosis chip is shown in Figure 5.1. The central loop is the key component, at which the DNA hybridization probes are laid down along the ring on top of the glass substrate. DNA samples and later fluorescent intercalating dyes can enter from the two branches of the top T-channel. On/off states of each microvalves are controlled by external pneumatic valves (LHDA1211111H; The Lee Company, Westbrook, CT) which either apply 50-kPa air pressure to the microvalves or vent them to the atmosphere. A maximum cycling frequency of 75 Hz has been demonstrated with complete opening and closing of the valves (Chapter 3). Snapshots of a final assembled device are shown in Figure 5.2.

5.3 Results
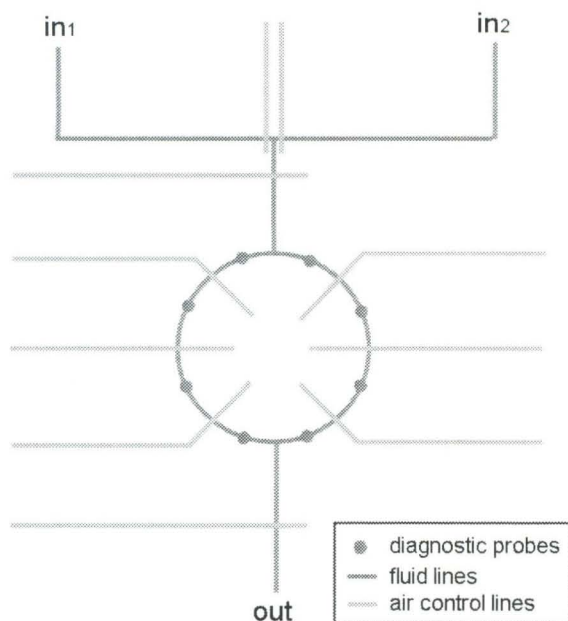
Figure 5.1: Illustration of the design of a multiple disease diagnosis chip. Any intersection of the bottom fluid channel and a top air control channel forms a microvalve. Three valves in series along the central loop become a peristaltic pump when an appropriate on/off sequence is applied.

(a).

(b).
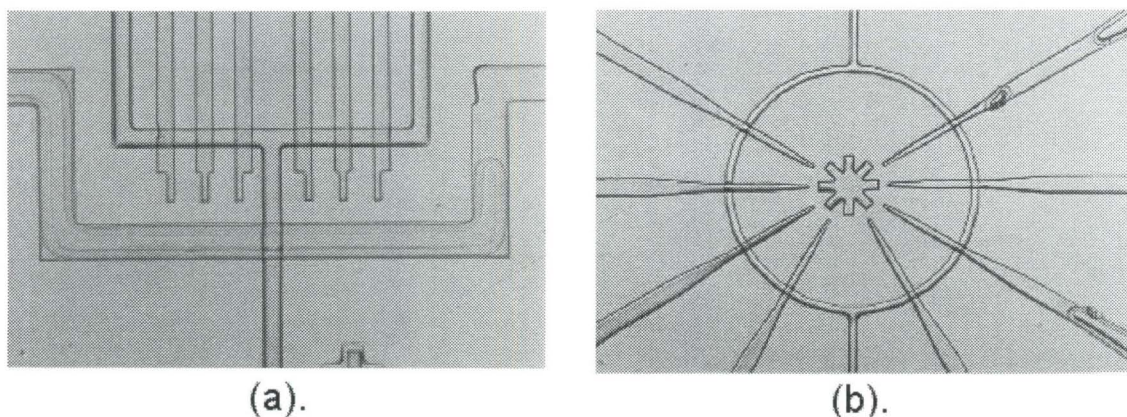
Figure 5.2: Snapshots of a two-layer DNA diagnosis chip. (a) shows the input mixing T-shaped fluid channel and six corresponding control microvalves. The wide $100\text{-}\mu$m air channel is used to close the inlet when the peristaltic pump at the central loop starts operating for hybridization. (b) shows the central fluid loop for DNA hybridization. Any three of the finger air channels form a peristaltic pump. Fluid channel width: $50~\mu$m.

5.3.1 Surface Patterning

We developed two independent methods of surface patterning. The first method allows patterning of the protein streptavidin, a common biochemical "glue" that binds biotin with nearly covalent strength. With the streptavidin surfaces, one can selectively anchor biotin-labeled reagents, including proteins and nucleic acids. The second method allows direct attachment of amine-modified DNA molecules to the surface using a commercially available surface chemistry from the company Surmodics.

In the first method, we derivatized half of the surface of a cover slip (VWR #1) with biotin[18, 78]. We then attached channels and flowed avidin-fluorescein conjugate down them, after which we flushed the channels with water, removed the channels, and flushed the entire cover slip again. The avidin molecules bound to the derivatized part of the surface with high affinity in the regions defined by the channels, forming fluorescent stripes as shown in Figure 5.3 (a). The regions that were not derivatized with biotin functioned as a control and showed a much lower level of avidin binding.

We were also able to perform successive patterning steps to the surface. In this case, we patterned the surface with non-fluorescent streptavidin by bonding an elastomeric device with channels to the substrate and flowing the streptavidin down the channels. As before, the streptavidin bound selectively to the surfaces that were exposed to the channels, and not to the surface covered by the elastomer. Since streptavidin is a tetramer, each molecule has at least two exposed groups free to bind more biotin. We demonstrated this by then removing the elastomeric channels and re-bonding in an orientation that was rotated by 90°. We flowed biotin-fluorescein conjugates down the channels and then washed with water. From the images in Figure 5.3 (b), it is clear that the fluorescent biotin binds selectively to the regions that are derivatized with streptavidin.

We also prepared surfaces patterned with DNA using commercially available silanized slides (3D-Link; Surmodics, Eden Prairie, MN). DNA samples were prepared by PCR of a 2 kpb region of λ-phage DNA using amino-terminated primers. The DNA was attached in situ by flowing it through an elastomeric channel replica made from the air channel mold of the diagnosis chip, i.e, the finger pattern in Figure 5.2 (b). After overnight incubation, the elastomeric device was peeled off from the slide, and washing and immobilization steps were followed according to the 3D-Link protocol. To show that the DNA was attached to the sur-
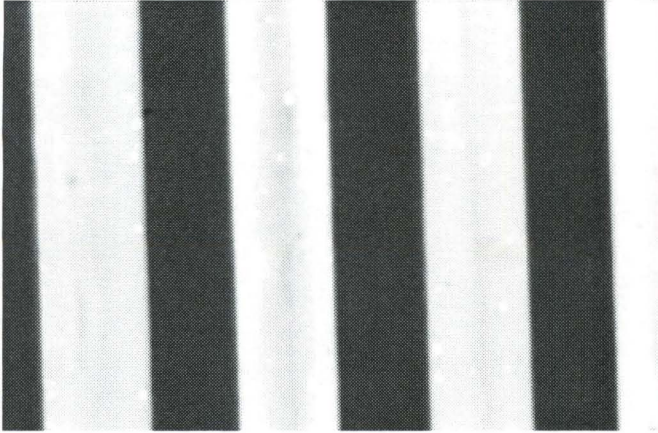
(a).
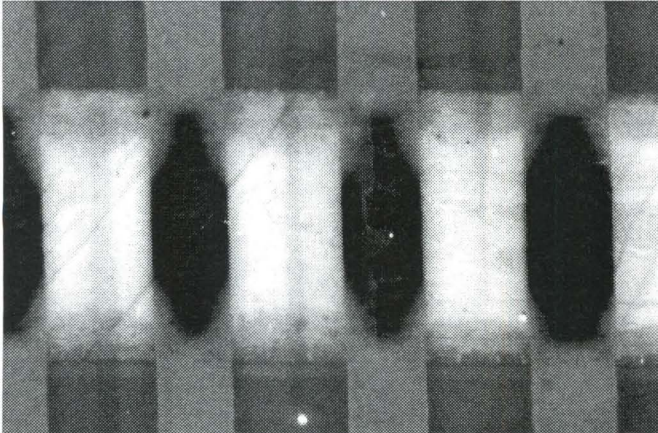
(b).
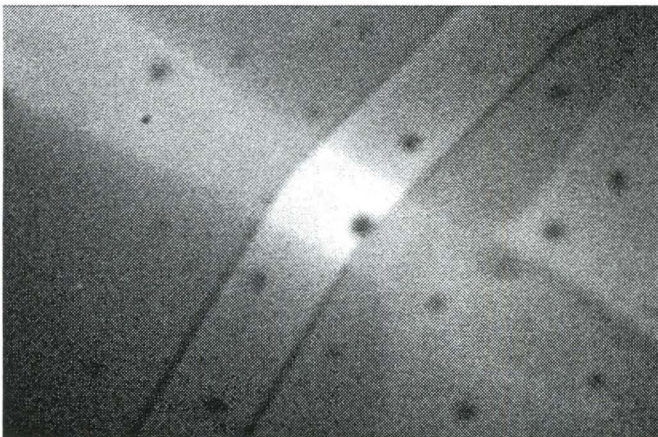
(c).

Figure 5.3: Images of chemically patterned cover slips. (a) A line pattern obtained by flowing avidin-fluorescein conjugates vertically on a biotinylated cover slip. (b) A checkerboard pattern obtained by flowing streptavidin horizontally (200 μm) and biotin-fluorescein conjugates vertically (100 μm). (c) DNA patterned on a Surmodics slide lights up when fluorescent dye PicoGreen was flowing in the central ring loop. Top-left to bottom-right was DNA with slightly auto-fluorescence. Top-right to bottom-left was part of the central ring of a diagnosis chip under a dark-field illumination.

face, we aligned and attached a diagnostic RTV device (as shown in Figure 5.2) to the same slide. Then we flowed the DNA intercalating dye PicoGreen (P-7581; Molecular Probes) through the bottom fluid channel, of which the central ring intersected with every DNA finger pattern on the slide. The intersection of the channels fluoresced, as shown in Figure 5.3 (c).

In summary, we have demonstrated two methods of chemical patterning of surfaces using soft lithography, and shown that the chemical patterns can also be interfaced with elastomeric microfluidics. These methods are the starting point for proof of principle of DNA diagnostics, and provide the foundation to demonstrate sensitive and selective DNA detection on chip. It is a straightforward extension to use protein-binding assays with these fluidic systems as well. One issue that remains to be addressed is the strength of adhesion — the elastomer adheres to derivatized surfaces, but not with the same strength as to clean glass.

5.3.2 Inline Mixing and Rotary Pumping

Our prototype DNA diagnostic chip has a junction for mixing and metering reagents, which then leads into a fluidic loop (Fig. 5.2). The probe molecules will be anchored in the loop so that the targets can circulate around. The loop has a peristaltic pump around it to control circulation. The fluidic connections into and out of the loop are controlled by input and output valves, respectively.

We have demonstrated mixing and metering in the first part of the chip. A solution containing fluorescent dye can be mixed with an aqueous solution — the flows can be alternated with two different valve-firing schemes. If the valves are opened and closed in synchrony, the fluid mixing is controlled by diffusion. One observes two segregated flows when the valves are open, which quickly mix by diffusion when the valves are closed. If the valves are opened and closed alternately, then slugs of fluid are injected into the stream.

We have also pumped fluid within the closed loop using the peristaltic pumps on the perimeter. The channels were loaded with fluorescent beads (2.5 μm in diameter). The beads could be visualized as the fluid circulated around the loop and clearly showed rotary motion with no net flux into or out of the loop. Thus reagents can be repetitively exposed to diagnostic probes anchored on the surface, and their binding will not be limited by diffusion. All target DNA in a sample should be eventually captured by their corresponding probes
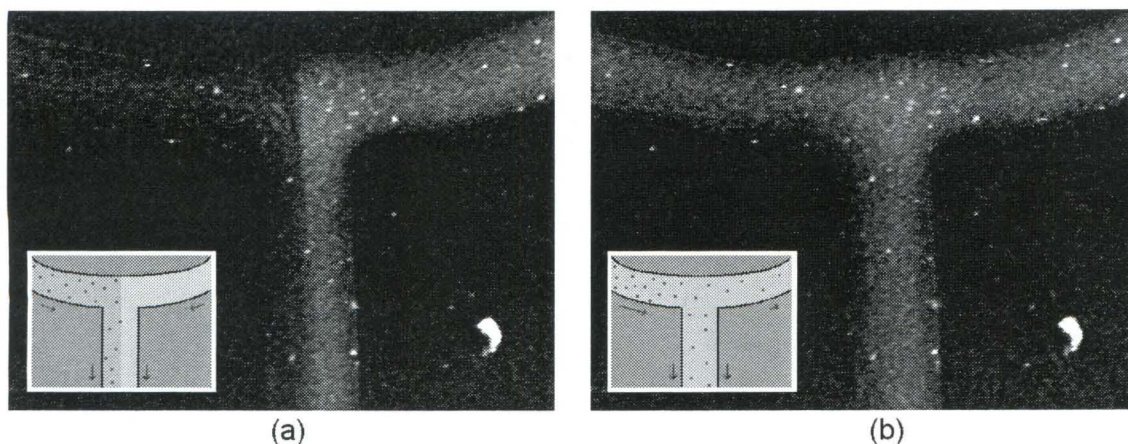
Figure 5.4: Inline mixing by rotary pumping. (a) No pumping. Buffer containing fluorescent beads (left) and buffer containing fluorescent dye (right) don't mix with each other because of laminar flow profile. (b) Active rotary pumping. The peristaltic pump at the ring, where the liquids come from, is turned on. Both dye and beads are well mixed at the output channel. (Insets) Illustrations of the distribution of beads and fluorescent dye in the fluidic channels.

after several passages. None of those precious target DNA molecules will be wasted, and therefore PCR amplification would no longer be necessary in most cases.

Such a device was also used to rapidly mix viscous liquids, since the parabolic flow profile of the fluid tends to "wrap" the two fluids around each other. Figure 5.4 shows an example of this 'inline rotary mixing'. Buffer containing fluorescent beads came in from the left input channel at the T-junction while buffer containing fluorescent dye FITC came in from the other side (Fig. 5.2 (a)). Because of laminar flow profile, these two fluids didn't mix with each other and actually split the flow channel into halves, one side with only beads and the other side with fluorescent dye. When they enter the central ring, the ring was also split into two distinct parts: On the left-hand side, there were just beads flowing through and on the right-hand side, there was only bright and uniform fluorescent dye. At the bottom of the ring, these two flows met with each other again as shown in Figure 5.4 (a). The channel was split into two distinct portions again. However, once we turned on the peristaltic pumping at the central ring, the situation suddenly changed significantly. Both dye and fluorescent beads were well mixed at the output channel as shown in Figure 5.2 (b). Part of the fluid was actually pumped back to the input of the ring and forced the two distinct streams to mix with each other. Such a fast inline mixing by rotary pumping would be very useful

in many microfluidic systems where time and space is critical, especially when the solution contains substances with small diffusion constants, such as DNA and micron-sized beads.

5.3.3   A Biotin/Avidin Model System

In order to visualize the binding reaction easily, a biotin/avidin model system was built to show the significant difference in terms of detection efficiency between a *passive* and an *active* diagnosis chip. An RCA-cleaned cover slip was first patterned by flowing biotinylation solution though an attached RTV device with eight finger channels, which was actually made from the air-channel mold as in Fig. 5.2 (b). After overnight incubation, the RTV device was peeled off and the cover slip was washed by DI water. A multiple disease diagnosis device (Fig. 5.2) was then attached with its center aligned to the center of biotinylated fingers. Therefore, the central ring would be able to intersect with all biotin fingers and form eight diagnostic spots. The pattern shown in Figure 5.3 (c) was made in exactly the same manner except that the DNA molecules were anchored on the surface there instead of biotin molecules.

After the biotin/avidin diagnosis device was made, 1-μm fluorescent beads (F-8776; Molecular Probes) coated with NeutrAvidin, a derivative of avidin with less nonspecific binding, was introduced into the ring from the input channel. Once the ring was filled, the flow was shut off right away. Because of the strong affinity between avidin and biotin, beads that were close to the biotinylated spots would be grabbed onto them and show positive diagnostic signals. However, when we simply relied on passive diffusion, no difference of bead concentration between biotinylated spots and the regular channel was observed even after we waited for 30 minutes. For one device, we actually waited for 4 hours and the biotinylated spots finally started to show up. Most of the beads within about 50 μm to the biotin pad were grabbed onto it. It is a very slow process and beads on one side of the ring would never have a chance to get onto the detection spots on the other side, a necessary condition for sensitive *multiple* disease diagnostics[3]. However, on the other hand, once we turned on the peristaltic pump, beads were actively moved in a loop now. Within 4 minutes,

---

[3]The diffusion constant D of 1-μm beads is $\sim 2.5 \times 10^{-9}$ cm^2/s [4], 40 times slower than 1-kpb DNA molecules ($D = \sim 1 \times 10^{-7}$ cm^2/s). So, 4 hours would equal to 6 min for 1-kbp DNA molecules. It is still a slow process for them to diffuse only across 50 μm in comparison the active pumping scheme, several millimeters in 4 minutes. At least, two orders of magnitude in speed can be achieved even for the 1-kpb DNA molecules.
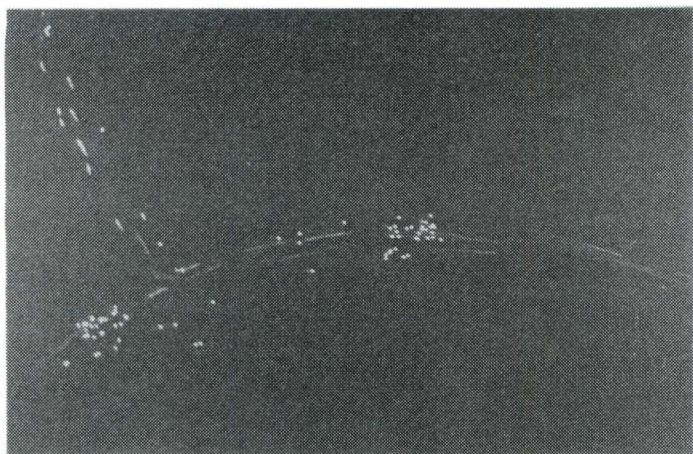
Figure 5.5: A snapshot of a running biotin/avidin diagnosis chip, where two biotin pads at the central ring are shown. This picture was taken 4 minutes after the peristaltic pump started. Clearly a lot of fluorescent NeutrAvidin beads had bound onto those biotin pads. Thin stripes are beads which was still moving in the ring loop while this picture was taken.

more than 80% beads in the central ring were quickly grabbed onto those biotinylated spots as shown in Figure 5.5. Therefore, as we all predicted, huge time difference was shown between a passive and an active diagnostic devices.

5.4 Conclusion

The first integrated microfluid lab-on-a-chip system based on monolithic elastomeric microvalves and micropumps was demonstrated. It includes surface patterning using elastomeric flow channels[19, 38], switching flow-control valves, a peristaltic pump and a biotin/avidin diagnosis scheme. Strong time differences between passive diffusion and active pumping methods were seen clearly. More than two orders of magnitude improvement in terms of diagnostic speed was obtained. Moreover, fast inline mixing was demonstrated with the same active pumping mechanism. Laminar flow and diffusion limitation in this low-Reynolds number regime can be overcome easily by this active pumping agitation.

For a multiple DNA diagnosis chip, various DNA hybridization primers bearing a biotin function group at the end could be brought into different finger channels during the surface patterning process. Therefore, multiple hybridization spots would form along the central ring when the active RTV device is aligned and attached. Target DNA could then be brought in from the top, circulated several times in the central ring loop and eventually they would find the right spots to hybridized on. After flushing the residue out to the bottom outlet, fluorescent dye used to determine the hybridization could be brought in

from another input channel. Multiple disease diagnosis could then be made in this fashion.

With the power of multilayer soft lithography, many complicated functions can easily be designed and fabricated as we have shown here. We anticipate that more active lab-on-a-chip devices will be developed rapidly. The problem of buffer depletion due to electrolysis in electroosmotic or electrophoretic flow control does not exist in these devices. Rotary pumping, rapid cell sorting, precise chemical metering and time-controlled reactions are all possible.

Appendix A   Abbreviations

AIDS Acquired immune deficiency syndrome.

APD Avalanche photodiode.

BAC Bacteria artificial chromosome.

BSA Bovine serum albumin.

DMSO Dimethylsulfoxide ($(CH_3)_2SO$).

FACS Fluorescence-activated cell sorter.

FITC Fluorescein isothiocyanate ($C_{21}H_{11}O_5$-N=S).

HMDS Hexamethyldisilazane ($(CH_3)_3Si)_2NH$.

HIV Human immunodeficiency virus.

IPA Isopropanol (C_3H_7OH).

LAAPD Large-area avalanche photodiode.

MEMS Microelectromechanical systems.

NA Numerical aperture (see [3]).

PCR Polymerase chain reaction.

PDMS Poly(dimethylsiloxane) ($(CH_3)_2SiO)_n$.

PFGE Pulsed-field gel electrophoresis.

PMMA Poly(methyl methacrylate) ($C_5H_8O_2)_n$.

PMT Photomultiplier tube.

RFLP Restriction fragment length polymorphism.

RIE Reactive ion etch.

SDS Sodium dodecyl sulfate ($C_{12}H_{25}SO_4Na$).

SEM Scanning electron microscope.

SMS Single-molecular sizing.

TMCS Trimethylchlorosilane $(CH_3)_3ClSi$.

VNTR Variable number of tandem repeats.

YAC Yeast artificial chromosome.

Appendix B   Protocols

B.1   RCA Cleaning

Step 1

Samples, such as glass cover slips, are first cleaned by microcleaning soap, such as Micro-90 from Cole-Parmer, in a heated ultrasonic tank for about 20 minutes. Then, rinse several times by DI water to get rid of any soap residues. Soaking in DI water once in-between could help if time is permitted.

Step 2

Make RCA cleaning solution, 6:4:1 $H_2O:NH_4OH(37\%):H_2O_2(30\%)$. Heat it up on a hot plate to $\sim55°C$, at which the solution just starts bubbling. Put samples into it for one to two hours. Rinse several times with DI water. For long-term storage, keep samples in DI water after rinsing. Blow dry before usage.

Note 1:

RCA is a well-known cleaning procedure for silicon and glass substrate. It could clean out most of organic and metal contamination's because of its strong oxidation activity. It also leaves hydroxyl groups on the finished surface and thus renders the surface extremely hydrophilic. Moreover, at aqueous condition of pH 8 – 9, the surface is strongly negative-charged, which makes it suitable for many subsequent surface treatments.

Note 2:

Long-term RCA treatment, more than an hour, would make the surfaces of glasses a little bit rough. It actually helps the adhesion of an RTV device to the glass substrate because of more contact area. However, the treated glass cover slips are not suitable for some ultra flat measurements, such as atomic force microscopy (AFM).

B.2 YOYO-1 DNA Staining

B.2.1 Buffers

STE Buffer:

Deionized water containing 10 mM Tris-HCl, 0.1 mM EDTA and 5 mM NaCl with a final pH 7.5 and filtered by a 0.2-μm filter. Store at 4°C. Because of the carbon dioxide in the air, deionized water typically has pH around 5 to 6. A stock solution of 1 M Tris-HCl of pH 8.5 should give a final solution of pH $\sim$7.5 when diluted by 100 times with this slightly acidic deionized water.

Running Buffer:

STE buffer with 0.5% Tween-20, 100 nM YOYO-1 and 0.5%–1.0% β-mercaptoethanol.

B.2.2 YOYO-1 Solutions

10 μM YOYO-1 Working Stock:

$$
\begin{cases}
178\ \mu l & \text{STE buffer,} \\
20\ \mu l & \beta\text{-mercaptoethanol (antioxidant),} \\
2\ \mu l & 1\ \text{mM YOYO-1 stock in DMSO (-20°C).}
\end{cases}
$$

Mix well and store at 4°. This is good for about a month.

1 μM YOYO-1 Staining Solution:

Dilute 10 μM YOYO-1 solution by STE buffer by a factor of 10.

0.2 μM YOYO-1 Staining Solution:

Dilute 1 μM YOYO-1 solution by STE buffer by a factor of 5. Add β-mercaptoethanol to about 1%.

B.2.3 Staining Process

DNA staining should be carried out at a concentration no more than 20 pM molecules to prevent the clamping effect described in section 4.3.6. Therefore, prepare a diluted DNA

sample of concentration less than 40 pM, heat it up at 65°C for 10 minutes to separate any hybridized DNA strains, and then mix thoroughly by gentle pipetting with an equal volume of 0.2 μM YOYO-1 staining solution. However, if the average length of DNA molecules is more than 20 kbp, the concentration of DNA base pairs may exceed 400 μM[1]. In this case, the amount of YOYO-1 dye should be increased accordingly to maintain a minimum dye:bp ratio of 1:4. After mixing, heat the sample up again at 65°C for two hours or 50°C for four hours. Keep the tube light-tight during the heating process. If time is not an issue, 50°C staining is strongly recommended. Stained DNA samples can be kept in the refrigerator of 4°C up to three days before actual measurement under the SMS system. Generally speaking, the sample stored overnight in the fridge gives the best results (lowest C.V.) because the dye distribution is very uniform among all DNA molecules. However, the improvement of C.V. is around 0.5% or less. So, it is not necessary in most cases. Nevertheless, mixing is very important during the whole process. A good mixing gives consistent and nice sizing results.

B.2.4   Dilution for SMS Runs

The stained DNA samples should be diluted to about 100–200 fM by the Running Buffer (in B.2.1) before running through the SMS system. The concentration can be lower than 100 fM but the running time would be longer. For a sample of $\sim$ 150 fM DNA molecules, the normal sizing rate in the SMS system is about 5 molecules per second.

B.3   Molecular Fingerprinting on SMS

Step 1: Restriction Digestion

DNA samples are first digested with a specific restriction enzyme, such as Bgl II, EcoR I, Hind III or Xho I, following the recipe given by the manufacturer. Multiple digestions can also be done if necessary. However, a final mixture of DNA molecules of a few thousands of base pairs are preferred.

In case that the buffer used above is not compatible with the following steps, exchange of buffer by dialysis or ethanol precipitation should be conducted.

---

[1]The concentration of nucleic acids in solution can be checked easily by measuring the light absorbance at 260 nm. The absorption coefficient ϵ for dsDNA bases is 6,600 cm^{-1}M^{-1}.

Step 2: DNA Extension with Primers and Fluorescent Nucleotides

1. Make 10× nucleotide mix: 250 μM dATP, 500 μM fluorescein-12-dATP (NEL465; NEN), and 750 μM dTTP, dCTP and dGTP.

2. Prepare 10× primer solution: 1 μM.

3. Dilute DNA sample in STE buffer to get a final 10× concentration: $\sim$ 5–50 ng/μl. This strongly depends on the average size of DNA fragments in the digested sample and also the relative amount of DNA templates that will hybridize with the primers. Generally speaking, 1 nM of DNA templates (10×) gives the best result.

4. Make Mix #1:

   - 2 μl ultra-pure water;

   - 1 μl 10× nucleotide mix;

   - 1 μl 10× primer;

   - 1 μl 10× DNA samples.

5. Make Mix #2 (Gibco ELONGASE Enzyme Mix), total 100 μl:

   - 16 μl 5× Buffer A (from the enzyme package);

   - 24 μl 5× Buffer B (from the enzyme package);

   - 4 μl ELONGASE Enzyme Mix;

   - 56 μl ultra-pure water.

6. Add equal volume of Mix #2 into Mix #1. Mix them well. 100 μl of Mix #2 can be used for 20 different DNA samples (in Mix #1). Therefore, the total volume of Mix #2 should be adjusted according to the number of DNA samples to run.

7. Polymerase reaction:

   - Denaturing — 94°C for one minute;

   - Annealing — the annealing temperature T_m of the primer for one minute;

   - Extension — 68° for an hour. The actual extension time depends on the lengths of the DNA fragments we would like to obtain.

8. Use dialysis or spin columns to clean out unused fluorescent single nucleotides (fluorescein-12-dATP).

Step 3: SMS Analysis

1. Dilute the fluorescently-labeled DNA samples to about 100 fM. (1,000× if the original 10× template concentration is 1 nM).

2. Run 10 μl of the diluted sample on an SMS system, using 10 mW laser power and 2,400-volt LAAPD bias for 10 to 30 minutes.

3. Analyze data using DNA size distribution or a threshold algorithm based on a pre-selected fluorescent level.

Bibliography

[1] A. Agronskaia, J. M. Schins, B. G. de Grooth, and J. Greve. Polarization effects in flow cytometric DNA sizing. *Appl. Opt.*, 38(4):714–719, 1999.

[2] J. S. Bader, R. W. Hammond, S. A. Henck, M. W. Deem, G. A. McDermott, J. M. Bustillo, J. W. Simpson, G. T. Mulhern, and J. M. Rothberg. DNA transport by a micromachined Brownian ratchet device. *PNAS*, 96(23):13165–13169, 1999.

[3] M. Bass, editor. *Handbook of Optics*. McGraw-Hill, 2nd edition, 1995.

[4] J. P. Brody and P. Yager. Low reynolds number micro-fluidic devices. In *Proc. of Solid-State Sensor and Actuator Workshop*, pages 105–108. Hilton Head, June 1996.

[5] L. Buchaillot, E. Farnault, M. Hounmady, and H. Fujita. Silicon nitride thin films young's modulus determination by an optical non-destructive method. *Jpn. J. Appl. Phys.*, 2(36 (6B)):L794–L797, 1997.

[6] M. Burmeister and L. Ulanovsky, editors. *Pulsed-Field Gel Electrophoresis: Protocols, Methods and Theories*. Humana, Totowa, NJ, 1992.

[7] W. W. Cai, J. P. Jing, B. Irvin, L. Ohler, E. Rose, H. Shizuya, U. J. Kim, M. Simon, T. Anantharaman, B. Mishra, and D. C. Schwartz. High-resolution restriction maps of bacterial artificial chromosomes constructed by optical mapping. *PNAS*, 95(7):3390–3395, 1998.

[8] C. R. Cantor, C. L. Smith, and M. K. Mathew. Pulsed-field gel electrophoresis of very large DNA-molecules. *Ann. Rev. Biophys. & Biophys. Chem.*, 17:287–304, 1988.

[9] C. Carlsson, M. Jonsson, and B. Åkerman. Double bands in DNA gel electrophoresis caused by bis-intercalating dyes. *Nucleic Acids Research*, 23(13):2413–2420, 1995.

[10] A. Castro, F. R. Fairfield, and E. B. Shera. Fluorescence detection and size measurement of single DNA molecules. *Anal. Chem.*, 65(7):849–852, 1993.

[11] M. Chee, R. Yang, E. Hubbell, A. Berno, X. C. Huang, D. Stern, J. Winkler, D. J. Lockhart, M. S. Morris, and S. P. A. Fodor. Accessing genetic information with high-density DNA arrays. *Science*, 274(5287):610–614, 1996.

[12] Y.-F. Chen, Y.-T. Dai, H.-P. Chou, D.-C. Chang, C.-Y. Chang, and P.-J. Wang. Observation of quantum confinement effects in strained SiGe/Si quantum wells at room temperature. *Appl. Phys. Lett.*, 62(21):2713–2715, May 1993.

[13] Y.-F. Chen, Y.-T. Dai, H.-P. Chou, and I.-M. Chang. Photoinduced absorption studied by photothermal deflection spectroscophy: Its application to the determination of the energy of dangling-bond states in a-Si:H. *Chinese J. Phys.*, 31(6):767–772, Dec. 1993.

[14] H.-P. Chou, C. Spence, A. Scherer, and S. Quake. A microfabricated device for sizing and sorting DNA molecules. *PNAS*, 96(1):11–13, Jan. 1999.

[15] H.-P. Chou, C. Spence, A. Scherer, and S. R. Quake. Microfabricated devices for sizing DNA and sorting cells. *Proc. SPIE*, 3258:181–187, Jan. 1998.

[16] H.-P. Chou, M. A. Unger, A. Scherer, and S. Quake. Integrated elastomer fluidic lab-on-a-chip – surface patterning and DNA diagnostics. In *Proc. of Solid-State Sensor and Actuator Workshop*. Hilton Head, June 2000.

[17] P. J. Crossland-Taylor. A device for counting small particles suspended in a fluid through a tube. *Nature*, 171:37–38, 1953.

[18] G. Decher. Fuzzy nanoassemblies: Toward layered polymeric multicomposites. *Science*, 27:1232–1237, 1997.

[19] E. Delamarche, A. Bernard, and H. Schmid. Patterned delivery of immunoglobulins to surfaces using microfluidic networks. *Science*, 276(5313):779–781, 1997.

[20] D. C. Duffy, J. C. McDonald, O. J. A. Schueller, and G. M. Whitesides. Rapid prototyping of microfluidic systems in poly(dimethylsiloxane). *Anal. Chem.*, 70(23):4974–4984, 1998.

[21] C. S. Effenhauser, G. J. M. Bruin, and A. Paulus. Integrated capillary electrophoresis on flexible silicone microdevices: Analysis of DNA restriction fragments and detection of single DNA molecules on microchips. *Anal. Chem.*, 69(17):3451–3457, 1997.

[22] J. Fahrenberg, W. Bier, D. Maas, W. Menz, R. Ruprecht, and W. K. Schomburg. A microvalve system fabricated by thermoplastic molding. *J. Micromech. Microeng.*, 5(2):169–171, 1995.

[23] S. Fiedler, S. G. Shirley, T. Schnelle, and G. Fuhr. Dielectrophoretic sorting of particles and cells in a microsystem. *Anal. Chem.*, 70(9):1909–1915, 1998.

[24] A. Y. Fu, H.-P. Chou, and S. R. Quake. Microfabricated devices for rapid particular sorting using pressure-driven scheme and embeded microvalves. Under development, 2000.

[25] A. Y. Fu, C. Spence, A. Scherer, F. H. Arnold, and S. R. Quake. A microfabricated fluorescence-activated cell sorter. *Nature Biotechnol.*, 17(11):1109–1111, Nov. 1999.

[26] M. J. Fulwyer. Electronic separation of biological cells by volume. *Science*, 150:910–911, 1965.

[27] C. Goll, W. Bacher, B. Bustgens, D. Maas, W. Menz, and W. K. Schomburg. Microvalves with bistable buckled polymer diaphragms. *J. Micromech. Microeng.*, 6(1):77–79, 1996.

[28] P. M. Goodwin, M. E. Johnson, J. C. Martin, W. P. Ambrose, B. L. Marrone, J. H. Jett, and R. A. Keller. Rapid sizing of individual fluorescently stained DNA fragments by flow cytometry. *Nucleic Acids Research*, 21(4):803–806, 1993.

[29] X. H. Guo, E. J. Huff, and D. C. Schwartz. Sizing single DNA–molecules. *Nature*, 359(6398):783–784, 1992.

[30] S. Gurrieri, K. S. Wells, I. D. Johnson, and C. Bustamante. Direct visualization of individual DNA molecules by fluorescence microscopy: Characterization of the factors affecting signal/background and optimization of imaging conditions using YOYO. *Anal. Chem.*, 249(1):44–53, 1997.

[31] D. J. Harrison, K. Fluri, K. Seiler, Z. H. Fan, C. S. Effenhauser, and A. Manz. Micromachining a miniaturized capillary electrophoresis-based chemical-analysis system on a chip. *Science*, 261(5123):895–897, 1993.

[32] R. P. Haugland, editor. *Handbook of Fluorescent Probes and Research Chemicals*. Molecular Probes, 7th edition, 1999. URL: http://www.probes.com/handbook/sections/0000.html.

[33] L. J. Hornbeck and W. E. Nelson. Bistable deformable mirror device. *OSA Tech. Dig. Ser.*, 8:107, 1988.

[34] K. Hosokawa, T. Fuji, and I. Endo. Handling of picoliter liquid samples in a poly(dimethylsiloxane)-based microfluidic device. *Anal. Chem.*, 71(20):4781–4785, 1999.

[35] C.-H. Huang, C. K. Mirabelli, S. Mong, and S. T. Crooke. Intermolecular cross-linking of DNA through bifunctional intercalation of an antitumor antibiotic, luzopeptin a (bbm-928a). *Cancer Res.*, 43:2718–2724, 1983.

[36] S. C. Jacobson, R. Hergenroder, L. B. Koutny, and J. M. Ramsey. High-speed separations on a microchip. *Anal. Chem.*, 66(7):1114–1118, 1994.

[37] A. J. Jefferys, V. Wilson, and S. L. Thein. Hypervariable minisatellite regions in human DNA. *Nature*, 314(6006):67–73, 1985.

[38] R. S. Kane, S. Takayama, E. Ostuni, D. E. Ingber, and G. M. Whiteside. Patterning proteins and cells using soft lithography. *Biomaterials*, 20(23–24):2363, 1999.

[39] M. U. Kopp, A. J. de Mello, and A. Manz. Chemical amplification: Continuous-flow PCR on a chip. *Science*, 280(5366):1046–1048, 1998.

[40] B. Koren and M. Szawlowski. Large-are avalanche photodiodes challenge pmts. *Laser Focus World*, 34(11):71–80, 1998.

[41] L. Kuhn, E. Bassous, and R. Lane. Silicon charge electrode array for ink-jet printing. *IEEE Trans. Electron Devices*, ED-25(10):1257–1260, 1978.

[42] A. Larsson, C. Carlsson, M. Jonsson, and B. Albinsson. Characterization of the binding of the fluorescent dyes YO and YOYO to DNA by polarized light spectroscopy. *J. Am. Chem. Soc.*, 116(19):8459–8465, 1994.

[43] The Lee Company. *Electro-Fluidic Systems Technical Handbook*, 6th edition, 1994.

[44] P. H. Li and D. J. Harrison. Transport, manipulation, and reaction of biological cells on-chip using electrokinetic effect. *Anal. Chem.*, 69(8):1564–1568, 1997.

[45] L. Y. Lin, E. L. Goldstein, and R. W. Tkach. Free-space micromachined optical switches for optical networking. *IEEE J. Selected Top. Quantum Electron.*, 5(1):4–9, 1999.

[46] D. J. Lockhart, H. L. Dong, M. C. Byrne, M. T. Follettie, M. V. Gallo, M. S. Chee, M. Mittmann, C. W. Wang, M. Kobayashi, H. Horton, and E. L. Brown. Expression monitoring by hybridization to high-density oligonucleotide arrays. *Nature Biotechnol.*, 14(13):1675–1680, 1996.

[47] J. C. Lötters, W. Olthuis, P. H. Veltink, and P. Bergveld. The mechanical properties of the rubber elastic polymer polydimethylsiloxane for sensor applications. *J. Micromech. Microeng.*, 7(3):145–147, 1997.

[48] M. Madou. *Fundamentals of Microfabrication.* CRC Press, 1997.

[49] G. L. Mandell, J. E. Bennett, and R. Dolin. *Mandell, Douglas, and Bennett's Principles and Practice of Infectious Diseases.* Churchill Livingstone, 4th edition, 1995.

[50] J. C. McDonald, D. C. Duffy, J. R. Anderson, D. T. Chiu, H. Wu, O. J. A. Schueller, and G. M. Whitesides. Fabrication of microfluidic systems in poly(dimethylsiloxane). *Electrophoresis*, 21(1):27–40, 2000.

[51] X. Meng, K. Benson, K. Chada, E. J. Huff, and D. C. Schwartz. Optical mapping of lambda bacteriophage clones using restriction endonucleases. *Nature Genet.*, 9(4):432–439, 1995.

[52] A. Moldavan. Photo-electric technique for the counting of microscopical cells. *Science*, 80:188, 1934.

[53] H. Morgan, N. G. Green, M. P. Hughes, W. Monaghan, and T. C. Tan. Large-area travelling-wave dielectrophoresis particle separator. *J. Micromech. Microeng.*, 7(2):65–70, 1997.

[54] R. S. Muller and K. Y. Lau. Surface-micromachined microoptical elements and systems. *Proc. IEEE*, 86(8):1705–1720, 1998.

[55] U.-J. K. nad Bruce W. Birren, T. Slepak, V. Mancino, C. Boysen, H. L. Kang, M. I. Simon, and H. Shizuya. Construction and characterization of a human bacterial artificial chromosome library. *Genomics*, 34(2):213–218, 1996.

[56] Y. Nakamura, M. Leppert, P. Oconnell, T. H. R. Wolff, M. Culver, C. Martin, E. Fujimoto, M. Hoff, E. Kumlin, and R. White. Variable number of tandem repeat (vntr) markers for human-gene mapping. *Science*, 235(4796):1616–1622, 1985.

[57] S.-M. Nie and R. N. Zare. Optical detection of single molecules. *Ann. Rev. Bioph. Biom.*, 26:567–596, 1997.

[58] J. Nygren, N. Svanvik, and M. Kubista. The interactions between the fluorescent dye thiazole orange and DNA. *Biopolymers*, 46(1):39–51, 1998.

[59] R. Pethig. Delectrophoresis: Using inhormogeneous AC electrical fields to separate and manipulate cells. *Crit. Rev. in Biochem.*, 16(4):331–348, 1996.

[60] S. R. Quake, H.-P. Chou, C. Spence, A. Y. Fu, and A. Scherer. Disposable microdevices for DNA analysis and cell sorting. In *Proc. of Solid-State Sensor and Actuator Workshop*. Hilton Head, June 1998.

[61] G. Ramsay. DNA chips: State-of-the art. *Nature Biotechnol.*, 16(1):40–44, 1998.

[62] L. M. Roylance and J. B. Angell. A batch-fabricated silicon accelerometer. *IEEE Trans. Electron Devices*, ED-26(12):1911–1917, 1979.

[63] H. S. Rye, S. Yue, D. E. Wemmer, M. A. Quesada, R. P. Haugland, R. A. Mathies, and A. N. Glazer. Stable fluorescent complexes of double-stranded DNA with bis-intercalating asymmetric cyanine dyes: Properties and applications. *Nucleic Acids Research*, 20(11):2803–2812, 1992.

[64] R. B. M. Schasfoort, S. Schlautmann, J. Hendrikse, and A. van den Berg. Field-effect flow control for microfabricated fluidic networks. *Science*, 286(5441):942–945, 1999.

[65] M. Schena, D. Shalon, R. W. Davis, and P. O. Brown. Quantitative monitoring of gene-expression patterns with a complementary-DNA microarray. *Science*, 270(5235):467–470, 1995.

[66] D. C. Schwartz and C. R. Cantor. Separation of yeast chromosome-sized DNAs by pulsed field gradient gel electrophoresis. *Cell*, 37:67–75, 1984.

[67] H. M. Shiparo. *Practical Flow Cytometry*. Wiley-Liss, 3rd edition, 1995.

[68] H. Shizuya, B. Birren, U.-J. Kim, V. Mancino, T. Slepak, Y. Tachiiri, and M. Simon. Cloning and stable maintenance of 300-kilobase-pair fragments of human DNA in Escherichia coli using an f-factor-based vector. *PNAS*, 89(18):8794–8797, 1992.

[69] S. Shoji. Fluids for sensor systems. *Top. Curr. Chem.*, 194:163–188, 1998.

[70] V. L. Singer, L. J. Jones, S. T. Yue, and R. P. Haugland. Characterization of PicoGreen reagent and development of a fluorescence-based solution assay for double-stranded DNA quantitation. *Anal. Biochem.*, 249(2):228–238, 1997.

[71] P. M. Small, P. C. Hopewell, S. P. Singh, A. Paz, J. Parsonnet, D. C. Ruston, G. F. Schecter, C. L. Daley, and G. K. Schoolnik. The epidemiology of tuberculosis in san francisco. *New Eng. J. of Med.*, 330(24):1703–1709, 1994.

[72] J. G. Smits. Piezoelectric micropump with three valves working peristaltically. *Sensor. Actuat. A*, 21(1–3):203–206, 1990.

[73] E. Stokstad. Drug-resistant tb on the rise. *Science*, 287(5462):2391, 2000.

[74] R. G. Sweet. High frequency recording with electrostatically deflected ink jets. *Rev. Sci. Inst.*, 36:131–133, 1965.

[75] O. N. Tufte, P. W. Chapman, and D. Long. Silicon diffused-element piezoresistive diaphragms. *J. Appl. Phys.*, 33:3322, 1962.

[76] R.-C. Tyan, A. A. Salvekar, H.-P. Chou, C.-C. Cheng, A. Scherer, P.-C. Sun, F. Xu, and Y. Fainman. Design, fabrication and characterization of form-birefringent multilayer polarizing beam splitter. *J. Opt. Soc. Am. A*, 14(7):1627–1636, July 1997.

[77] M. A. Unger, H.-P. Chou, T. Thorsen, A. Scherer, and S. R. Quake. Microfabricated valves and pumps using multi-layer soft lithography. *Science*, 288(5463):113–116, Apr. 2000.

[78] M. A. Unger, E. Kartalov, and S. R. Quake. Manuscript in preparation.

[79] H. T. G. van Lintel, F. C. M. van de Pol, and S. Bouwstra. A piezoelectric micropump based on micromachining of silicon. *Sensor. Actuat.*, 15(2):153–167, 1988.

[80] J. C. Venter, H. O. Smith, and L. Hood. A new strategy for genome sequencing. *Nature*, 381(6581):364–366, 1996.

[81] L. C. Waters, S. C. Jacobson, N. Kroutchinina, J. Khandurina, R. S. Foote, and J. M. Ramsey. Microchip devices for cell lysis, multiplex PCR amplification, and electrophoretic sizing. *Anal. Chem.*, 70(1):158–162, 1998.

[82] G. K.-S. Wong, J. Yu, E. C. Thayer, and M. V. Olson. Multiple-complete-digest restriction fragment mapping: Generating sequence-ready maps for large-scale DNA sequencing. *PNAS*, 94(10):5225–5230, 1997.

[83] S. S. Woo, J. M. Jiang, B. S. Gill, A. H. Paterson, and R. A. Wing. Construction and characterization of a bacterial artificial chromosome library of sorghum-bicolor. *Nucleic Acids Research*, 22(23):4922–4931, 1994.

[84] A. T. Woolley, K. Q. Lao, A. N. Glazer, and R. A. Mathies. Capillary electrophoresis chips with integrated electrochemical detection. *Anal. Chem.*, 70(4):684–688, 1998.

[85] Y. N. Xia, E. Kim, X. M. Zhao, J. A. Rogers, M. Prentiss, and G. M. Whitesides. Complex optical surfaces formed by replica molding against elastomeric masters. *Science*, 273(5273):347–349, 1996.

[86] Y. N. Xia and G. M. Whitesides. Soft lithography. *Angewandte Chemie - Int. Ed.*, 37(5):551–575, 1998.

[87] X. Yang, C. Grosjean, Y.-C. Tai, and C.-M. Ho. A MEMS thermopneumatic silicone rubber membrane valve. *Sensor. Actuat. A*, 64(1):101–108, 1998.

[88] N. Yazdi, F. Ayazi, and K. Njafi. Micromachined inertial sensors. *Proc. IEEE*, 86(8):1640–1659, 1998.

[89] A. M. Young, T. M. Bloomstein, and S. T. Palmacci. Contoured elastic-membrane microvalves for microfluidic network integration. *J. Biomech. Eng. – Trans. ASME*, 121(1):2–6, 1999.